

NASA/TM—2012–217456



# **Analytical Round Robin for Elastic-Plastic Analysis of Surface Cracked Plates: Phase I Results**

*D.N. Wells and P.A. Allen  
Marshall Space Flight Center, Huntsville, Alabama*

---

**March 2012**

## The NASA STI Program...in Profile

Since its founding, NASA has been dedicated to the advancement of aeronautics and space science. The NASA Scientific and Technical Information (STI) Program Office plays a key part in helping NASA maintain this important role.

The NASA STI Program Office is operated by Langley Research Center, the lead center for NASA's scientific and technical information. The NASA STI Program Office provides access to the NASA STI Database, the largest collection of aeronautical and space science STI in the world. The Program Office is also NASA's institutional mechanism for disseminating the results of its research and development activities. These results are published by NASA in the NASA STI Report Series, which includes the following report types:

- **TECHNICAL PUBLICATION.** Reports of completed research or a major significant phase of research that present the results of NASA programs and include extensive data or theoretical analysis. Includes compilations of significant scientific and technical data and information deemed to be of continuing reference value. NASA's counterpart of peer-reviewed formal professional papers but has less stringent limitations on manuscript length and extent of graphic presentations.
- **TECHNICAL MEMORANDUM.** Scientific and technical findings that are preliminary or of specialized interest, e.g., quick release reports, working papers, and bibliographies that contain minimal annotation. Does not contain extensive analysis.
- **CONTRACTOR REPORT.** Scientific and technical findings by NASA-sponsored contractors and grantees.
- **CONFERENCE PUBLICATION.** Collected papers from scientific and technical conferences, symposia, seminars, or other meetings sponsored or cosponsored by NASA.
- **SPECIAL PUBLICATION.** Scientific, technical, or historical information from NASA programs, projects, and mission, often concerned with subjects having substantial public interest.
- **TECHNICAL TRANSLATION.** English-language translations of foreign scientific and technical material pertinent to NASA's mission.

Specialized services that complement the STI Program Office's diverse offerings include creating custom thesauri, building customized databases, organizing and publishing research results...even providing videos.

For more information about the NASA STI Program Office, see the following:

- Access the NASA STI program home page at <http://www.sti.nasa.gov>
- E-mail your question via the Internet to [help@sti.nasa.gov](mailto:help@sti.nasa.gov)
- Fax your question to the NASA STI Help Desk at 443-757-5803
- Phone the NASA STI Help Desk at 443-757-5802
- Write to:  
NASA STI Help Desk  
NASA Center for AeroSpace Information  
7115 Standard Drive  
Hanover, MD 21076-1320

NASA/TM—2012–217456



# **Analytical Round Robin for Elastic-Plastic Analysis of Surface Cracked Plates: Phase I Results**

*D.N. Wells and P.A. Allen  
Marshall Space Flight Center, Huntsville, Alabama*

National Aeronautics and  
Space Administration

Marshall Space Flight Center • Huntsville, Alabama 35812

---

**March 2012**

## Acknowledgments

The authors would like to acknowledge the support of the ASTM Committee on Fatigue and Fracture (E08), with a special note to James Joyce (U.S. Naval Academy, Retired), Richard Link (U.S. Naval Academy), and Robert Tregoning (U.S. Nuclear Regulatory Commission) for their support during the development of the revised surface crack testing standard and encouraging this analytical round robin to go forward. As always, our mentor Robert H. Dodds Jr. (University of Illinois at Urbana-Champaign) has provided a continuous stream of support and guidance. Clearly, the most important part of any round robin study is the group of participants graciously lending their time and effort to the undertaking. We would like to thank each of them sincerely: Steven Altstadt at Stress Engineering Services, Mark Messner at the University of Illinois at Urbana-Champaign with the support of Robert Dodds, Ramesh Mageshwaren, and Marc Scibetta at SCK CEN (Belgian Nuclear Research Center), Matt McCutcheon at NASA Marshall Space Flight Center (MSFC) (Propulsion Structures), Dawn Phillips and Brian Steeve at MSFC (Vehicle Structures), Howard Rathbun at the U.S. Nuclear Regulatory Commission, Guowu Shen at CANMET (Canada Centre for Mineral and Energy Technology), Greg Thorwald and Chris Tipple at Quest Integrity Group, Igor Varfolomeev at the *Fraunhofer-Institut fuer Werkstoffmechanik IWM* (Germany), Xin Wang at Carleton University (Canada), Stefan Bickelmaier and Michael Windisch at MT Aerospace AG (Germany), and Yoshiki Yamada at NASA Glenn Research Center. Our work on surface cracks at MSFC would not be possible without the support of Vann Bradford, Tommy Stewart, and Damon Cleghorn. We greatly appreciate their efforts in helping us move the new surface crack test standard forward.

Available from:

NASA Center for AeroSpace Information  
7115 Standard Drive  
Hanover, MD 21076-1320  
443-757-5802

This report is also available in electronic form at  
<<https://www2.sti.nasa.gov/login/wt/>>

## TABLE OF CONTENTS

1. INTRODUCTION .....	1
1.1 Motivation for the Inter-Laboratory Study .....	1
1.2 Scope and Objectives for Phase I of the Inter-Laboratory Study .....	1
2. PROBLEM STATEMENT, PHASE I .....	3
3. PARTICIPANT OVERVIEW .....	5
4. RESULTS AND DISCUSSION .....	8
4.1 Tying Analysis to Experiment .....	10
4.2 J-Integral Results .....	19
4.3 Assessing Sources of Variability .....	30
5. CONCLUSIONS .....	68
6. RECOMMENDED PRACTICES .....	69
APPENDIX A—PHASE I PROBLEM STATEMENT AND TABULAR DATA .....	71
APPENDIX B—EVALUATION OF INTER-LABORATORY STUDY RESULTS ASSUMING A NORMAL DISTRIBUTION .....	75
REFERENCES .....	79

## LIST OF FIGURES

1.	Surface crack test specimen configuration .....	3
2.	ILS specimen configured for testing .....	9
3.	ILS specimen fracture surface with tearing location indicated .....	10
4.	Experimental force versus CMOD response .....	11
5a.	Force versus CMOD for all ILS participants .....	12
5b.	Force versus CMOD for all ILS participants at end of test .....	13
6.	Deviation in predicted CMOD relative to lab-5 .....	14
7.	Elastic stiffness for each model relative to current $\pm 2.5\%$ limits .....	15
8a.	Overall force versus CMOD with “corner bracket” validity limit .....	16
8b.	Force versus CMOD, zoomed to “corner bracket” validity limit .....	17
9a.	Overall force versus CMOD with CMOD-based validity limit .....	18
9b.	Force versus CMOD, zoomed to CMOD-based validity limit .....	19
10a.	J-integral at $\phi = 17^\circ$ versus force .....	20
10b.	J-integral versus $\phi$ at 200 kN .....	21
10c.	J-integral versus $\phi$ at 252 kN .....	22
10d.	J-integral versus $\phi$ at 289 kN .....	23
10e.	J-integral versus $\phi$ at 200 kN normalized by maximum J-integral value .....	24
10f.	J-integral versus $\phi$ at 252 kN normalized by maximum J-integral value .....	25
10g.	J-integral versus $\phi$ at 289 kN normalized by maximum J-integral value .....	26
11.	J-integral versus CMOD at $\phi = 17^\circ$ .....	29

## LIST OF FIGURES (Continued)

12.	J-integral versus CMOD at $\phi = 17^\circ$ with CMOD-based evaluation criteria .....	30
13.	J-integral at $\phi = 17^\circ$ versus analysis code .....	33
14.	Typical $\frac{1}{4}$ symmetric surface crack finite element mesh .....	34
15.	J-integral at $\phi = 17^\circ$ versus model size parameter from equation (1) .....	35
16a.	Variation in elastic CMOD stiffness versus element integration order .....	36
16b.	J-integral at $\phi = 17^\circ$ versus element integration order .....	37
17.	Crack tip mesh with undeformed geometry on left and deformed on right for (a) collapsed elements with tied nodes, (b) collapsed elements with untied nodes, and (c) keyhole pattern .....	38
18.	J-Integral at $\phi = 17^\circ$ versus crack tip mesh geometry .....	39
19.	Illustration of typical J-integral results showing degrees of path dependency .....	40
20.	Illustration of dimension used to characterize domain size .....	41
21.	J-integral at $\phi = 17^\circ$ versus normalized domain size .....	42
22.	J-integral at $\phi = 17^\circ$ versus method used to evaluate J from multiple domains .....	43
23.	J-integral at $\phi = 17^\circ$ versus model boundary condition .....	44
24a.	Curved crack front with skewed elements relative to the crack front normal, a common source of oscillating J-integral solutions .....	45
24b.	Curved crack front with elements aligned with the crack front normal .....	46
25.	Oscillating J-integral solution affecting the lab-8 solution .....	46
26.	J-integral at $\phi = 17^\circ$ versus use of true or engineering stress-strain material properties .....	48
27.	J-integral at $\phi = 17^\circ$ versus use of small-strain or finite-strain formulation .....	49
28.	Stress-strain inputs in engineering stress-strain space .....	50

## LIST OF FIGURES (Continued)

29a.	Engineering stress versus plastic strain .....	51
29b.	Engineering stress versus plastic strain illustrating range of proportional limits .....	52
30.	J-integral at $\phi = 17^\circ$ versus proportional limit in constitutive inputs .....	53
31.	Area under the engineering stress-plastic strain curve as function of stress .....	54
32a.	Engineering stress-strain curves used in the proportional limit substudy .....	55
32b.	All variations in proportional limit occur prior to standard 0.2% offset strain yield definition .....	56
33.	Area under the engineering stress-plastic strain curve as function of stress for the proportional limit substudy .....	57
34.	Images (a) through (j) illustrate the effects of proportional limit on the resulting J-integral value as the model is loaded through the ILS load regime and beyond .....	58
35.	Bounding models at the tearing CMOD for the CMOD-matching substudy .....	65
36.	Comparison of scaled material property inputs for the CMOD-matching substudy .....	66
37.	Bounding models at the deformation-limited CMOD for the CMOD-matching substudy .....	67
38.	Probability plot for normal distribution of J-integral values .....	75
39.	Probability plot for normal distribution of elastic stiffness of modeled CMOD response .....	76
40.	Probability plot for normal distribution of the number of nodes used to model the crack front .....	77
41.	Probability plot for normal distribution of the model size parameter from equation (1) .....	77

## LIST OF TABLES

1.	List of ILS participants and affiliation .....	5
2.	Summary of J-integral results .....	27
3.	Summary of ILS model parameters for all participants .....	31
4.	Summary of results from CMOD-matching substudy .....	64

## LIST OF ACRONYMS

ASTM	American Society for Testing and Materials
CMOD	crack mouth opening displacement
CTOD	crack tip opening displacement
DCPD	direct current potential drop
FEA	finite element analysis
ILS	inter-laboratory study
MSFC	Marshall Space Flight Center
MSP	model size parameter
TM	Technical Memorandum

## NOMENCLATURE

$2c$	surface crack length (see fig. 1)
$a$	crack depth (see fig. 1)
$B$	specimen thickness (see fig. 1)
$E$	Young's modulus of elasticity
$K$	stress intensity factor
$L$	specimen height (see fig. 1)
$M_a$	deformation state characterized by crack length, i.e., $M_a = r_{\phi a} \sigma_{ys} / J_{\phi}$
$r_{\phi a}$ and $r_{\phi b}$	specimen characteristic length used to evaluate the deformation state (see inset in fig. 34a)
$W$	specimen width (see fig. 1)
$\mu$	mean of population (number of nodes)
$\nu$	Poisson's ratio
$\sigma$	standard deviation of the population (number of nodes)
$\sigma_{ys}$	material yield strength
$\ell$	local crack extension (see fig. 3)



## TECHNICAL MEMORANDUM

### ANALYTICAL ROUND ROBIN FOR ELASTIC-PLASTIC ANALYSIS OF SURFACE CRACKED PLATES: PHASE I RESULTS

#### 1. INTRODUCTION

The ASTM Committee on Fatigue and Fracture (E08) Task Group on Fracture Toughness of Surface Cracks (E08.07.03) is developing a new material test standard for the assessment of surface crack toughness in the linear-elastic and the elastic-plastic regime. While evaluation of the linear-elastic stress intensity factor,  $K$ , is well accepted for surface crack geometries through the Newman-Raju equations<sup>1,2</sup> or other existing tabulations,<sup>3</sup> the evaluation of elastic-plastic J-integral values requires the user to perform an analytical assessment of the experiment using methods that cannot be easily contained or conveyed within a test standard. The feasibility of allowing this latitude in assessment methodology in a testing standard requires validation through an inter-laboratory study (ILS). This Technical Memorandum (TM) provides an overview of the problem statement and results of the first phase of the study.

##### 1.1 Motivation for the Inter-Laboratory Study

Existing mechanical testing standards for fracture mechanics applications, such as ASTM E1820,<sup>4</sup> include within the document all the necessary equations and supporting data to assess the experiment directly, producing a “standard” result. In the case of a surface crack in a flat plate, no openly available method exists for accurately evaluating the J-integral under elastic-plastic conditions along the full perimeter of a surface crack that can feasibly be reduced to equation form for inclusion into a test standard. However, the ability to assess this problem using methods of analysis such as finite elements has progressed considerably in recent years and may now be a suitable substitute for assessment of experimental results in lieu of fixed relations within the document. Codes defining standard practice for structural evaluation of defects, such as the API Recommended Practice 579, Fitness-for-Service,<sup>3</sup> allow for such external analysis methods. This study is designed to evaluate the feasibility of an external analysis method for experimental data assessment.

##### 1.2 Scope and Objectives for Phase I of the Inter-Laboratory Study

This ILS is planned to develop in phases based on need and observations made as the study progresses. Additional phases are likely to investigate different crack shapes, bending as opposed to tension loading, and different materials. This first phase approached the ILS concept differently than most experimentally based studies—the analysis methodology was not specified to participants and key experimental results were withheld, as explained below. This made the study “blind”

in the sense that the participants did not have the experimental force and displacement information available to them to validate their model, or to potentially alter their model to converge on the experimental result, and they were free to approach the analysis using any method of choice. This approach allowed this first phase of the ILS to serve as a current measure of the state of the art for elastic-plastic fracture mechanics analysis. An open study of this nature regarding elastic-plastic analysis methods has not been performed for some time.<sup>5,6</sup>

Given this approach, the ILS phase I results are representative of the surface crack test standard providing essentially no guidance regarding the method of test analysis; however, analysis guidelines are to be provided within the testing standard to maximize the likelihood that users will, to the extent possible, reach a “standardized” answer. These guidelines are expected to derive from three sources: an assessment of the causes of variability within the ILS results, a compilation of the best generally accepted modeling practices, and the commonality of methods chosen by the ILS participants.

## 2. PROBLEM STATEMENT, PHASE I

The initial effort, described as phase I—problem A, was an analysis of a surface crack in tension. The basic geometry and definition of parameters for a generic surface crack specimen are shown in figure 1. The complete problem statement as it was provided to each participant is included in appendix A along with the necessary tabular data for the reader to independently analyze the problem. The material properties for the problem were provided to all participants in the form of engineering stress versus strain data from a tensile test. The elastic properties ( $E = 74.46 \text{ GPa}$  and  $\nu = 0.33$ ) were defined to remove that potential source of variability from the study. The choice of constitutive models and treatment of the stress-strain data was left to the discretion of the participants.

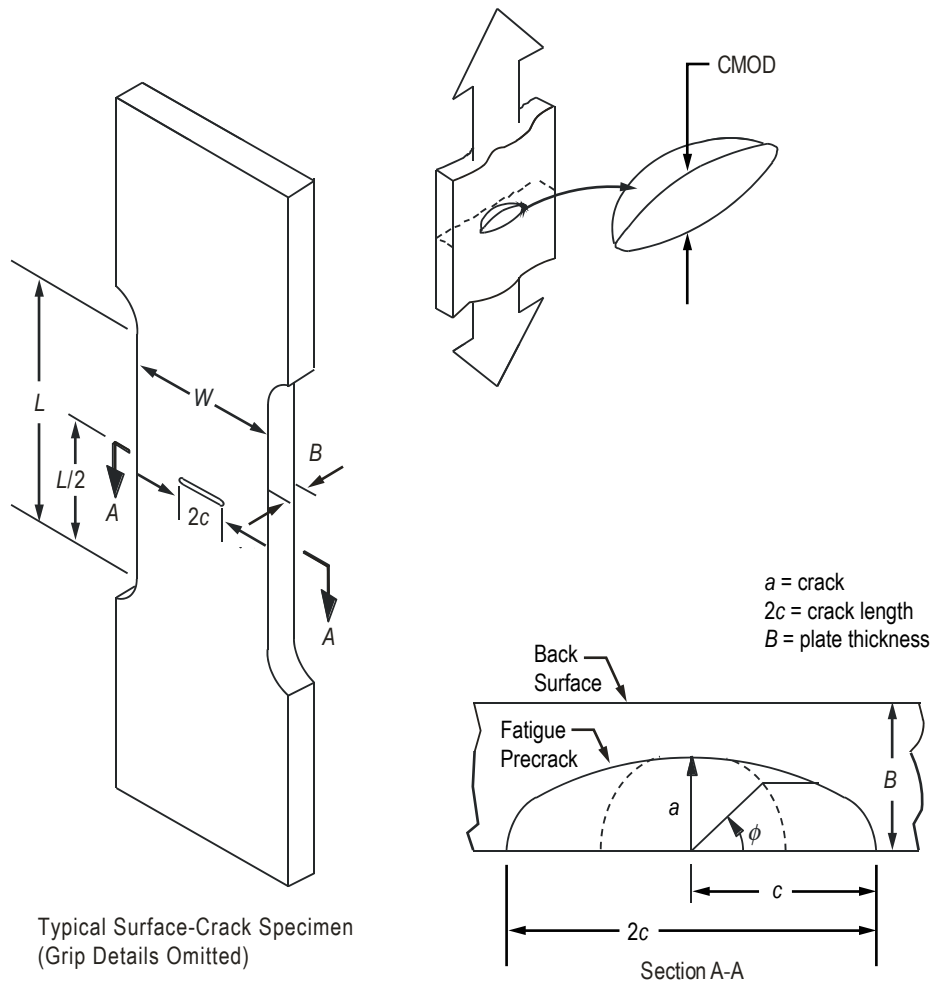


Figure 1. Surface crack test specimen configuration.

From their analysis, each participant was requested to provide three primary results, selected based on the nature of results required by the test method. Participants were requested to run their elastic-plastic analysis with sufficient quantity of load steps to report the following data:

- (1) Force versus crack mouth opening displacement (CMOD) throughout the test.
- (2) J-integral versus parametric angle location ( $\phi$ ) for a set of specific force values.
- (3) J-integral versus force throughout the test for a given parametric angle location ( $\phi$ ).

### 3. PARTICIPANT OVERVIEW

This phase of the study had 15 participants covering a range of industries, academia, and countries. There was also intent to include participants with a broad range of expertise in the study. The user community for the test standard is potentially broad; therefore, our intent was not to have only “experts” in the field participating. A study with only expert participants would not be properly representative. It could lead to overly optimistic results and a lack of comprehensive analytical recommendations for users of the test standard.

A list of the participants is included in table 1. All participants have been assigned a random designation from lab-1 to lab-15. All results remain anonymous, though each participant was informed of their lab identification.

Table 1. List of ILS participants and affiliation.

Name	Affiliation
Phillip Allen (lab-1)	MSFC Materials Laboratory
Steven Altstadt	Stress Engineering Services
Mark Messner/Bob Dodds	University of Illinois at Urbana-Champaign
Ramesh Mageshwaran	SCK CEN, Belgium
Matt McCutcheon	MSFC Propulsion Structures
Dawn Phillips	MSFC Vehicle Structures
Howard J. Rathbun	U.S. Nuclear Regulatory Commission
Guowu Shen	MTL/CANMET, Canada
Brian Steeve	MSFC Vehicle Structures
Greg Thorwald	Quest Integrity Group
Chris Tipple	Quest Integrity Group
Igor Varfolomeev	Fraunhofer-Institut fuer Werkstoffmechanik IWM
Xin Wang	Carleton University, Canada
Stephan Bickelmaier	MT Aerospace AG, Germany
Yoshiki Yamada	NASA Glenn Research Center

After receiving all contributions, the authors sent a survey to each participant to document the input parameters for each of the analyses. The questions in the survey were not exhaustive, but were selected with insight into expected sources of variation in these assessments. To minimize interpretation issues in the answers, a list of likely answers was provided; however, the survey always allowed the participant to provide any response along with explanatory comments. The survey requested the following information, with the standardized responses provided appearing in {brackets}:

- (1) General
  - (a) Principle background of analyst {materials, structures, other}
  - (b) Method of analysis used {finite elements, SINTAP, other}
  - (c) What code was used {ABAQUS, ANSYS, WARP3D, other}
  
- (2) Model specifics
  - (a) Total number of elements
  - (b) Total number of nodes
  - (c) Number of nodes along the crack front
  - (d) Type of element {linear hex (8-node), quadratic hex, (20+ node), other}
  - (e) Element integration order {full, reduced}
  - (f) Strain assumption {small strain, finite strain}
  
- (3) Crack tip modeling
  - (a) Crack tip elements/geometry {collapsed hex-untied nodes, collapsed hex-tied nodes, collapsed hex-tied nodes with  $\frac{1}{4}$  point mid-side node, key-hole or finite radius, no special crack tip meshing, other}
  
- (4) Boundary conditions
  - (a) Grip end modeling {simple rectangular flat plate, modeled grip end details (provide comments)}
    - (i) If grip end details modeled, description of boundary condition is required
    - (ii) If rectangular flat plate {uniform displacement, uniform pressure stress, other}
  - (b) Number of symmetry planes {none, 1, 2}
  
- (5) Material modeling (actual stress-strain inputs requested)
  - (a) Type of plasticity {incremental, nonlinear elastic/deformation}
  - (b) Engineering or true stress and strain {engineering, true}
  - (c) Stress-strain curve representation {bilinear, multilinear table, linear + power law, power law, other}
  
- (6) J-integral calculations
  - (a) Method {domain integral, crack tip opening displacement (CTOD), other}
  - (b) If domain integral was used
    - (i) Number of domains
    - (ii) Method to get J from multiple domains {average of all, average of all but first, average of converged, average of subset (e.g., last 4 of 10), maximum value of all domains, other}
    - (iii) Dimension of outermost domain.

An additional short survey was provided if the submitted analysis was not based on finite element methods. While a few participants did submit supplementary analysis that was not finite element based, these analyses were provided for reference purposes with the finite element results being the primary submittal to the study. All results included in the study were based on finite element models.

Each lab's submission was reviewed upon receipt. If there appeared to be any form of basic issue with the provided data, the authors contacted the participant for clarification. There were a few cases of errors created during the copy and paste process to move data from finite element code output to the requested Excel spreadsheet summaries. These corrections were allowed in order to avoid unwarranted variation in the results. In each case, the simple errors corrected in this process would have been easily noticed had the study not been blind to the experimental results.

#### 4. RESULTS AND DISCUSSION

As a basis for discussing the ILS results, it is helpful to present the experimental results upon which this phase of the ILS is based. The participants were not aware of these results at the time of their assessment.

The experiment consisted of a 2219-T8 aluminum specimen of the dimensions shown in appendix A. The photograph of the specimen during test (see fig. 2) shows the ring gauge used for CMOD as well as input current and probe wires for direct current potential drop (DCPD) measurements. Changes in the DCPD signal assisted as a nonquantitative indicator of crack extension during the test. The DCPD probe spacing was  $\approx 1$  mm using local platinum probe wires welded near the right-hand  $2c$  location of the precrack. The outer probe wires visible in the photograph provided a reference signal to normalize the DCPD measurement. The specimen was precracked in tension, instrumented, and then loaded monotonically until the combination of CMOD and DCPD signals indicated sufficient change to suggest local tearing had occurred. The specimen was partially unloaded and the extent of the crack tearing was marked using a sodium hydroxide solution. The solution was rinsed from the crack and the crack dried while the partial load was maintained. The specimen was then subjected to fatigue marking cycles at  $\approx 60\%$  of the tearing load to help accentuate the ductile tearing fracture surface. Finally, the specimen was monotonically loaded to failure using the same instrumentation.

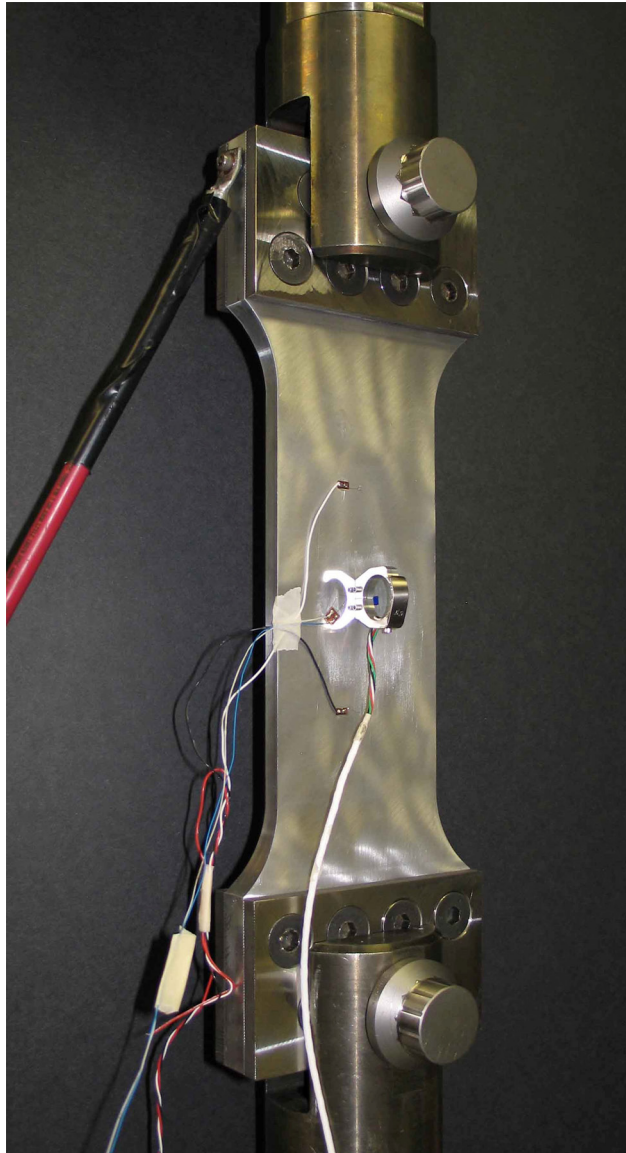


Figure 2. ILS specimen configured for testing.

The proposed surface crack test method relies on a multispecimen technique to narrow in on appropriate amounts of crack tearing for test assessment. The fracture surface for the ILS test, annotated in figure 3, reveals the local (maximum) crack extension ( $\ell$ ) was 0.5 mm, at a parametric angle of  $17^\circ$ . This information, combined with the tearing force of 251.8 kN and the corresponding CMOD, constitute the experimental test result. The intent of the proposed surface crack standard is to define the crack tip conditions at the initiation of ductile tearing. Therefore, the analysis requested by the ILS was to estimate the J-integral at the parametric angle  $\phi = 17^\circ$  at the tearing force of 252 kN, and to predict the force versus CMOD response throughout the test. Though experimental results cannot be compared beyond this force level, the requested analysis was extended to a force of 289 kN in order to provide insight into analysis variability at higher deformation levels.

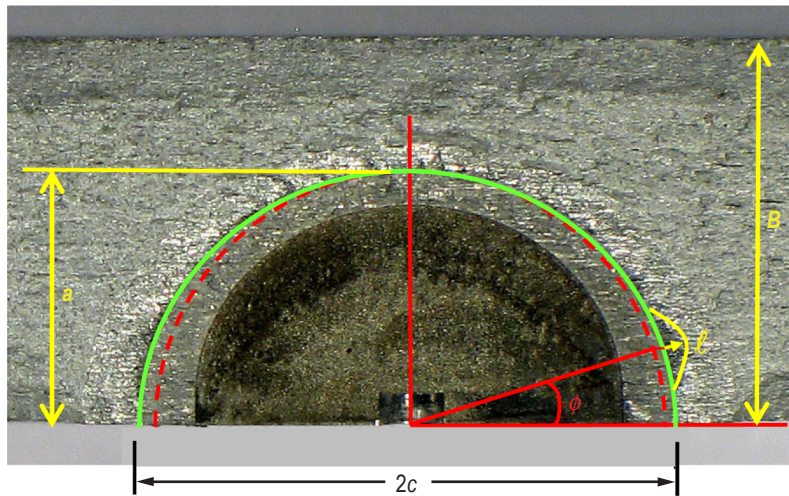


Figure 3. ILS specimen fracture surface with tearing location indicated.

#### 4.1 Tying Analysis to Experiment

The only physical tie between the analysis and experiment is the force versus CMOD response. Based on this metric, the proposed test standard requires agreement between analysis and experiment in two ways: (1) the slope of the force-CMOD elastic response and (2) the final analytical force-CMOD prediction. The limits of acceptable agreement for these metrics are still under review and studies such as this ILS will help determine the required bounds.

The force-CMOD response from the experiment is shown in figure 4. The nonlinearity in the test record and the permanent CMOD offset of  $\approx 0.015$  mm are indicators of elastic-plastic conditions in the specimen. The force-CMOD predictions from the 15 ILS labs are plotted along with the experimental record in figures 5a and 5b. Consistent agreement is found in the elastic slope with only lab-2 predicting a slightly stiffer response. The predicted nonlinearity of the force-CMOD response due to plasticity is also reasonably consistent up to the tearing force of 252 kN. The deviation in CMOD prediction increases significantly at force levels above 252 kN. Figure 6 illustrates the variation in CMOD predictions relative to the arbitrarily chosen lab-5 result. Three response families are visible in the result: lab-2 stands unique; labs -6, -14, and -15 share a slightly stiffer response; and the remaining labs are grouped as a general family largely within the  $\pm 1$  standard deviation lines shown. The appropriateness of applying normal distribution statistics to various ILS data is discussed in appendix B.

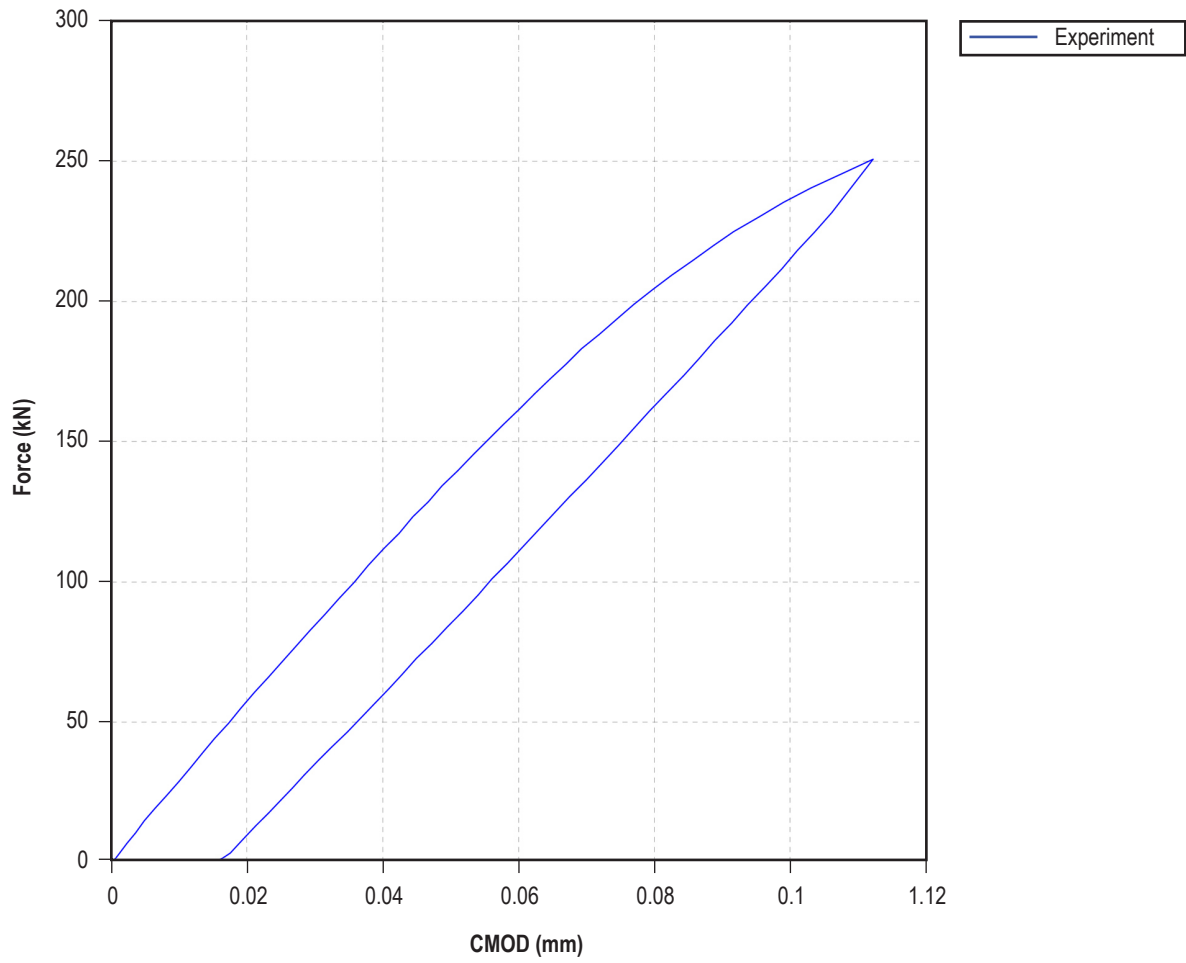


Figure 4. Experimental force versus CMOD response.

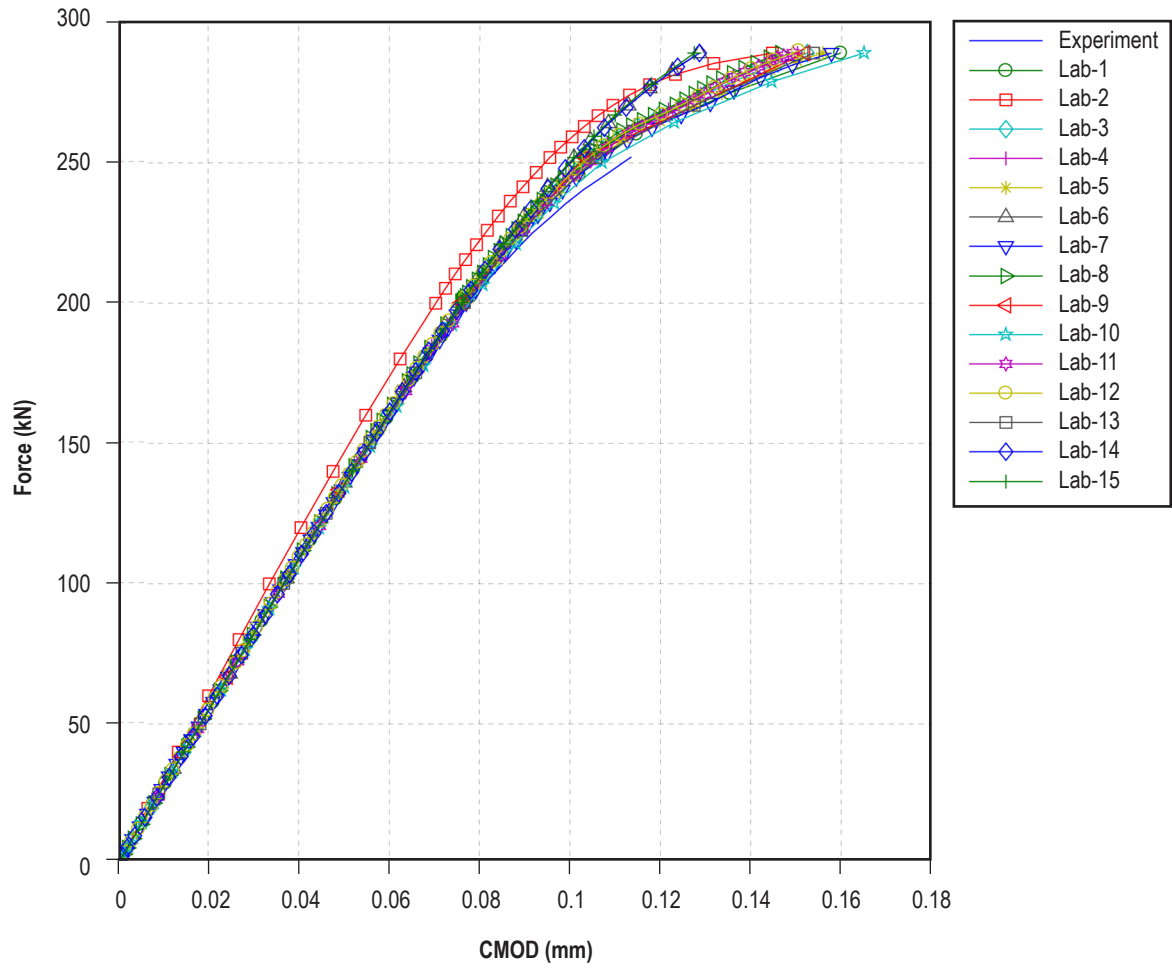


Figure 5a. Force versus CMOD for all ILS participants.

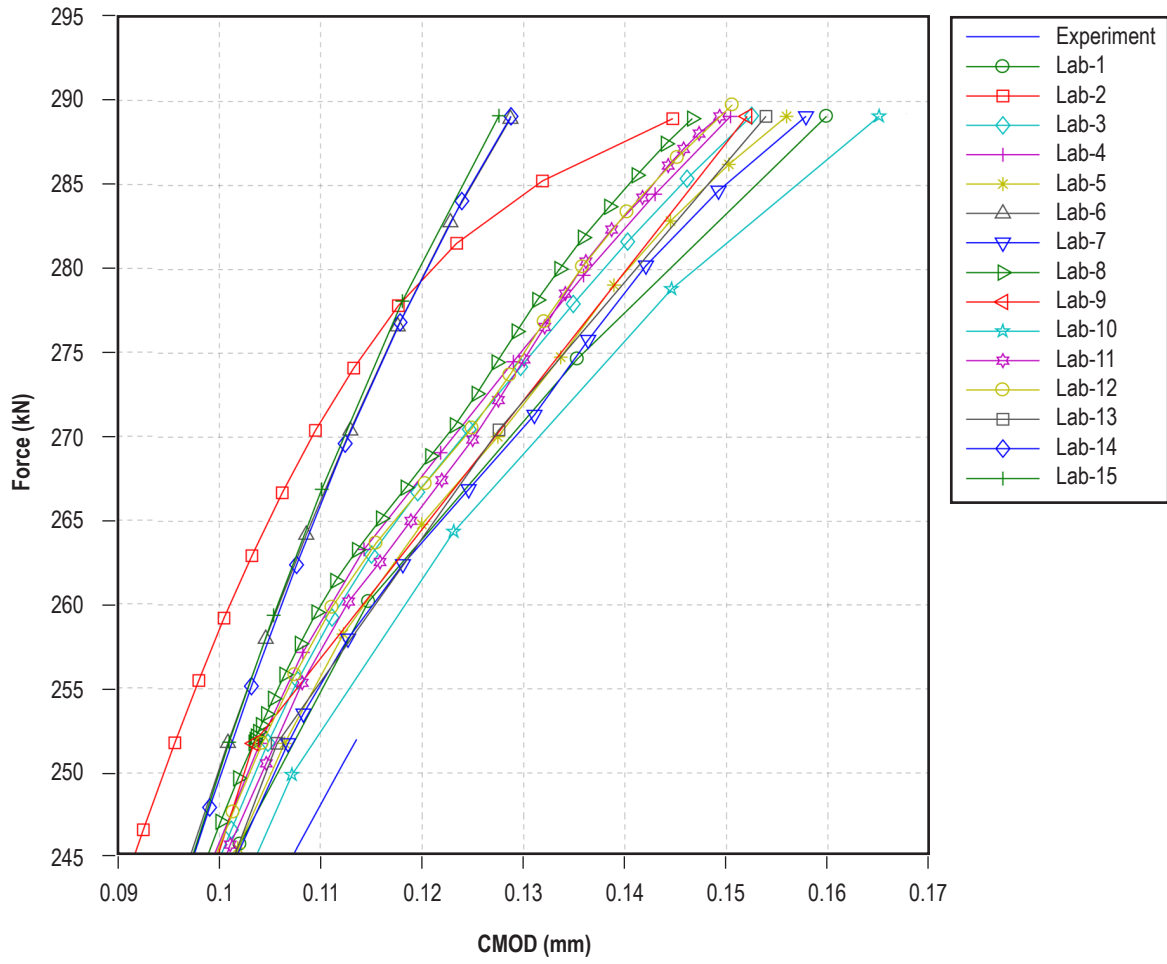


Figure 5b. Force versus CMOD for all ILS participants at end of test.

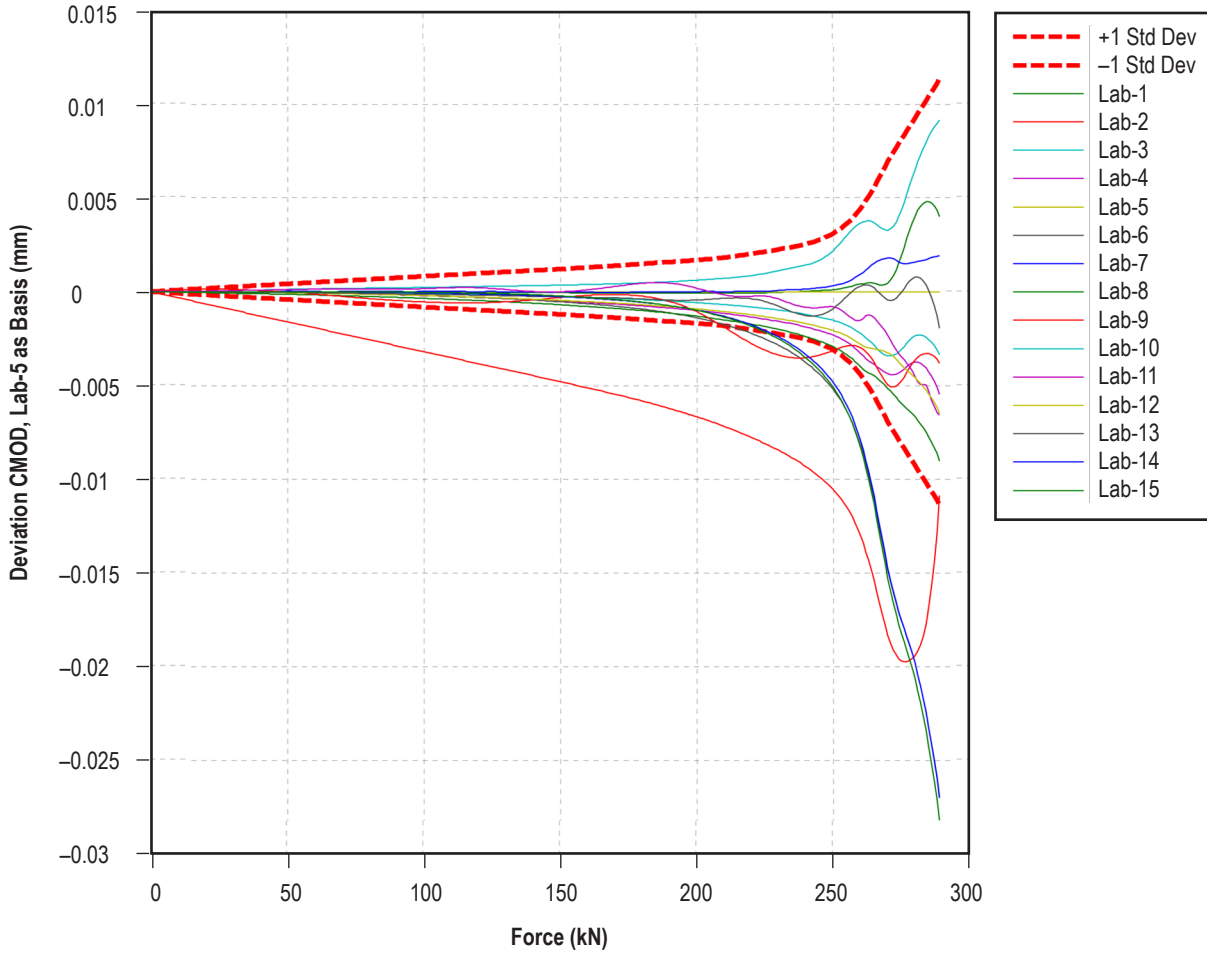


Figure 6. Deviation in predicted CMOD relative to lab-5.

To maintain acceptable bounds on the analytical assessment of the experiment, the force-CMOD traces must agree using reasonable metrics. Currently, two metrics are proposed. The first is a simple evaluation of the elastic stiffness of the force-CMOD relationship. This evaluation provides a broad check on numerous basic inputs to the analysis, including the specimen and crack geometry, the elastic stiffness in the material constitutive model, and to a lesser degree, the modeled boundary conditions. Many fundamental analysis mistakes can be screened with this evaluation. Currently, the test standard's allowable range for the analytical prediction is  $\pm 2.5\%$  of the experimental stiffness. Figure 7 shows the modeled stiffness for each of the labs relative to the experiment along with the  $\pm 2.5\%$  bounding lines. The stiffness was determined by a regression of force-CMOD data between 30 and 150 kN. Thirteen of 15 labs matched the experimental stiffness within these limits with their blind analysis. It is important to note that in this phase of the ILS, the elastic modulus of the material ( $E = 74.46$  GPa) was provided directly as part of the problem statement. The inevitable variability of selecting an elastic modulus from literature, handbooks, or test data is not reflected in this part of the study. The most direct means of correcting the analytically predicted specimen stiffness is through changing the model's elastic modulus. Additional guidance will be required to appropriately limit the liberties taken with the modulus in order to match experimental

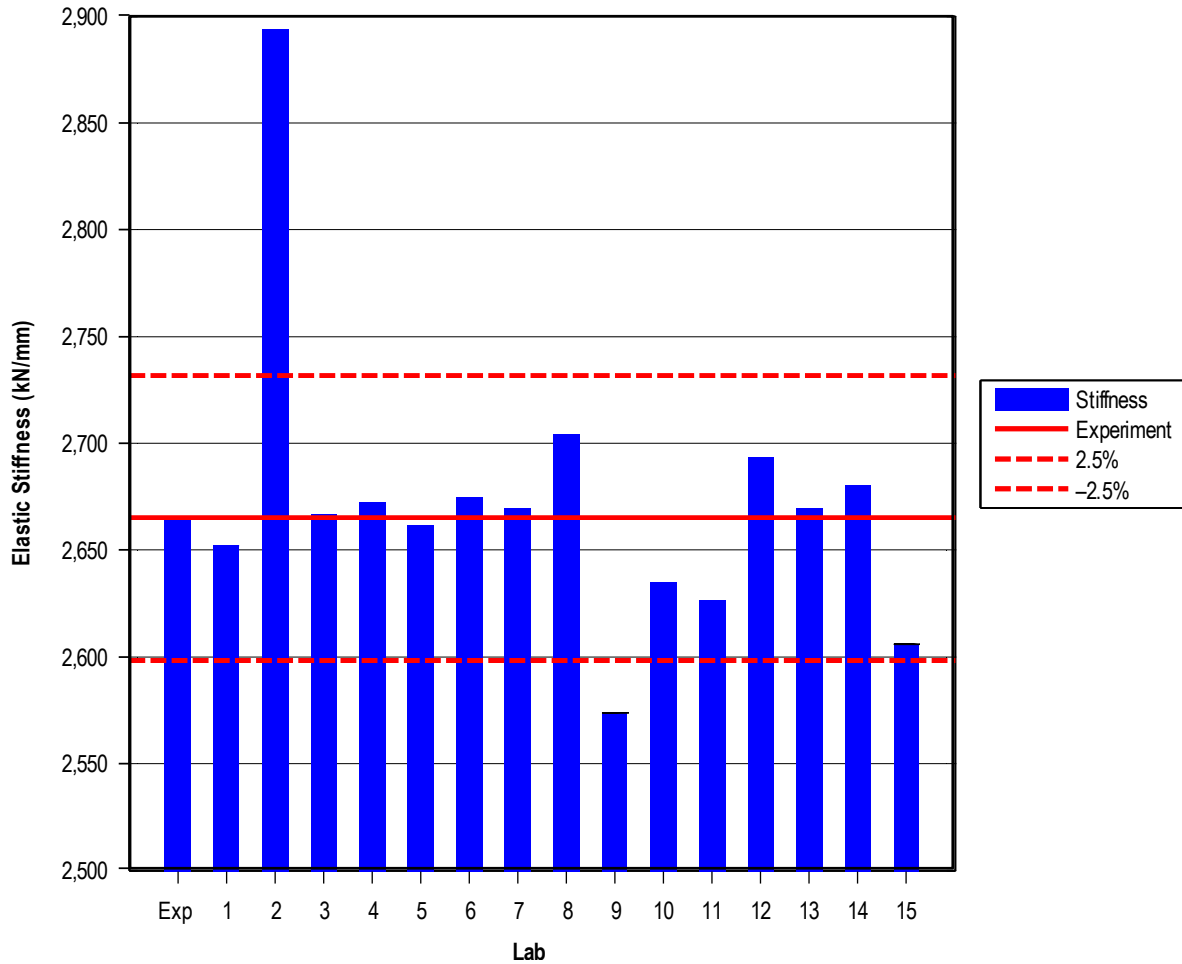


Figure 7. Elastic stiffness for each model relative to current  $\pm 2.5\%$  limits.

results. A need to alter the modulus value in the analysis by more than a few percent to match the experiment is an indicator that some other aspect of the analysis or experimental data is in error.

The second proposed metric to match the analysis results to the test results concerns the maximum force and CMOD recorded during the test. This is the point in the test when the specimen is unloaded after the initiation of tearing. It is unlikely the test and analysis records will match exactly, so there is a potential to evaluate the test result based on the analysis matching either the test force or the test CMOD. The current draft of the test standard proposes test evaluation when the analysis reaches either the maximum experimental force or CMOD, whichever is first. This evaluation method is illustrated in figures 8a and 8b. The corner bracket shown at the end of the experimental record represents a limit on force, allowing up to  $-10\%$  error in CMOD prediction, or a limit on CMOD allowing up to a  $-10\%$  error in force prediction. All ILS analyses reflect a model stiffer than the experiment regarding the response to plastic deformation. This is an expected result from two perspectives:

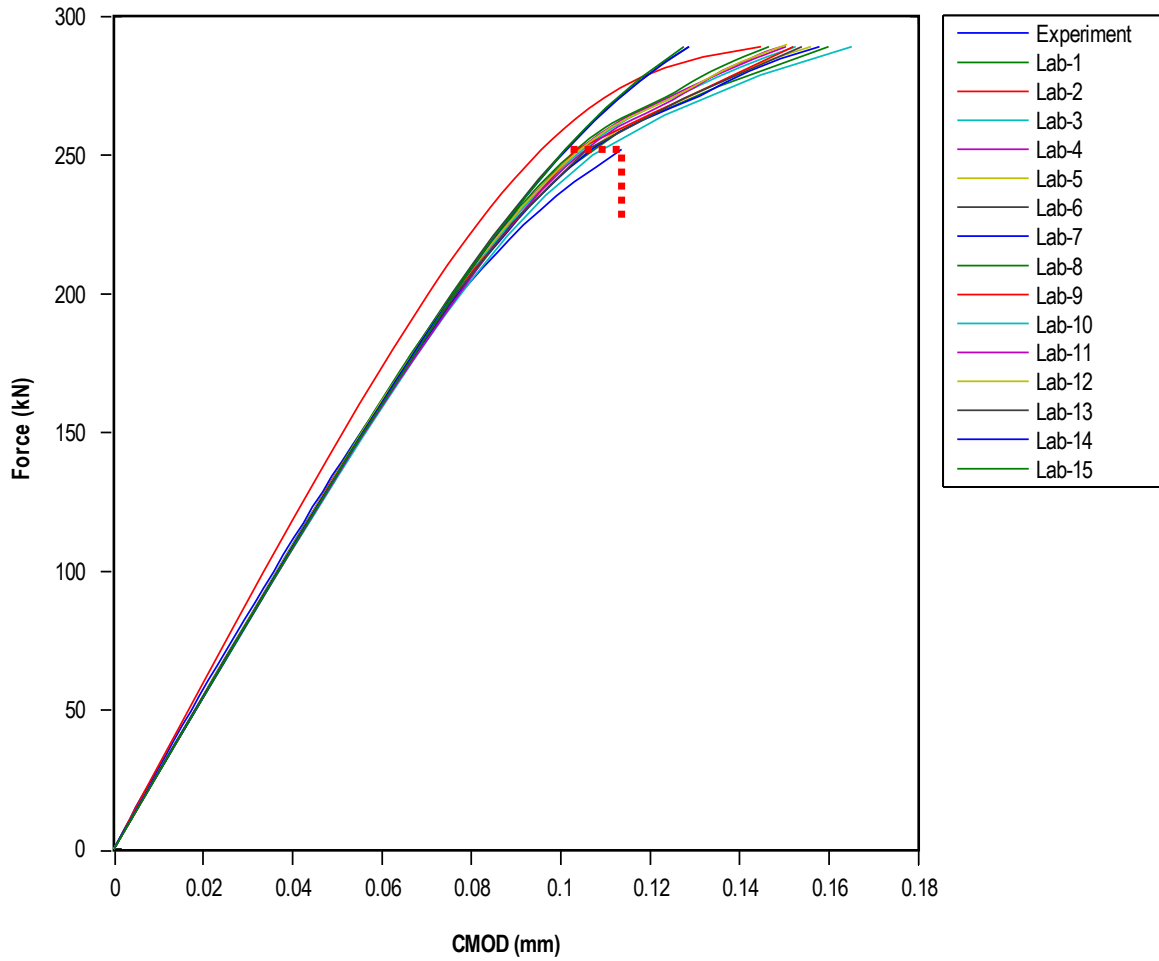


Figure 8a. Overall force versus CMOD with “corner bracket” validity limit.

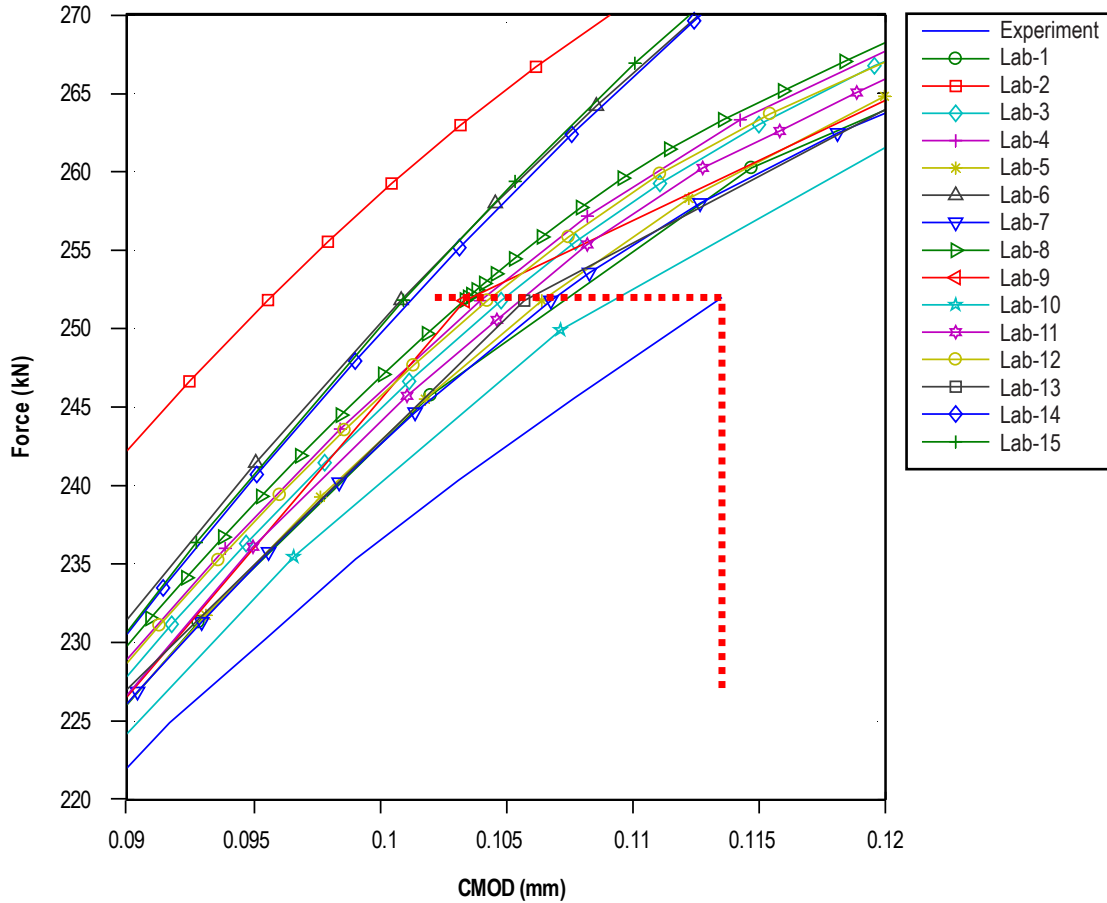


Figure 8b. Force versus CMOD, zoomed to “corner bracket” validity limit.

(1) The finite element methodology discretizes the geometry and enforces an assumed displacement field within each of the elements, creating a model response stiffer than reality.

(2) The nonlinearity in the experimental force-CMOD trace incorporates plasticity as well as geometric changes such as localized tearing; therefore, the test record nonlinearity may have plastic CMOD offset and elastic compliance changes due to crack extension superimposed.

The crack geometry in the analysis does not change—creating a stiffer analytical response. It is important that the test record not have excessive compliance change due to crack extension (tearing) in order for this assessment methodology to apply; i.e., the crack shape after tearing should not be appreciably different from the precrack shape. The proposed test standard sets limits on the amount of crack tearing allowed.

More clearly visible in figure 8b, 11 of 15 analyses satisfy the criteria of matching CMOD within 10% at the maximum test force of 252 kN. The stiffer results of labs -2, -6, -14, and -15 underpredict the CMOD by slightly more than 10%. Note that lesser values of CMOD at a given force correspond to a lower value of the J-integral. Setting limits using the force-CMOD corner

bracket ensures a conservative assessment of the experiment. The maximum J-integral evaluated from the test would result from an exact match of the experimental record—hitting the corner of the bracket. Any deviations from the experimental force CMOD record are truncated by this method and will reduce the resulting J value. Anticipating the use of this methodology, this ILS problem statement requested reporting of J-integral values at specific force levels.

Tests that result in tearing under predominantly linear-elastic conditions are well characterized by either force or CMOD. Tests extending into the elastic-plastic regime behave differently, with the value of J increasing as a strong exponential of the force and varying more directly proportional to increases in crack opening displacements, characterized by the CTOD and, as related mostly by geometry, the CMOD. Therefore, as plastic effects begin to dominate at the crack front, the CMOD becomes a better behaved and more reliable indicator of the crack tip conditions than applied force. Based on these arguments, a CMOD-based criterion for comparing test and analysis records may be a more accurate way to determine J. Figures 9a and 9b illustrate the use of this criterion. The error bar represents a  $\pm 5\%$  allowable error in force prediction at the experimental CMOD. The same subset of results is valid by this evaluation as was valid in the case of the corner bracket method. While potentially more accurate, this approach allows evaluation of the test result

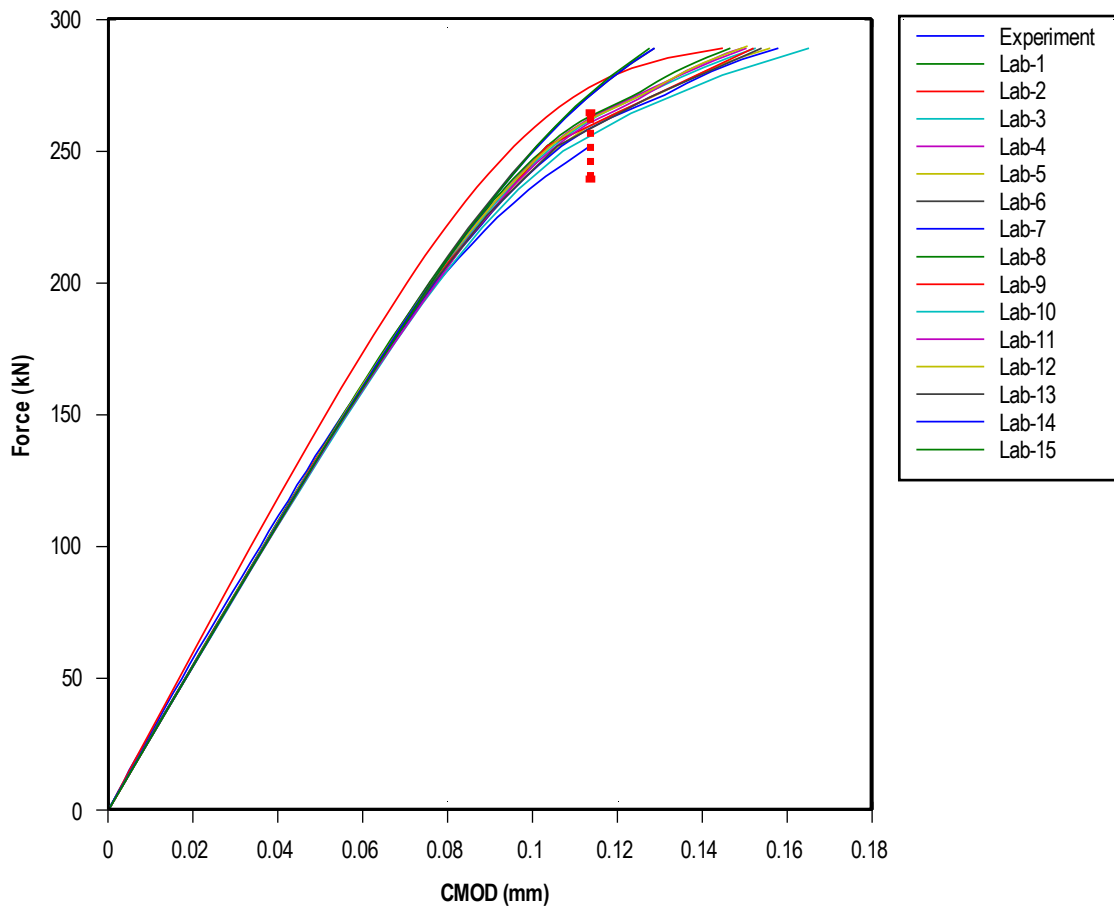


Figure 9a. Overall force versus CMOD with CMOD-based validity limit.

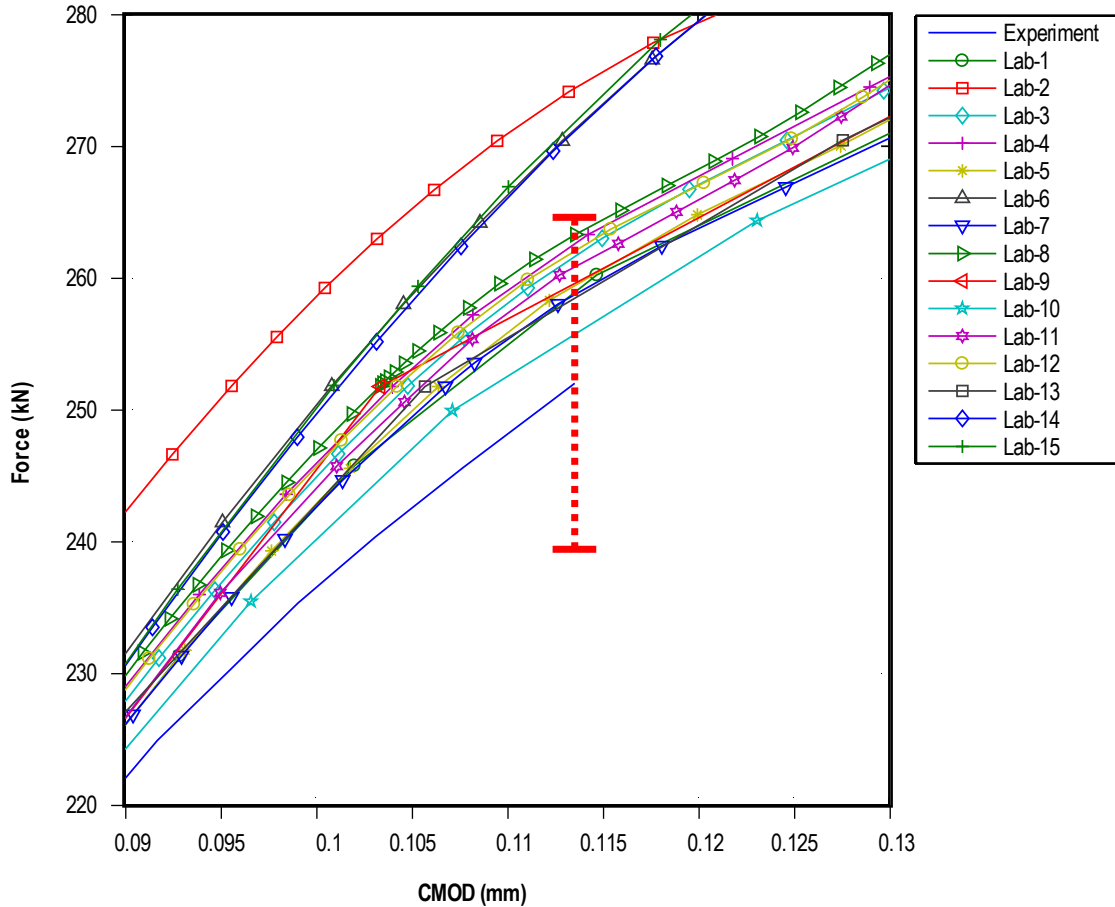


Figure 9b. Force versus CMOD, zoomed to CMOD-based validity limit.

at a force higher than that actually achieved in the experiment. The result is that an exact match to the experimental record represents the mean of allowable evaluations, not the maximum. Since analyses without crack extension are biased towards a stiffer response (higher force for given CMOD), this method will be biased toward producing higher J-integral values. This method is likely to produce more consistent test evaluations when the force-CMOD record is highly nonlinear due to plasticity and has achieved a near zero slope at tearing. However, most tests producing this type of force-CMOD record are not likely within the currently established limits of deformation for the elastic-plastic regime established by the proposed test standard. Further review of the effects of these evaluation methods follow during discussion of J-integral results and the influence of constitutive modeling choices.

#### 4.2 J-Integral Results

The reported J-integral values from each of the ILS labs are presented in figures 10a through 10g. The surface crack is a three-dimensional crack case, which results in a strong variation in J around the crack perimeter. Ideally, the experimental results will indicate where along the perimeter the maximum amount of crack extension occurred. In the case of this ILS problem, the location of maximum tearing occurred at a parametric angle,  $\phi = 17^\circ$ . In analysis of this test, the

ILS labs reported J values at each analytical load step from zero to 289 kN at this  $\phi = 17^\circ$  location. Additionally, the J values were requested at discrete forces (200, 252, and 289 kN) to be reported along the crack perimeter for  $0^\circ \leq \phi \leq 90^\circ$ .\* Figure 10a presents the J-integral versus force results for all labs at  $\phi = 17^\circ$ . The variability across labs is not extensive up to the test force of 252 kN. At higher forces, the variability increases, but not exorbitantly, considering the blind nature of the study. The values of J at  $\phi = 17^\circ$  are tabulated along with their average, range, and standard deviation in table 2 to assist with quantitative comparison.

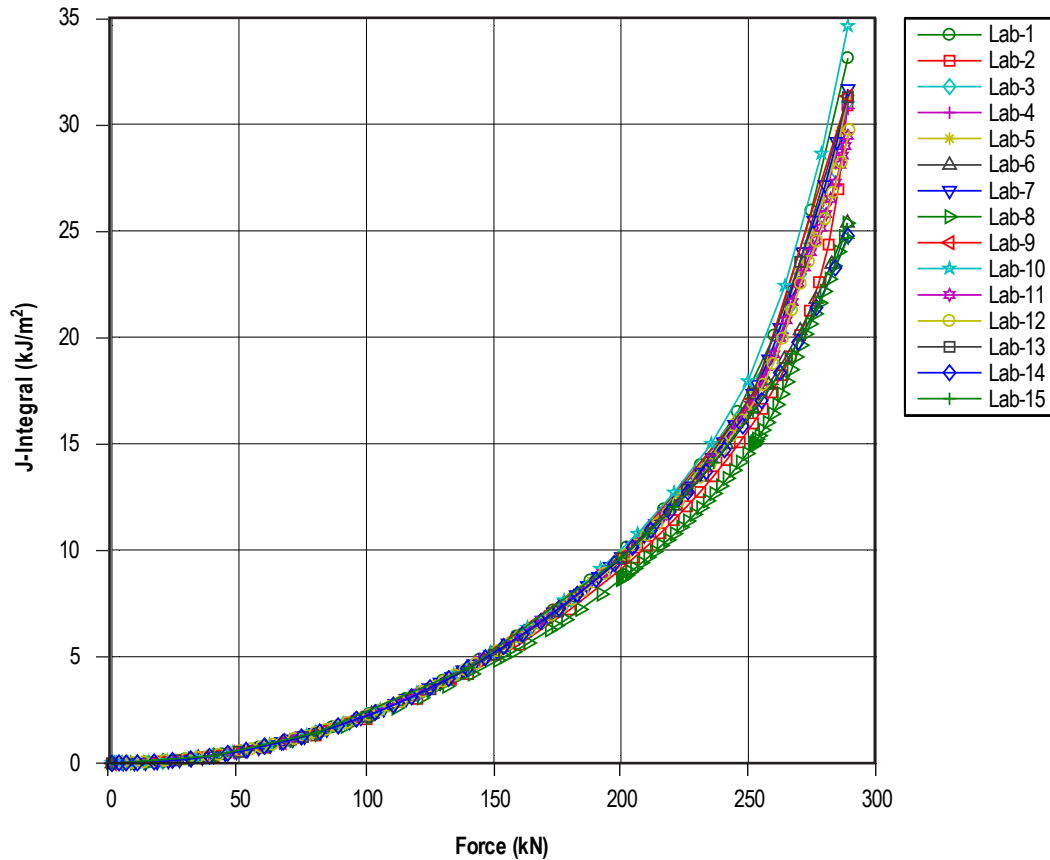


Figure 10a. J-integral at  $\phi = 17^\circ$  versus force.

\* Some participants cautioned against the use of their J results for  $\phi \leq 5^\circ$  due to the strong gradient created by the loss of the crack singularity at the free surface. The proposed surface crack test standard prohibits evaluation of J in this range of  $\phi$ ; therefore, these values are not significant to the study.

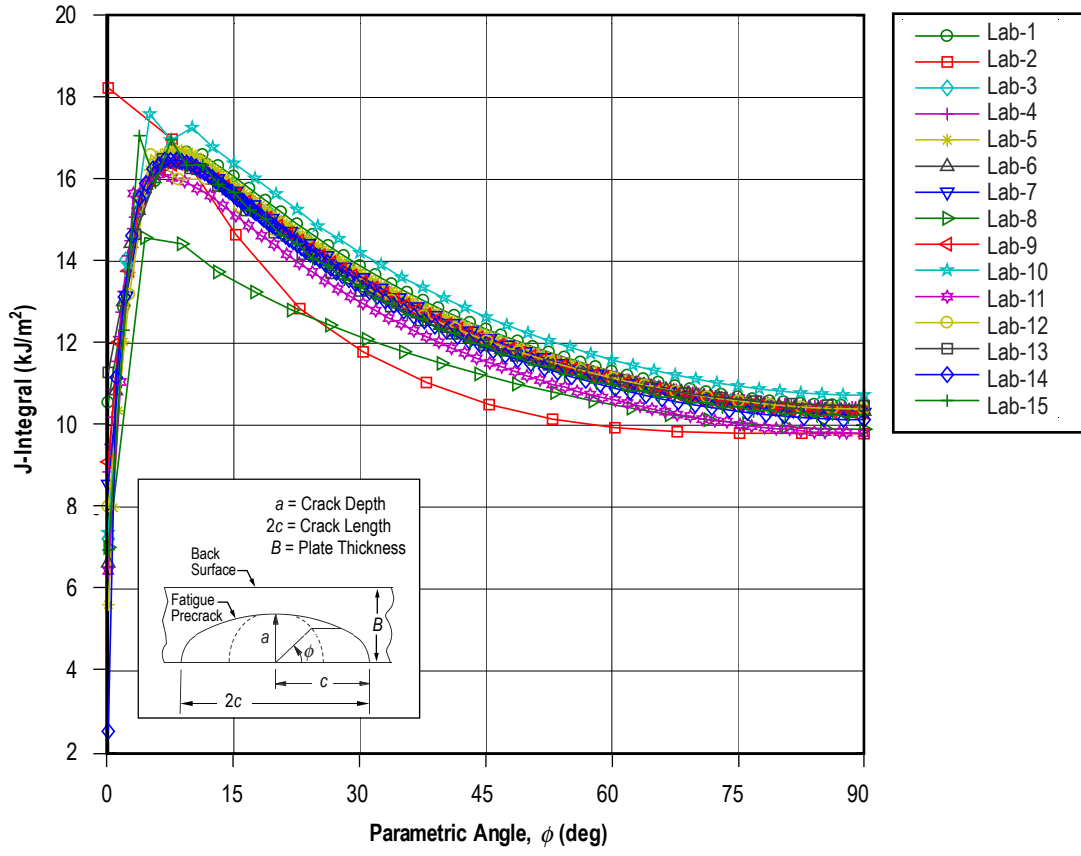


Figure 10b. J-integral versus  $\phi$  at 200 kN.

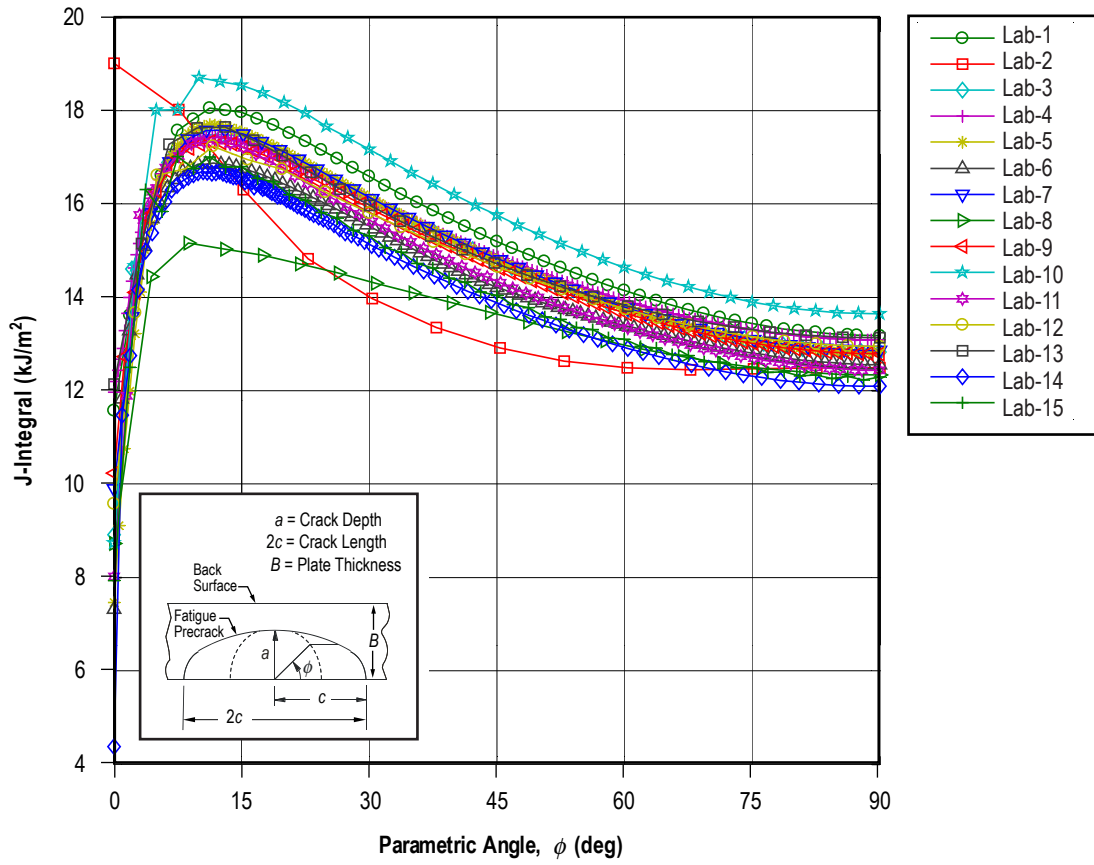


Figure 10c. J-integral versus  $\phi$  at 252 kN.

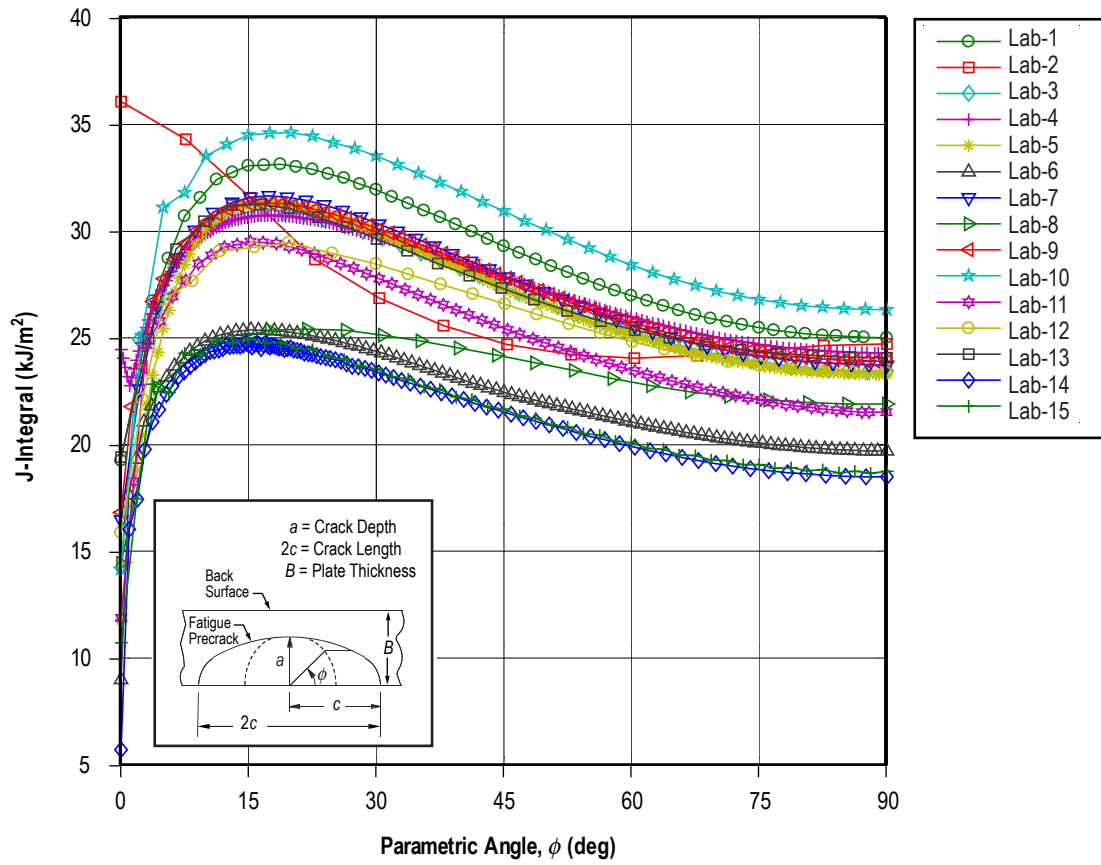


Figure 10d. J-integral versus  $\phi$  at 289 kN.

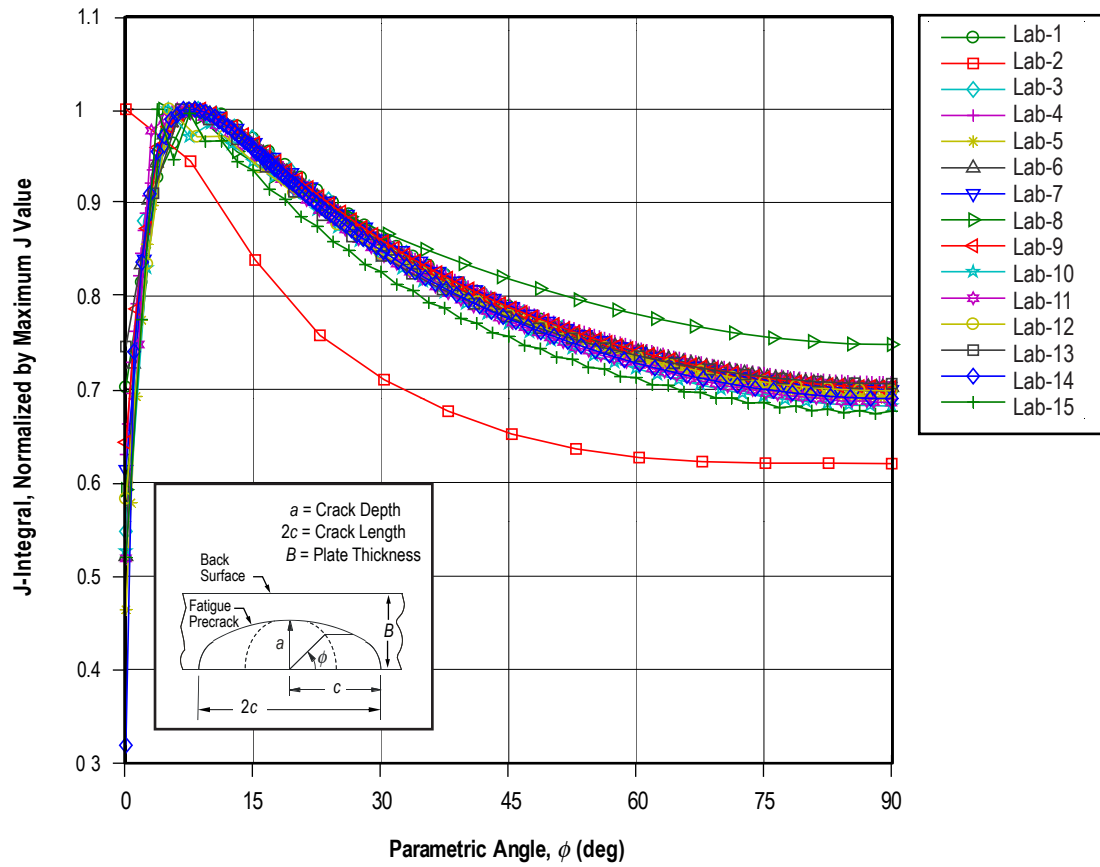


Figure 10e. J-integral versus  $\phi$  at 200 kN normalized by maximum J-integral value.

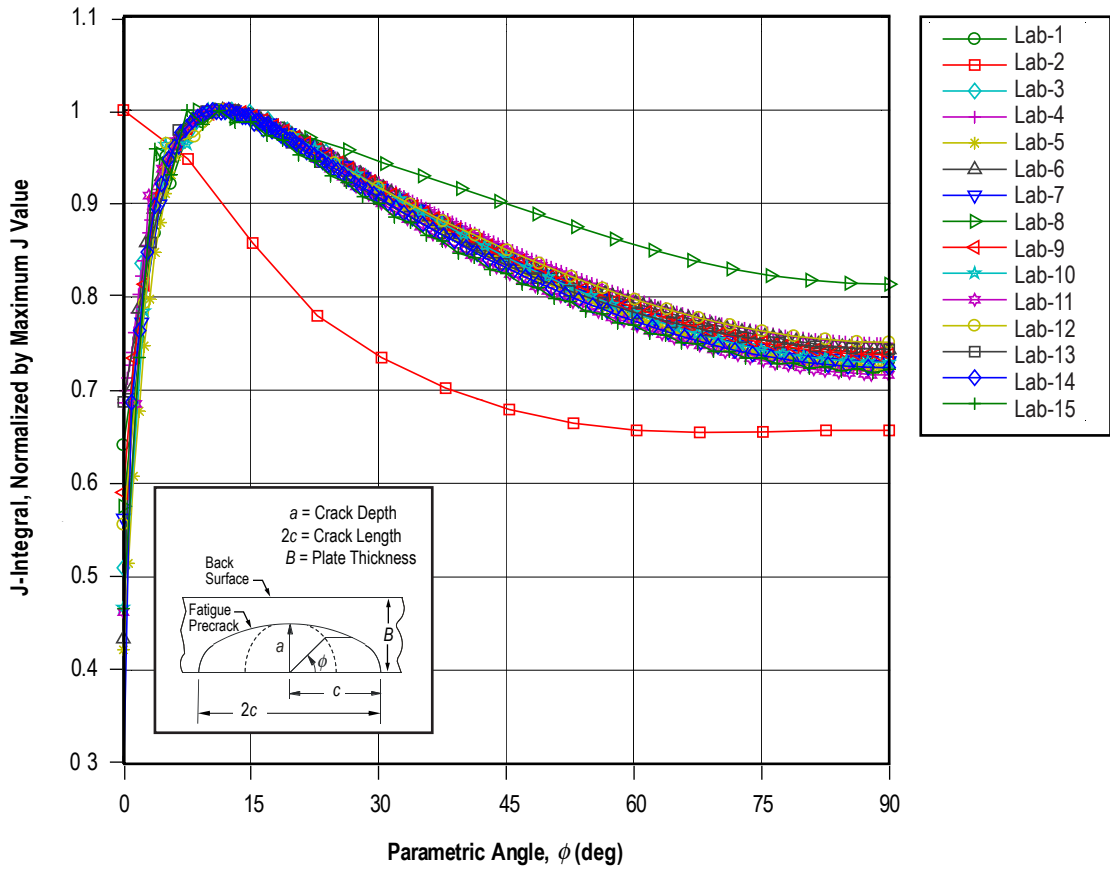


Figure 10f. J-integral versus  $\phi$  at 252 kN normalized by maximum J-integral value.

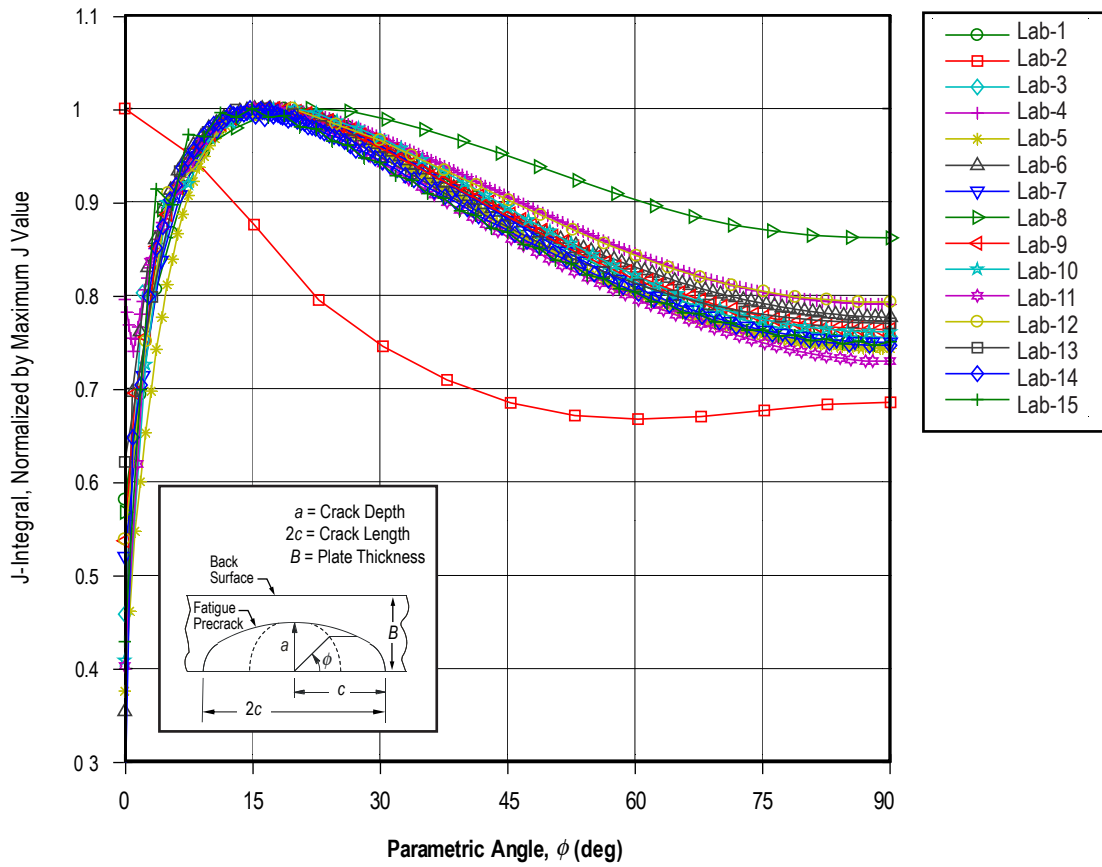


Figure 10g. J-integral versus  $\phi$  at 289 kN normalized by maximum J-integral value.

Table 2. Summary of J-integral results.

J-Integral at $\phi=17^\circ$ (kJ/m <sup>2</sup> )					
Assessment Condition	200 kN	252 kN	CMOD at Crack Tearing	289 kN	CMOD at 0.15 mm
Max	10.05	18.42	20.94	34.59	32.51
Avg	9.58	16.95	19.35	29.66	30.28
Min	8.65	14.92	17.02	24.74	26.20
Std Dev	0.34	0.82	0.83	3.15	1.49

	CMOD (mm)	J at $\phi=17^\circ$ (kJ/m <sup>2</sup> )	
Lab-2	0.0956	15.9	
Lab-6	0.1009	16.7	
Lab-15	0.1009	16.5	
Lab-14	0.1012	16.4	
Lab-8	0.1034	14.9	} Max 18.42 Avg 17.38 Min 16.85 Std Dev 0.44
Lab-9	0.1034	17.1	
Lab-4	0.1040	17.2	
Lab-12	0.1043	16.9	
Lab-3	0.1048	17.3	
Lab-11	0.1055	17.0	
Lab-13	0.1057	17.3	
Lab-5	0.1064	17.4	
Lab-1	0.1066	17.8	
Lab-7	0.1068	17.4	
Lab-10	0.1089	18.4	

For evaluation of the surface crack J at a particular angle  $\phi$ , variation can be considered in terms of the general magnitude of J as well as the distribution of J as a function of  $\phi$  around the perimeter of the crack. Figures 10b–10d show the computed J values around the crack at the three discrete force values, 200, 252, and 289 kN, respectively. The progression of the J versus  $\phi$  distributions with increasing load further illustrates the increasing variability shown in figure 10a. All but two labs (lab-2 and lab-8) have computed a response that appears to vary principally in magnitude of J with a consistent response of J as a function of  $\phi$ . To better evaluate this effect, figures 10e–10g reflect the same data normalized by each lab’s maximum J value. These figures illustrate a magnitude-independent evaluation of the  $\phi$ -dependence of J. The near-surface loss of singularity is consistently predicted in all solutions except lab-2, which utilized a different analytical method. For all other solutions, the predicted  $\phi$  location of maximum J is consistent despite no standardization of crack mesh refinement for this study. The difference visible in the lab-8 solution for  $30^\circ < \phi < 90^\circ$  is of more interest since the analytical method used here is the same as the other consistent solutions (domain integral). The cause of the lab-8 difference is discussed in further detail in section 4.3.4. Overall, these results strongly support the ability of current analytical techniques to reliably compute the  $\phi$ -dependence of J.

Figure 11 illustrates the  $J$  versus CMOD response for each of the labs. The discrete force values are identified along each trajectory. In the linear elastic regime,  $J$  varies quadratically with CMOD. Once the linear elastic regime has been exceeded, the response between  $J$  and CMOD is mostly linear, as follows from the relation of  $J$  proportional to CTOD. When compared to the highly sensitive response between force and  $J$  in the elastic-plastic regime (see fig. 10a), there is an advantage to the use of CMOD as the criterion to anchor analysis to experiment. Figure 12 shows the same data with the experimental CMOD at 252 kN and the trajectory lines removed. Valid solutions at a force of 252 kN with predicted CMOD within 10% of the experiment provide a solution range from 14.9 to 18.4 kJ/m<sup>2</sup>. Symbols plotted along the experimental CMOD line represent  $J$  values interpolated from the provided solutions at this CMOD. In this case, valid solutions within 5% of the 252 kN force (see fig. 9b) provide a range of  $J$  values from 17.3 to 20.1 kJ/m<sup>2</sup>. Use of the CMOD criterion reduces the variability in the solutions relative to the force criterion, but for most analyses, this will correspond to analysis at a force higher than the experiment and therefore higher  $J$  values. As deformation levels increase, the use of the CMOD criteria becomes more effective at containing variability. A set of  $J$  values is estimated at a CMOD of 0.15 mm by interpolating (or extrapolating) each lab's result. Again, the represented variability is reduced by approximately half. Note that including the lab-8 result nearly doubles the variability in the solution to the experiment at 252 kN, 19% with lab-8 versus 8.5% without.

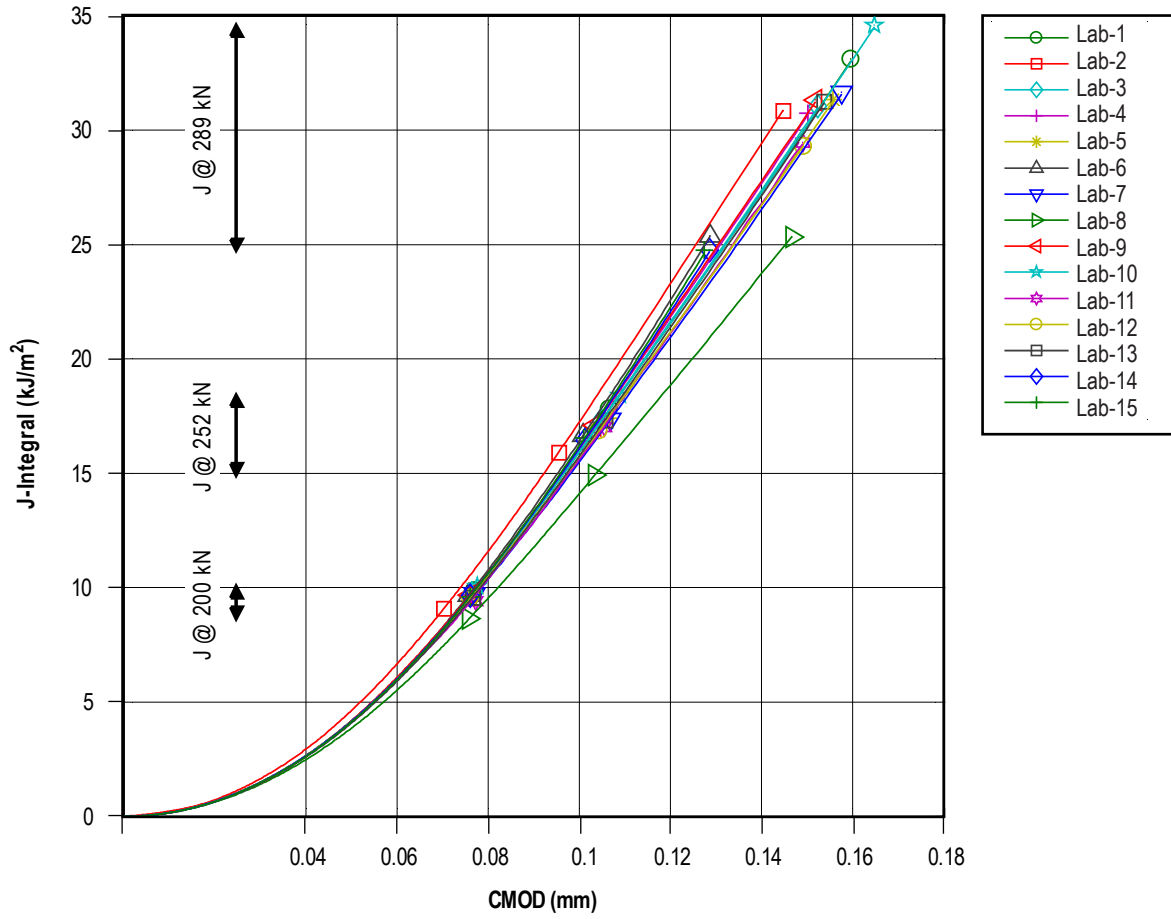


Figure 11. J-integral versus CMOD at  $\phi = 17^\circ$ .

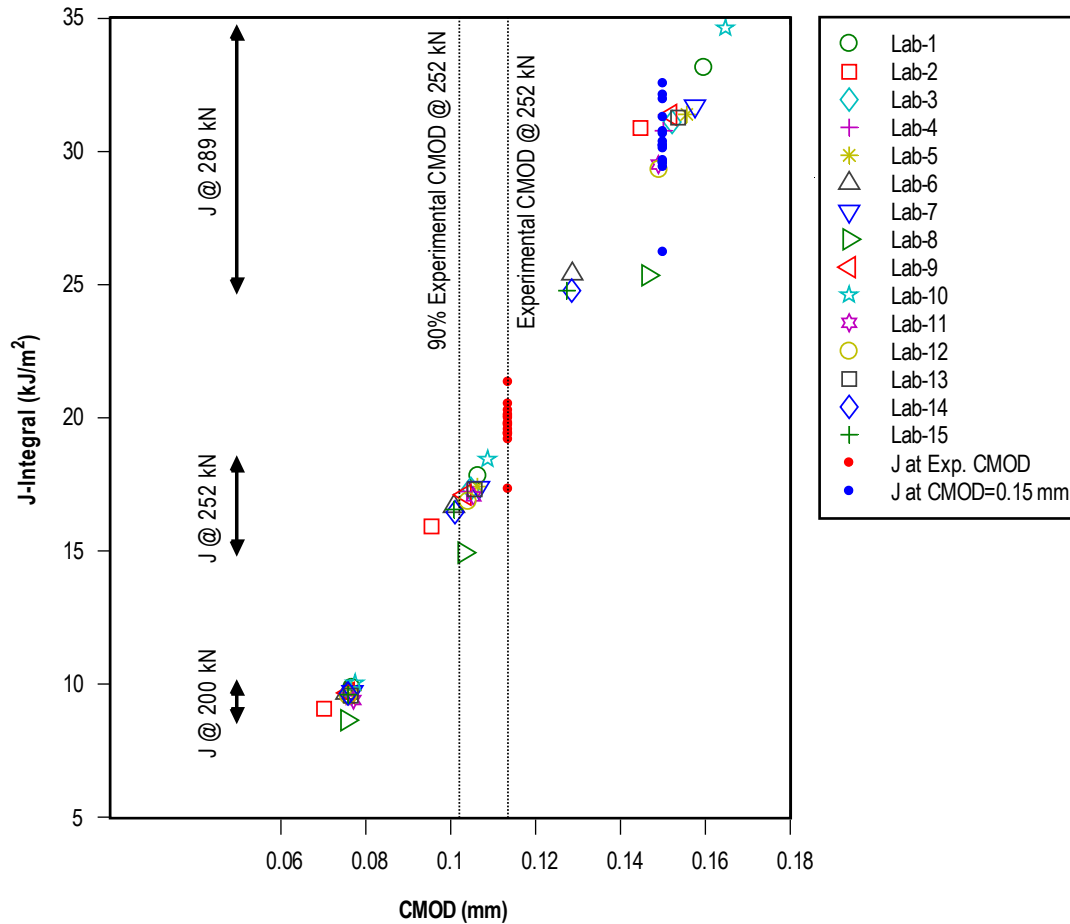


Figure 12. J-integral versus CMOD at  $\phi = 17^\circ$  with CMOD-based evaluation criteria.

### 4.3 Assessing Sources of Variability

To address various potential contributions to variability, the analysis methodology of each lab was collected through the survey previously discussed. Table 3 presents a summary of the reported parameters utilized in each model. The parameters are assessed independently by observing the reported J values at  $\phi = 17^\circ$  as a function of each parameter. This provides a rough guide to likely causes of variation, but cannot be fully conclusive because the parameters are not always fully independent, i.e., other influences which happen to correlate may produce trends in data which are not actually due to the observed parameter. The following section steps through a series of observations from table 3.

Tables 3. Summary of ILS model parameters for all participants.

Lab ID	Analyst Background	Code	Model Size					Formulation		
			No. Elem.	No. Nodes	CF Nodes	CF Density	Model Size	Elem. Type	Integration	Strain
Lab-1	Structures	WARP3D	4,780	22,716	49	-0.37	-1.65	Quad	Reduced	Small
Lab-2	Structures	ADINA	10,416	46,859	24	-0.91	-1.37	Quad	Full	Small
Lab-3	Structures	ABAQUS	12,348	53,459	41	-0.54	-0.78	Quad	Full	Small
Lab-4	Structures	WARP3D	25,195	111,228	181	2.48	4.20	Quad	Reduced	Finite
Lab-5	Structures	WARP3D	9,624	45,222	145	1.70	1.18	Quad	Reduced	Small
Lab-6	Materials	ANSYS	22,742	90,547	101	0.75	1.77	Quad	Reduced	Finite
Lab-7	Structures	WARP3D	14,316	64,281	42	-0.52	-0.39	Quad	Reduced	Small
Lab-8	Structures	ABAQUS	11,032	50,585	41	-0.54	-0.88	Quad	Full	Finite
Lab-9	Structures	ANSYS	20,479	70,249	73	0.15	0.48	Quad	Reduced	Small
Lab-10	Structures	ABAQUS	2,248	16,805	37	-0.63	-2.11	Quad	Reduced	Small
Lab-11	Structures	ABAQUS	13,999	62,699	61	-0.11	-0.04	Quad	Reduced	Small
Lab-12	Structures	ABAQUS	9,055	41,718	25	-0.89	-1.52	Quad	Reduced	Finite
Lab-13	Structures	ABAQUS	100,000	110,000	25	-0.89	0.79	Linear	Full	Small
Lab-14	Structures	ABAQUS	21,648	91,297	97	0.67	1.71	Quad	Full	Small
Lab-15	Structures	ABAQUS	6,584	30,102	49	-0.37	-1.40	Quad	Reduced	Finite

Lab ID	Crack Tip Mesh	Specimen Grip	Boundary Condition	Constitutive Model			Formulation			
				Plasticity	Eng/True	SS-Curve	J Method	No. Dom.	Avg. Method	Dom. Size
Lab-1	C-UT	Simple	Stress	Incr	Eng	Table	Domain	10	Maximum	0.89
Lab-2	C-UT	Simple	Stress	NLE	<b>True</b>	Eq	VCE	-	-	0.00
Lab-3	C-T_1/4	Simple	Stress	Incr	<b>True</b>	Table	Domain	8	Drop 2	2.20
Lab-4	KH	Simple	Stress	Incr	True	Table	Domain	16	Maximum	2.12
Lab-5	C-UT	Simple	Stress	Incr	<b>True</b>	Table	Domain	6	Drop 1	0.74
Lab-6	C-UT	Simple	Disp	Incr	True	Table	Domain	10	Converged	0.63
Lab-7	C-UT	Simple	Stress	Incr	Eng	Table	Domain	5	Drop 1	0.60
Lab-8	C-UT	Simple	F w/C	Incr	True	Table	Domain	10	Maximum	0.50
Lab-9	C-T_1/4	Simple	Stress	Incr	<b>True</b>	Table	Domain	10	Subset	1.08
Lab-10	C-UT	Simple	Stress	Incr	Eng	Table	Domain	5	(5 only) Drop 1	1.01
Lab-11	KH	Simple	Stress	Incr	<b>True</b>	Table	Domain	5	Drop 0	0.47
Lab-12	C-UT	Details	RS	Incr	True	Table	Domain	10	Subset	0.94
Lab-13	C-UT	Details	F w/C	Incr	Eng	Table	Domain	5	(3-6)	2.26
Lab-14	C-T	Simple	Stress	Incr	<b>True</b>	Table	Domain	10	Maximum	0.82
Lab-15	KH	Simple	Disp	Incr	True	Table	Domain	10	Converged Maximum	0.75

Tables 3. Summary of ILS model parameters for all participant (Continued).

CF Nodes = Number of nodal locations along the crack perimeter	Stress = Uniform pressure stress
Quad = Element with quadratic shape functions	Disp = Uniform displacement condition
Linear = Element with linear shape functions	RS = Rigid surface contact for pin(s)
	F w/C = Force with coupling
CF Density = See equation (1)	Incr = Incremental plasticity
Model Size = See equation (1)	NLE = Non-linear elasticity
Full = Quadrature integrates stiffness exactly for undistorted elements	Eng = Engineering stress and strain material properties
Reduced = Quadrature at a lower order than full	True = True stress and strain material properties
	<b>True</b> = True stress and strain properties used small-strain formulation
Small = Nodal geometry is not updated due to strain	Table = Stress strain values supplied as a look-up table for interpolation
Finite = Nodal geometry is updated due to strain	Eq = Stress-strain values determined by an equation
C-UT = Collapsed hex, untied nodes	Domain = Domain integral method used
C-T = Collapsed hex, tied nodes, standard mid-side nodes	VCE = Virtual crack extension (other than domain integral)
C-T_1/4 = Collapsed Hex, tied nodes, 1/4 point mid-side nodes	Maximum = J reported is the maximum of all domain results
KH = Key-hole mesh	Drop X = The first X domain results were not included in the average
Simple = Rectangular flat plate	Converged = Value or average was taken from domains with unchanging value
Details = Some grip detail added using contact, coupling, or other methods	Subset = The domain value was selected from a single or group of domains
	Dom. Size = Radial size of outer domain divided by avg. domain size (1.01 mm)

Though not plotted, it is of interest that the background of all but one reported participant was “structures.” This could have a bearing on the ability of typical mechanical test labs to have the experience and capability to execute the analysis reliably. Most labs participating in the ILS were engineering organizations that include a damage tolerance assessment capability. Many material test organizations may not have adequate depth in structural analysis to reliably execute the assessment of surface crack tests to the new standard. This issue can readily be addressed by these organizations’ use of third party analysis capabilities within the commercial industry.

#### 4.3.1 Codes and Modeling Choices

Four analysis codes were represented in the study: ABAQUS,<sup>7</sup> WARP3D,<sup>8</sup> ANSYS,<sup>9</sup> and ADINA.<sup>10</sup> Figure 13 reports the J results at three force levels by lab for each of the codes. As expected, there are no visible trends based on analysis code; therefore, no restrictions on analysis code are likely in the test standard.

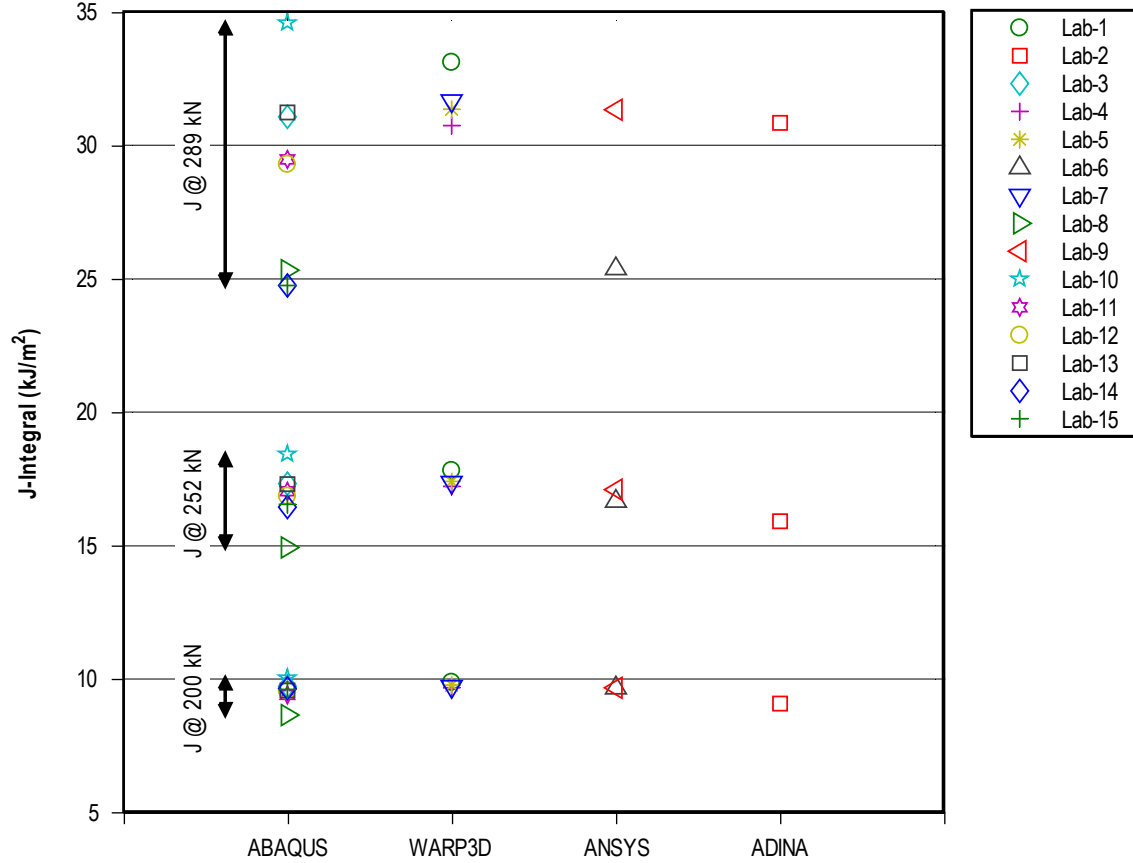


Figure 13. J-integral at  $\phi = 17^\circ$  versus analysis code.

A common concern for converged finite element analysis (FEA) is mesh refinement. To address this issue in a simple, yet quantitative manner, the authors requested the number of nodes and elements in the model as well as the number of nodal locations along the crack front perimeter. This cannot fully define the quality of a mesh in that it does not address the efficient use of elements or the quality of the element geometry, but it does allow a very basic assessment to see if the results are strongly model size dependent. Figure 14 shows a typical  $\frac{1}{4}$  symmetric surface crack finite element mesh and the associated mesh refinement near the crack tip and in the far field. To develop a parameter to represent model size, the number of nodes in each model was normalized to a standard normal space by subtracting the mean ( $\mu$ ) number of nodes and dividing by the standard deviation ( $\sigma$ ) of the number of nodes. To balance this parameter somewhat with a parameter representing the degree of refinement at the crack tip, the number of crack front nodes was similarly normalized and the two values summed. The model size parameter (MSP) is shown in equation form below:

$$\text{MSP} = \frac{(N_{\text{model}} - \mu_{\text{model}})}{\sigma_{\text{model}}} + \frac{(N_{\text{crack front}} - \mu_{\text{crack front}})}{\sigma_{\text{crack front}}}. \quad (1)$$

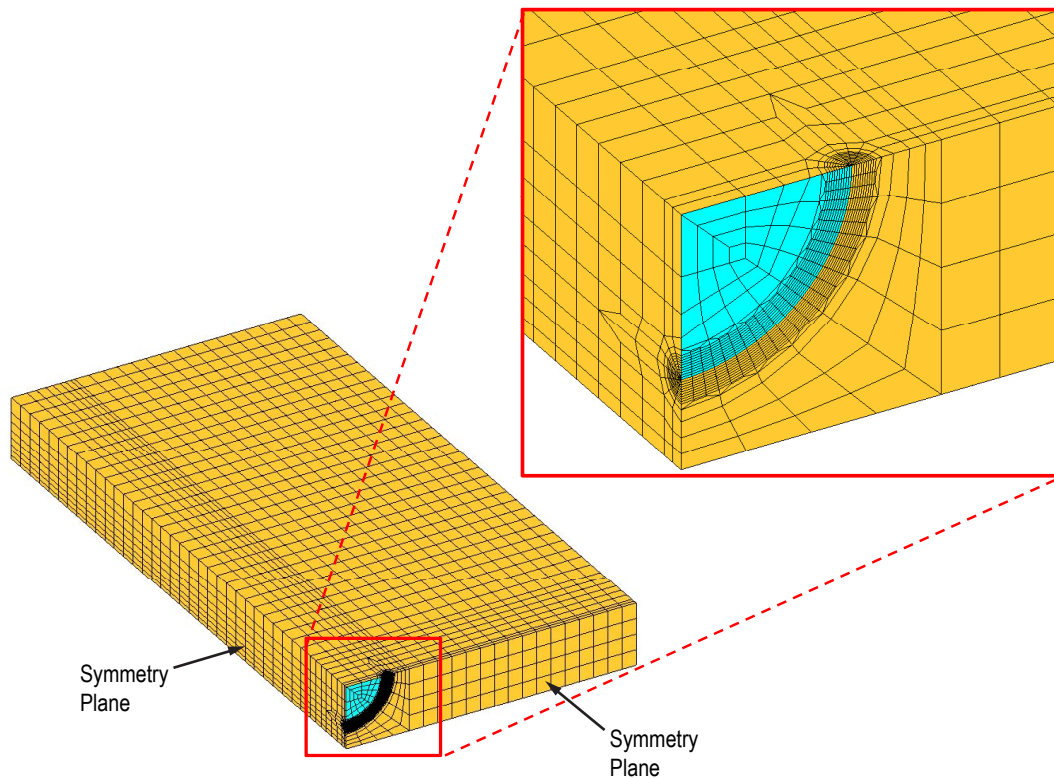


Figure 14. Typical  $\frac{1}{4}$  symmetric surface crack finite element mesh.

For the average model, the MSP will be zero. Negative values represent models smaller than average and positive values represent larger models. Lab-11 represents an “average size” model using this parameter. Figure 15 illustrates the influence of model size on the predicted J values. There are no distinct trends with model size. All models in the study were sufficiently refined to produce reliable J values. Based on the efficiency of computing resources and the robustness of the domain integral method for calculating J, this result is not unexpected.

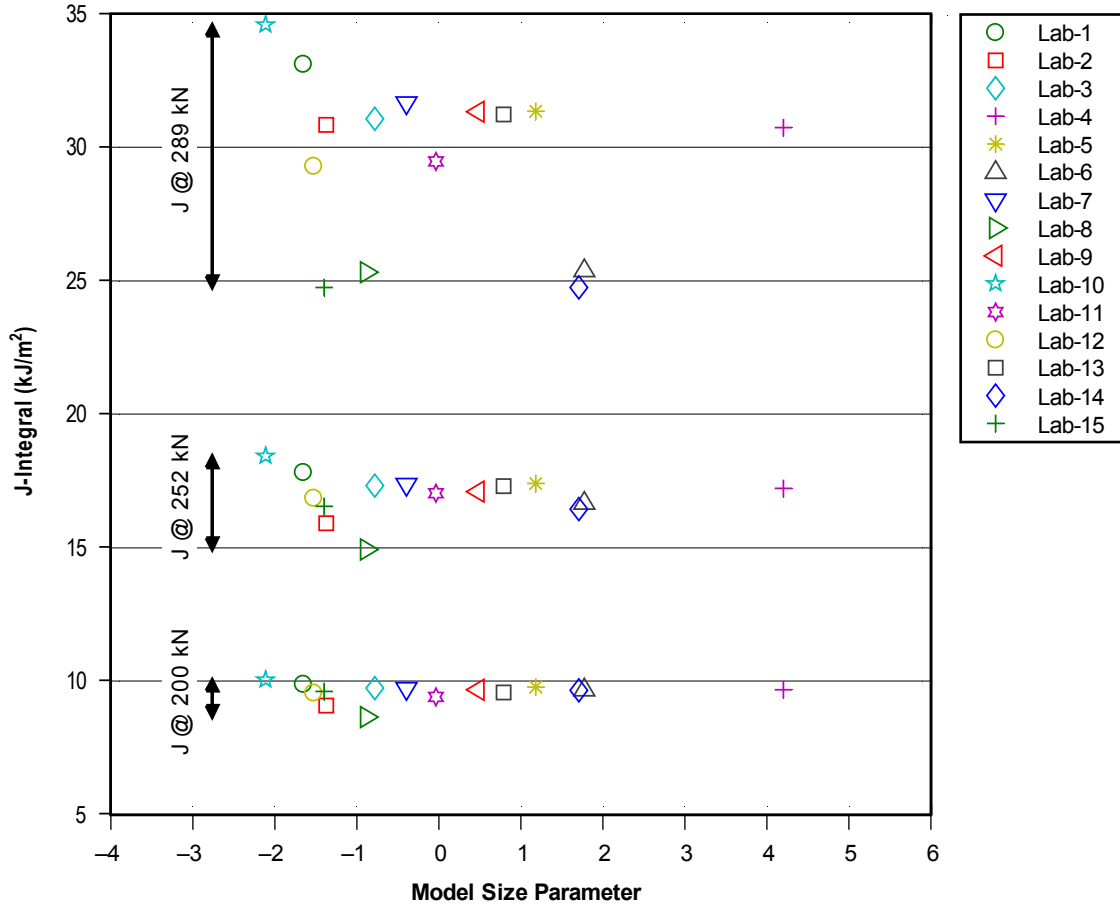


Figure 15. J-integral at  $\phi=17^\circ$  versus model size parameter from equation (1).

The MSP is a rough gauge of the refinement of the continuum discretization in the finite element models. The ability of the model to reproduce the displacements in the experiment is a function of this elemental discretization and the assumed shape of the displacement field within these elements. The need to discretize and assume displacement field shapes makes the typical finite element model stiffer than reality. Because the objective of this analysis is to reproduce the force and displacement results of the experiment as faithfully as possible, it is desirable to minimize the overprediction of stiffness. A common means to this end is to utilize an element formulation with “reduced integration.” Generally, reduced integration is defined as choosing a quadrature for element integration that is one order lower than the function used to estimate the displacement field. In this process, the higher order terms are removed from the integration of the element stiffness matrix and the element stiffness is slightly reduced. This has the desirable effect of offsetting, to some degree, the increased stiffness associated with the discretization process. A further benefit of reduced element integration vis-à-vis model stiffness is the elimination of “plasticity locking,” a manifestation of artificial stiffening in distorted, fully integrated, quadratic isoparametric elements due to their inability to properly represent the incompressibility assumption of the underlying plasticity theory.<sup>11</sup> The use of reduced integration comes at the potential cost of enabling zero-energy deformation modes into the solution. This is most likely to occur around the crack tip

and must be guarded against. The effect of using full versus reduced integration elements in the ILS problem is illustrated in figures 16a and 16b. In figure 16a, a weak trend is visible toward a less stiff elastic response with reduced integration elements. Note that this response may also be a function of mesh refinement. The trends in the J solutions with element integration are even weaker, as shown in figure 16b. Based on these observations, it is not likely that element integration order will have a substantial influence on J values for models with sufficient element density. If zero-energy deformation modes are avoided, the use of reduced integration is helpful at tempering the overly stiff response of the finite element solution and may assist in developing an acceptable match to the experimental force versus CMOD response.

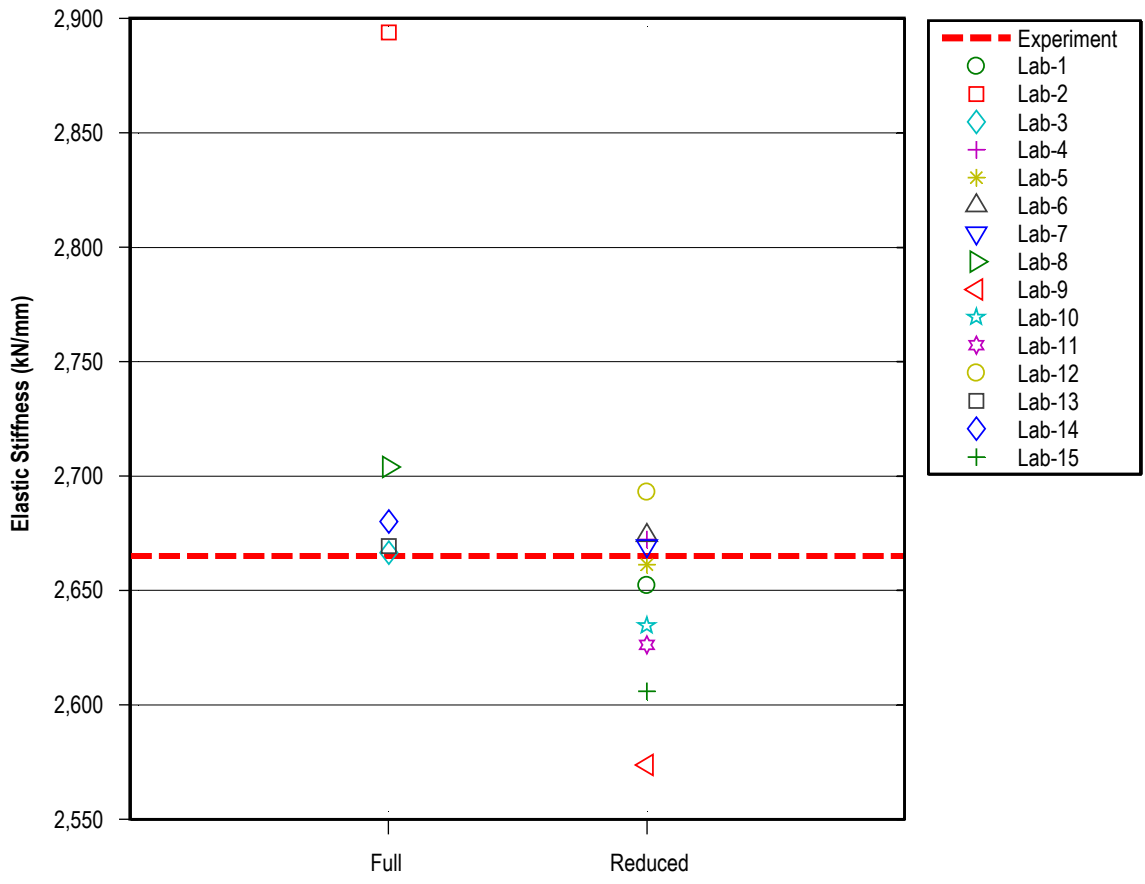


Figure 16a. Variation in elastic CMOD stiffness versus element integration order.

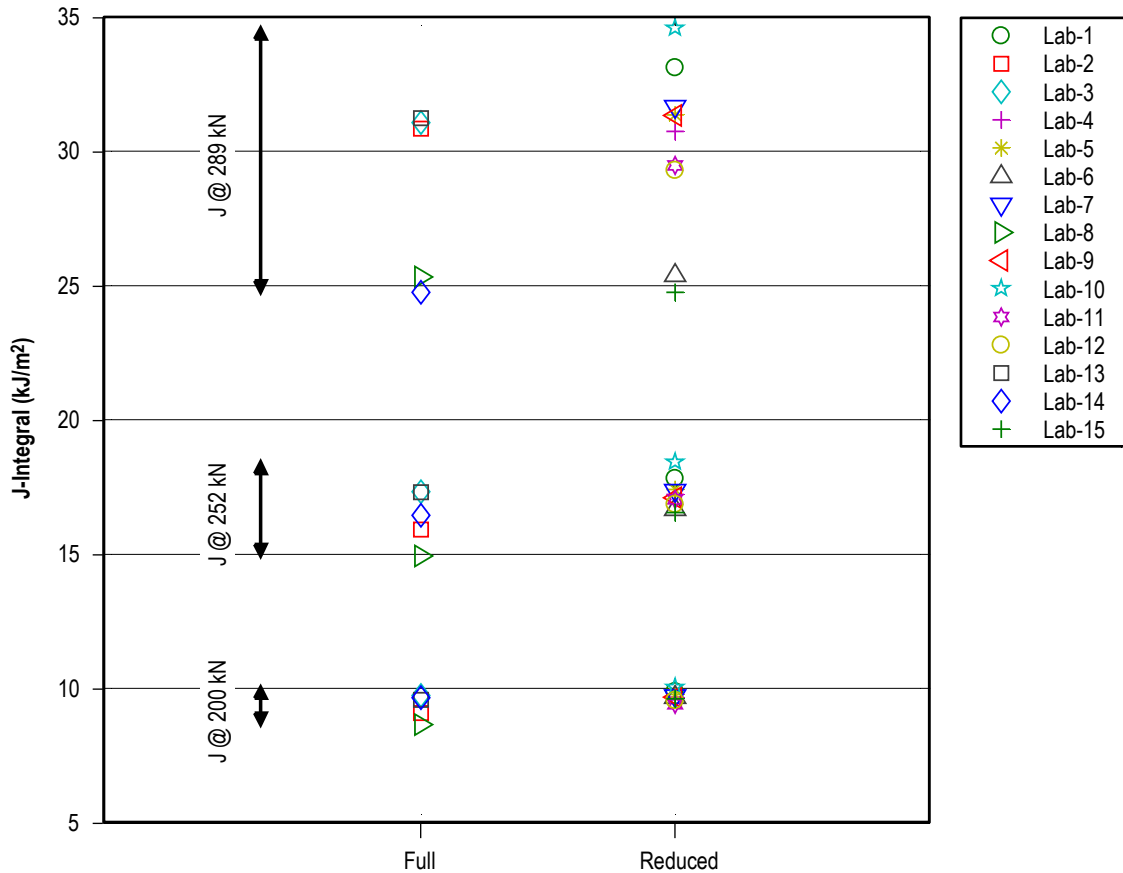


Figure 16b. J-integral at  $\phi = 17^\circ$  versus element integration order.

Another aspect of fracture mechanics modeling open to wide interpretation is the choice of meshing technique at the tip of the crack. A wide variety of practices exist that were developed with specific methodologies in mind, such as reproducing a linear-elastic singularity, or providing accurate crack face opening profiles for the displacement method of determining  $K$ , or perhaps getting the CTOD accurately modeled. In the ILS submittals, there were three different techniques of crack tip modeling represented:

- (1) Collapsed brick elements with tied nodes at the crack tip and mid-side nodes relocated to the quarter point.
- (2) Collapsed brick elements with duplicate, untied nodes at the tip.
- (3) A key-hole mesh pattern.

Figure 17 illustrates the three crack tips along with their deformed shapes. Figure 18 shows the resulting J values sorted relative to the crack tip meshing practice with no discernable influence on the results. None of the ILS submittals utilized a J evaluation scheme that is sensitive to the resolution of the near-crack tip fields. All were based on the virtual crack extension method, with

14 out of 15 labs using the domain integral approach for the implementation. These results illustrate precisely why the domain integral approach has become the *de facto* standard for such calculations. The fact that the most accurate  $J$  evaluations actually come from domains remote from the crack tip without need to accurately resolve these stress and strain fields is powerful. Other fracture mechanics assessments, such as resolving the CTOD or evaluating the constraint condition in the crack tip fields, require more care be taken in the meshing of the crack tip elements. For purposes of  $J$ -integral analysis in the elastic-plastic regime, the use of collapsed brick elements with duplicate nodes which can allow the crack tip to open under load is the recommended method for assessments related to the surface crack standard. (The method using tied crack tip nodes with quarter point mid-side nodes was developed to best represent the linear elastic fracture mechanics singularity and the solution for  $K$  and is not recommended for elastic-plastic analysis. The key-hole and initial radius methods are useful for properly resolving crack tip stress and strain fields under very high deformations. This is not required for an accurate evaluation of the  $J$ -integral if the domain integral method is used.)

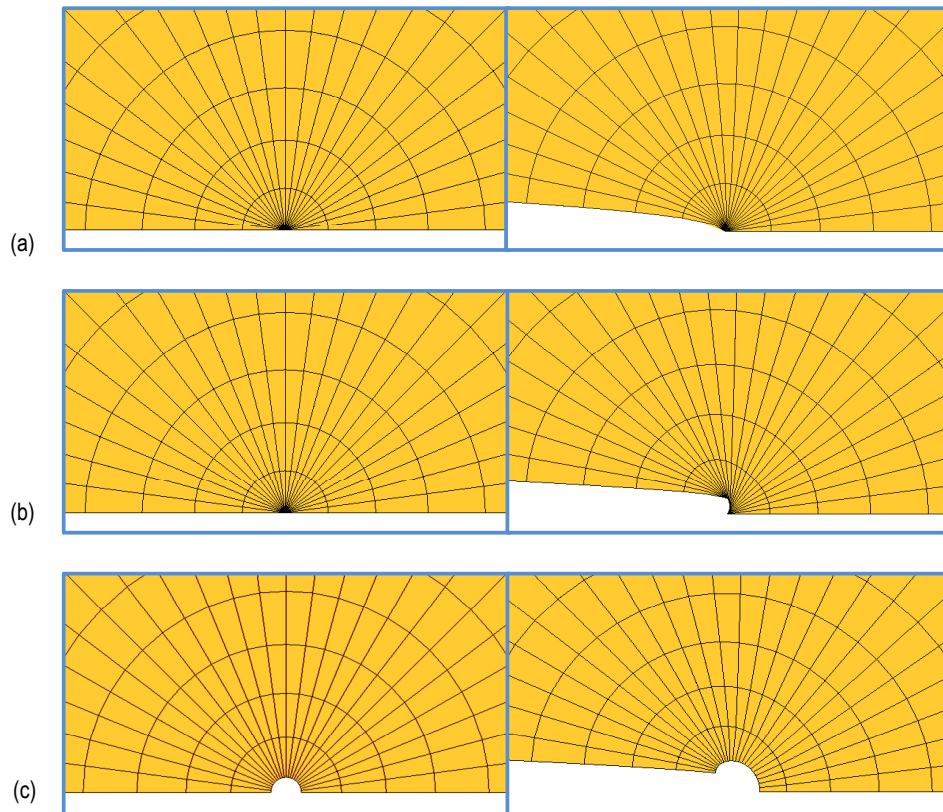


Figure 17. Crack tip mesh with undeformed geometry on left and deformed on right for (a) collapsed elements with tied nodes, (b) collapsed elements with untied nodes, and (c) keyhole pattern.

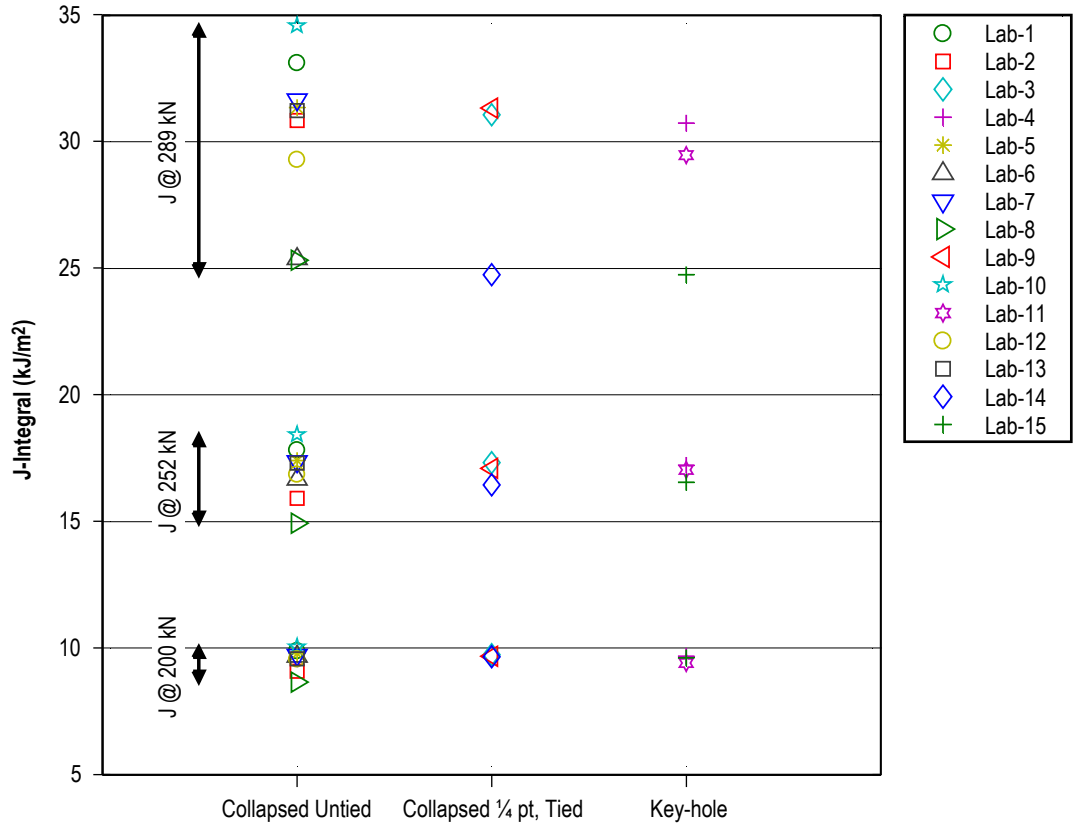


Figure 18. J-Integral at  $\phi = 17^\circ$  versus crack tip mesh geometry.

### 4.3.2 The Domain Integral

When using the domain integral method, the development of a crack tip mesh also involves establishing the orderly element patterns that make up the volume domains. Most finite element codes that support the domain integral calculation also have tools to assist in the generation of domains. Each domain is defined by a volumetric region encompassing the crack tip from one crack face to the other (or to a symmetry plane). Generally, there are multiple concentric domains which ideally render the same value based on the path-independent nature of the J-integral. When modeling elastic-plastic conditions, maintaining a true path-independent behavior requires the use of a constitutive model that does not violate the fundamental assumptions of the conservation integral—a conservative strain energy field. This is done using a hyperelastic (nonlinear elastic) constitutive model, referred to as deformation plasticity in much of the fracture mechanics literature.<sup>12</sup> These constitutive models are not universally available and are often limited in the manner in which they represent material flow behavior, such as allowing only power law representations of the stress-strain curve. The use of incremental plasticity is much more common, versatile, and representative of metallic plasticity; however, the nature of irreversible deformation and the local unloading and stress rearrangement that occurs violates the conservation integral assumptions and creates path dependence in the domain integral calculation. This can largely be avoided if

the domains are sufficiently remote to pass through material that remains predominantly elastic. Unfortunately, the most common method of domain generation starts directly at the crack tip; and, for most elastic-plastic analysis, this ensures that some of the near-tip domains will be substantially within the crack tip plastic zone. In incremental plasticity, the proper J value is that measured in the far-field, away from the influences of plasticity. J-integral values calculated within domains influenced by plasticity will be lower than the far-field J value. Determining the proper J value from a domain integral analysis requires evaluation of the path dependency of the domain results. The physical size of the domains relative to the state of deformation in the model (size of the plastic zone) will influence in the degree of path independence achieved. Figure 19 notionally illustrates a typical loss of path dependence as plasticity effects overwhelm the domains. The highest value in the most remote domain will be the best evaluation of the J-integral.<sup>13</sup>

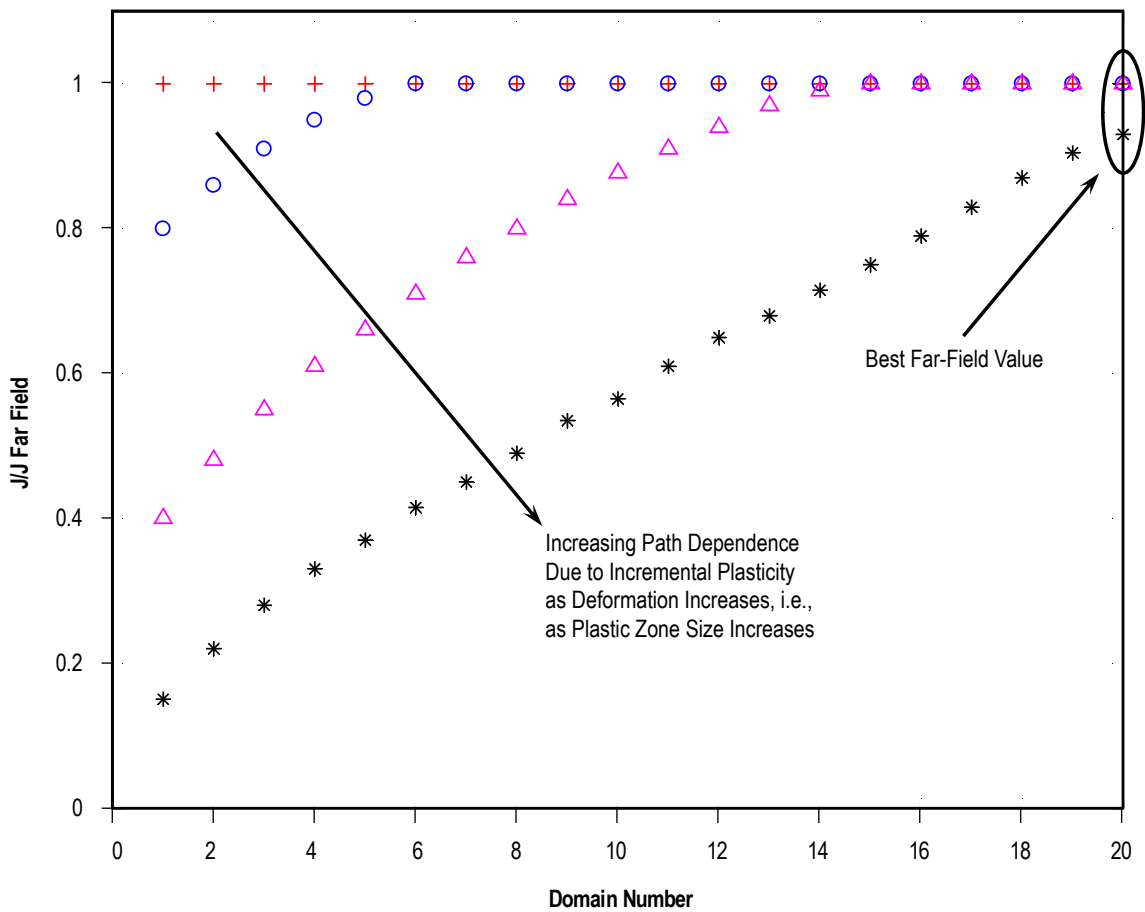


Figure 19. Illustration of typical J-integral results showing degrees of path dependency.

To determine if the size and treatment of the domain results is a source of variability for the ILS problem, the authors requested each lab using the domain integral to report the physical size (radius) of the outermost domain, as illustrated in figure 20, as well as a description of how path dependence was evaluated, i.e., how an answer was chosen from the multiple domain results. Figure 21 shows resulting J values versus the domain size normalized by the average domain size, which was 1.01 mm. For the ILS problem, the J results do not correlate with domain size, indicating that the domains used were sufficiently large to accommodate the deformation without large error, or that path dependence in domain results was properly handled. The method of handling the domain path dependence was grouped into three categories based on the survey results: (1) all but the first domain was averaged, (2) some smaller subset of the domain values was averaged, or (3) only the fully converged or maximum value was reported. Figure 22 illustrates the effect of these choices on the J-integral results. If these effects were significant in the models, a trend toward higher J values for the converged or maximum domain result would be likely when compared to results involving averaging over many domains. In fact, the family of lower J values at 289 kN each reported using converged/maximum domain value. This indicates other factors are present to cause these variations.



Figure 20. Illustration of dimension used to characterize domain size.

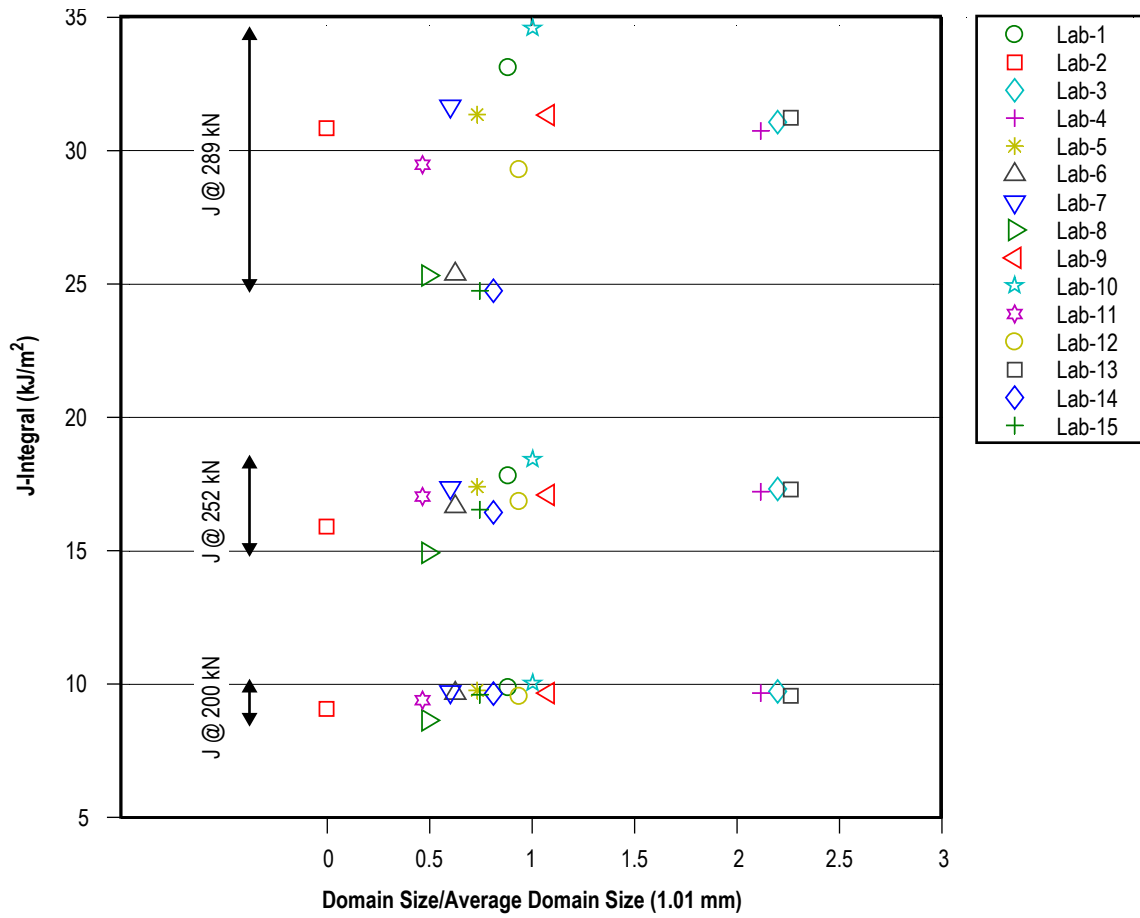


Figure 21. J-integral at  $\phi = 17^\circ$  versus normalized domain size.

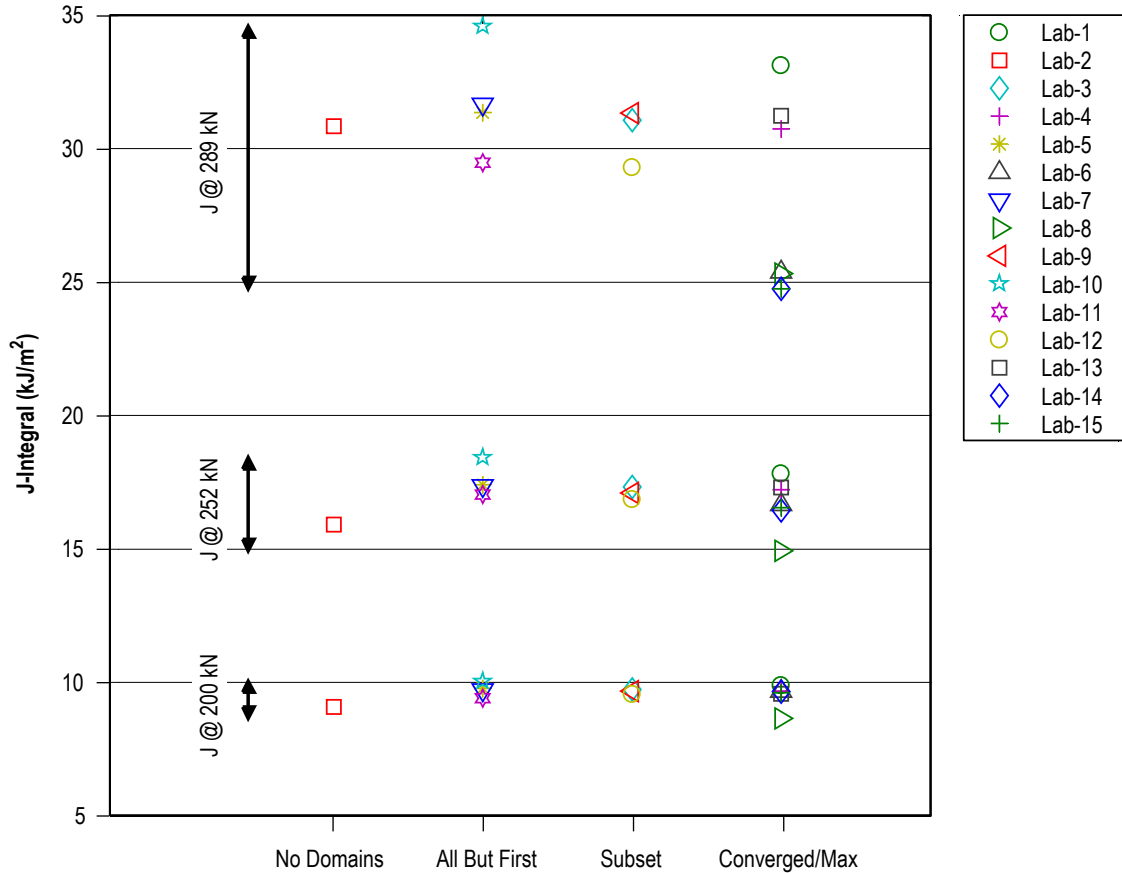


Figure 22. J-integral at  $\phi=17^\circ$  versus method used to evaluate J from multiple domains.

### 4.3.3 Boundary Conditions

Three basic types of model boundary conditions were reported by ILS participants: remote uniform pressure stress, remote uniform displacement, and a few with various forms of contact or the use of the ABAQUS force with coupling approach (\*COUPLE). Figure 23 reports the J results versus these three forms of boundary conditions, again without any significant trends. The surface crack test standard limits the specimen geometry, controlling the height ( $L$ ) and surface length of the crack ( $2c$ ) relative to the specimen width ( $W$ ) so that  $2c \leq W/5$  and  $L \geq 2W$  (see fig. 1). These limitations are in place to help minimize (but not eliminate) the influence of boundary conditions in both experiment and analysis. The family of solutions with lower J values actually spans all three types of boundary conditions. For a direct comparison, the lab-1 model was run with displacement boundary conditions to compare against the original solution using stress boundary conditions. The maximum difference in J was 2% between the two boundary conditions, indicating the variation in boundary conditions is not a significant source of the variation in the ILS problem.

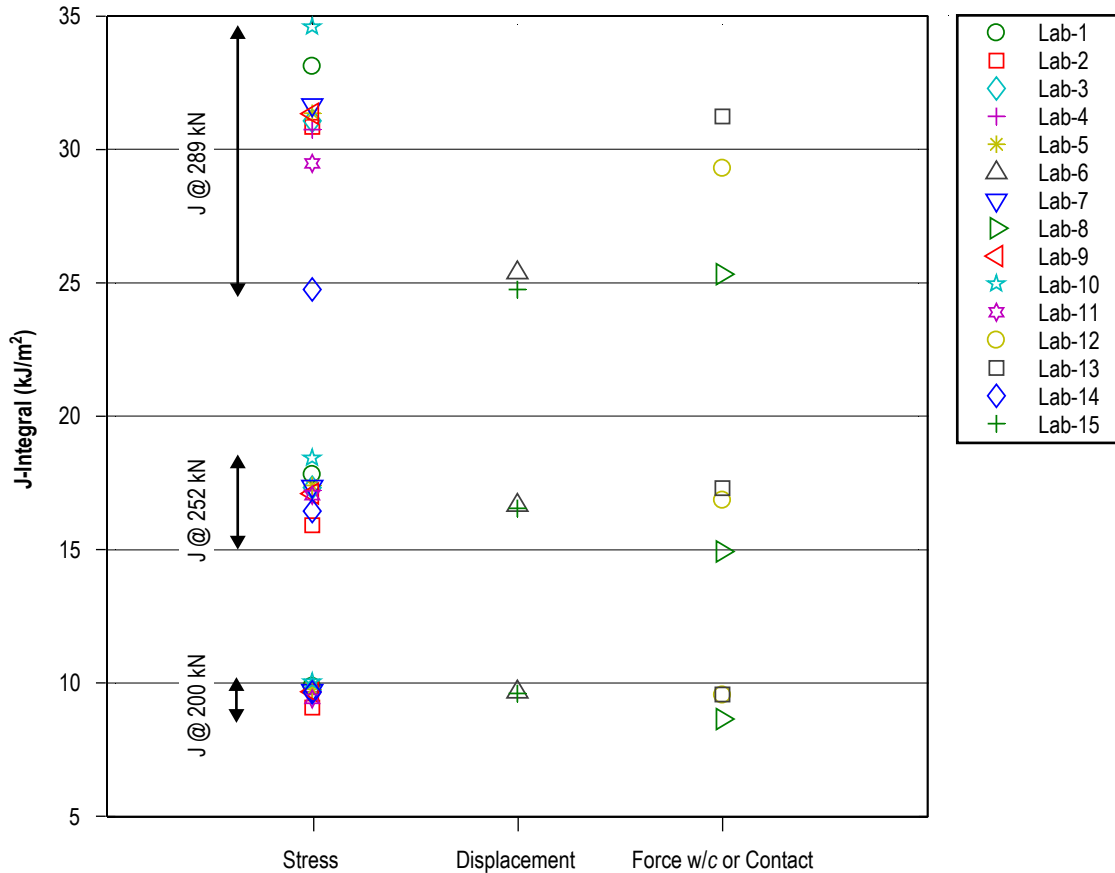


Figure 23. J-integral at  $\phi = 17^\circ$  versus model boundary condition.

#### 4.3.4 Variability Due to Element Skewing

Lab-8 kindly collaborated to uncover the source of variability in that solution. As discussed below, it is the only solution with significant differences not well explained by the constitutive input. In this case, a review of figures 6–9 illustrate that the predicted deflections from the model are reasonable, producing a force versus CMOD response that matches the experiment well and agrees with many other solutions. The series of graphs in figure 10 illustrates a slightly lower J-integral solution and a somewhat different  $\phi$ -dependence in the solution. Figure 11 is the strongest clue that there may be issues with the J-integral solution. If the CMOD has been well predicted, the J-integral solution should follow the clear trend from the other analyses. This solution tends to stand alone.

The most unique aspect of the lab-8 submittal is that the model geometry was created from a previously existing surface crack mesh and warped to meet the geometry of the ILS problem. Scaling fracture mechanics finite element meshes to meet new needs has long been a common practice; however, this is most successful for subtle changes in two-dimensional crack geometries. The curved front of the surface crack makes any but the smallest of mesh distortions problematic. In this case, the result was skewed elements along the crack front at a strong angle to the local crack front normal. Figures 24a and 24b illustrate an example of the skewed crack front element shape, though the mesh in these figures is not from the ILS problem. Despite previous statements regarding the robustness of the domain integral method with respect to mesh quality, this aspect of mesh integrity is important. The lab-8 solution has a strong oscillation in the J-integral solution from corner to mid-side nodes, shown in figure 25. These oscillations are frequently observed when the domain definition includes elements with such distortion. It is important to maintain elements along the crack front as perpendicular to the crack front as possible.

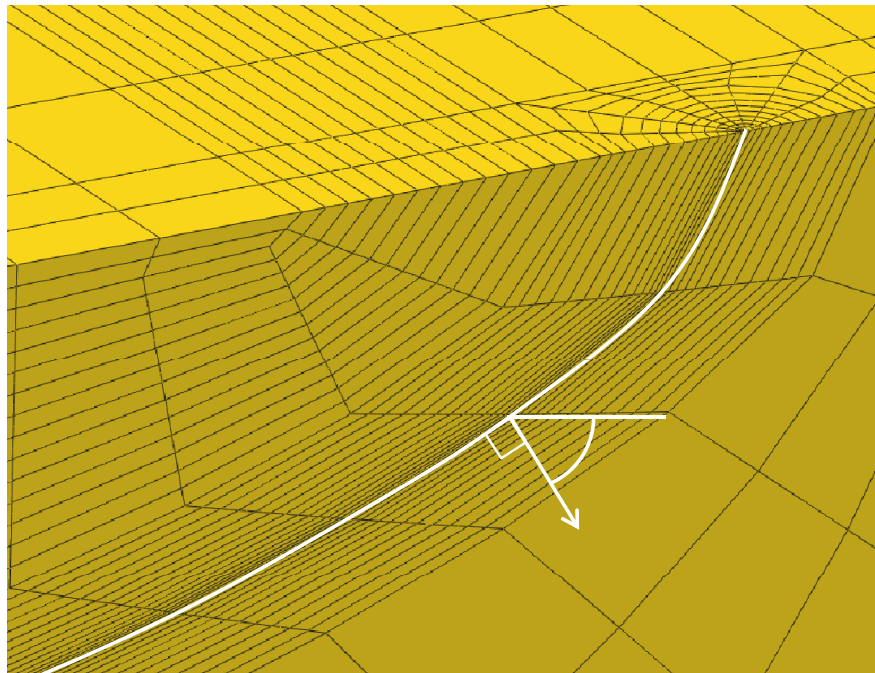


Figure 24a. Curved crack front with skewed elements relative to the crack front normal, a common source of oscillating J-integral solutions.

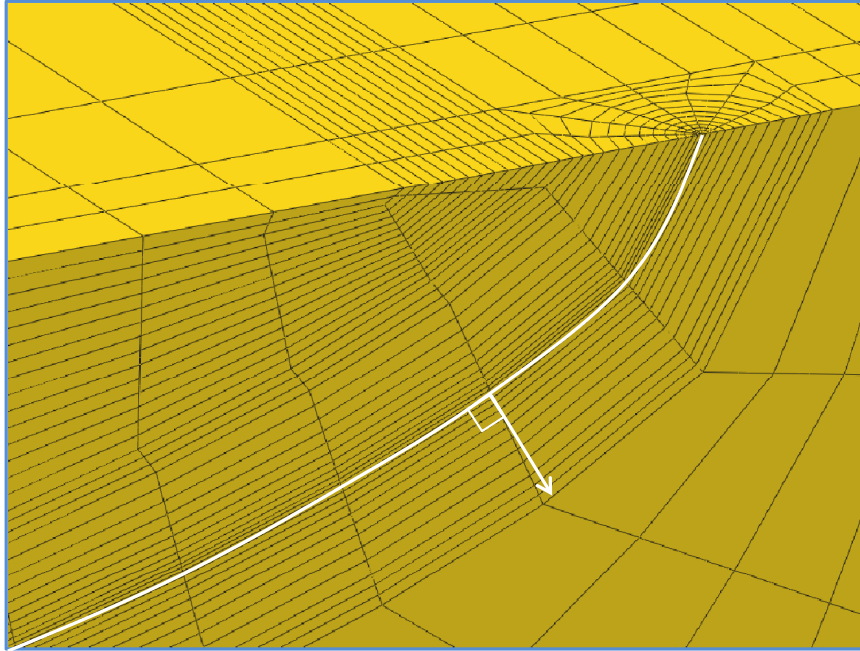


Figure 24b. Curved crack front with elements aligned with the crack front normal.

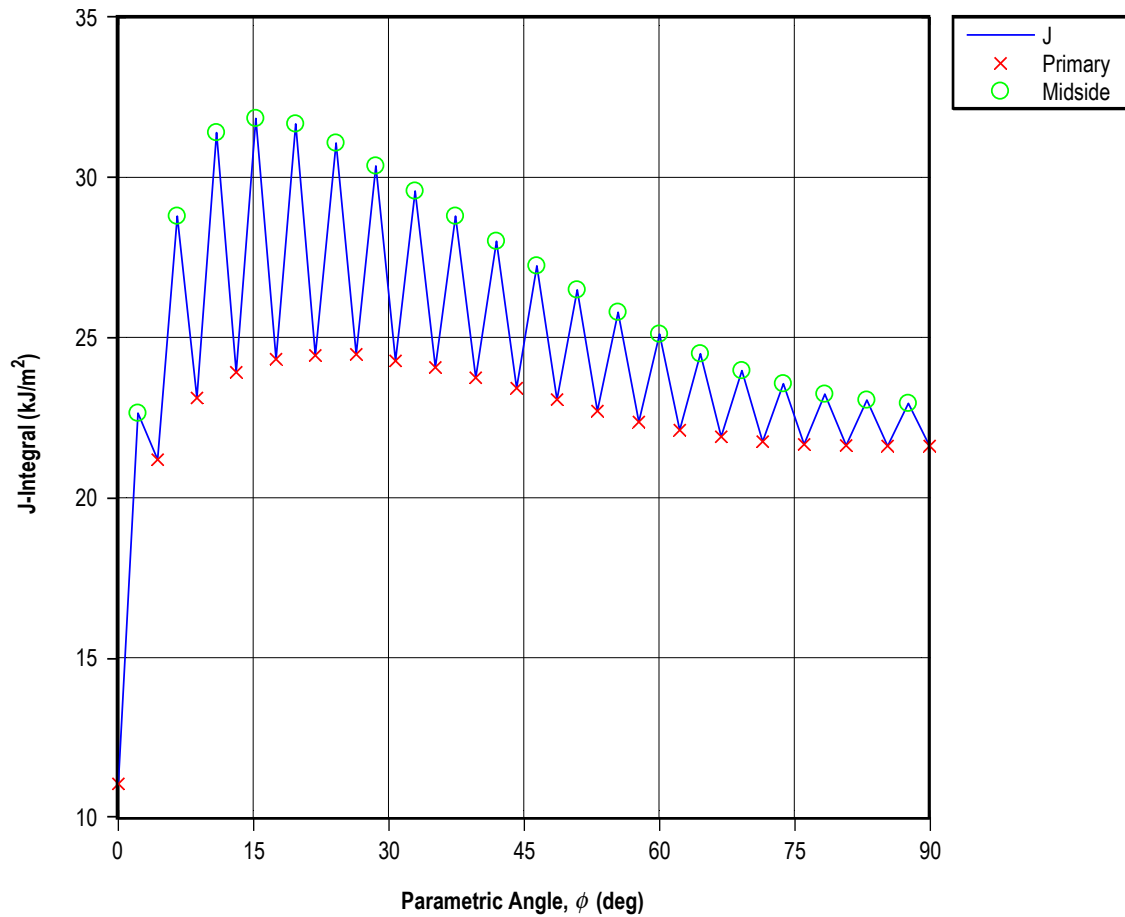


Figure 25. Oscillating J-integral solution affecting the lab-8 solution.

### 4.3.5 Constitutive Modeling

For modeling elastic-plastic behavior, the choices made regarding the constitutive properties of the material often have the largest impact on model results compared to other modeling choices. As expected, this follows through to the ILS problem as well. Each lab was provided with a spreadsheet containing a set of engineering stress-strain data, very much as it would appear from a test lab reporting a tensile test. See appendix A. Each participant was free to represent this material property in their model in any fashion they chose. In this case, the ILS problem was actually simplified because the value of elastic modulus (and Poisson's ratio) was provided in addition to the stress-strain data. This should have assisted with the evaluation of the stress-strain curve and likely minimized some of the variability in its representation. Fourteen of the 15 labs used a table of stress-strain data pairs to represent the stress-strain curve. Lab-2 fit a linear-plus-power law equation to the data for use with a nonlinear elastic representation of the curve. Beyond these consistencies, there was a wide variety in choices. The survey recorded the use of true stress-strain versus engineering stress-strain as well as the fidelity of the curve representation regarding proportional limit/yield point selection and hardening behavior. Though not constitutive in nature, the use of small strain assumptions (nodal geometry definition does not change) versus a finite strain formulation (nodal geometry updates due to displacements) was also documented since it relates to the constitutive inputs.

Figures 26 and 27 illustrate the J results relative to the choice of true versus engineering stress-strain and the use of small strain versus finite strain formulations, respectively. These choices are related in that one should generally follow the other. If small strain assumptions are used, the engineering stress-strain curve is appropriate, while if a finite strain formulation is used, the true stress-strain curve is proper. Based on the survey responses, 6 of the 15 labs used a true stress-strain input with small strain assumptions. In figures 26 and 27, these cases are indicated by a small arrow. J-integral evaluation is generally insensitive to the choice of small versus finite strains, except for an increase in path dependency with the finite strain formulation.<sup>13</sup> However, the transformation of the stress-strain curve into true stress-strain space elevates the curve and tends to suppress the resulting J values as plasticity becomes a large contributor. This trend is visible in figure 26.

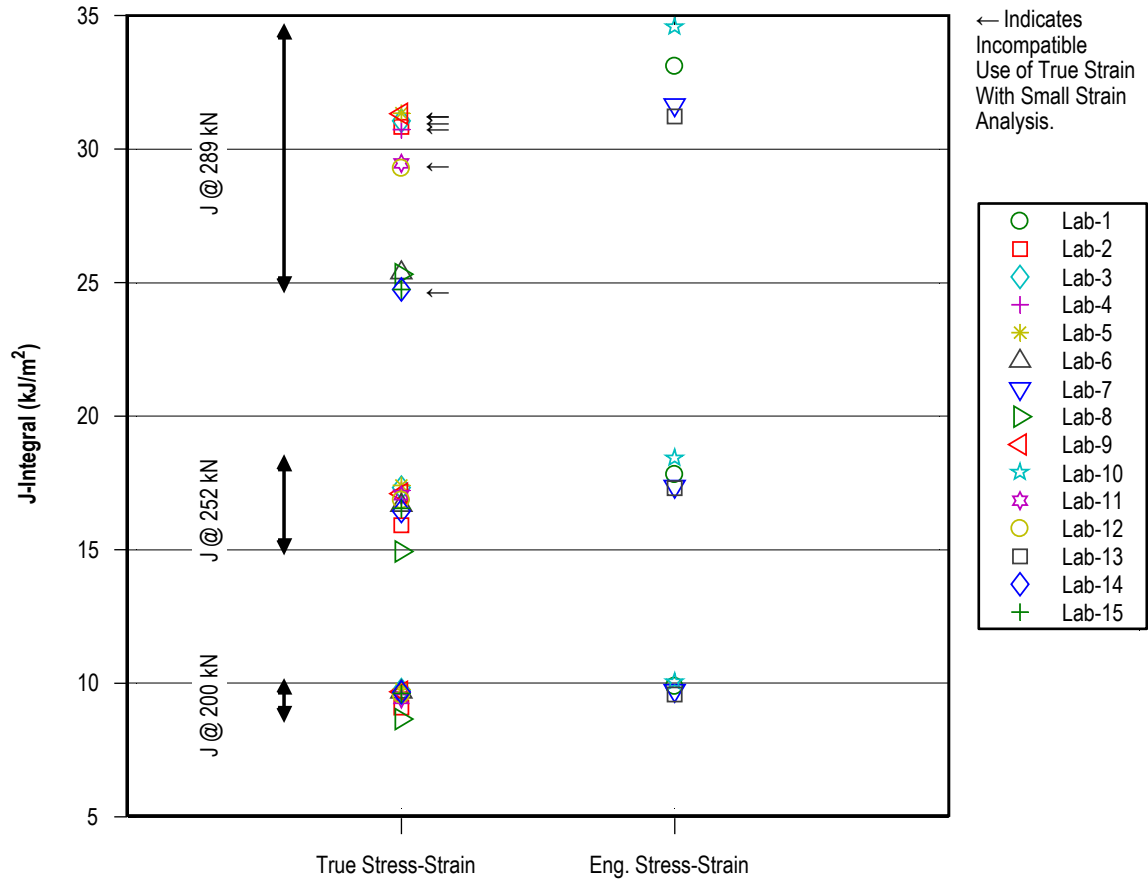


Figure 26. J-integral at  $\phi = 17^\circ$  versus use of true or engineering stress-strain material properties.

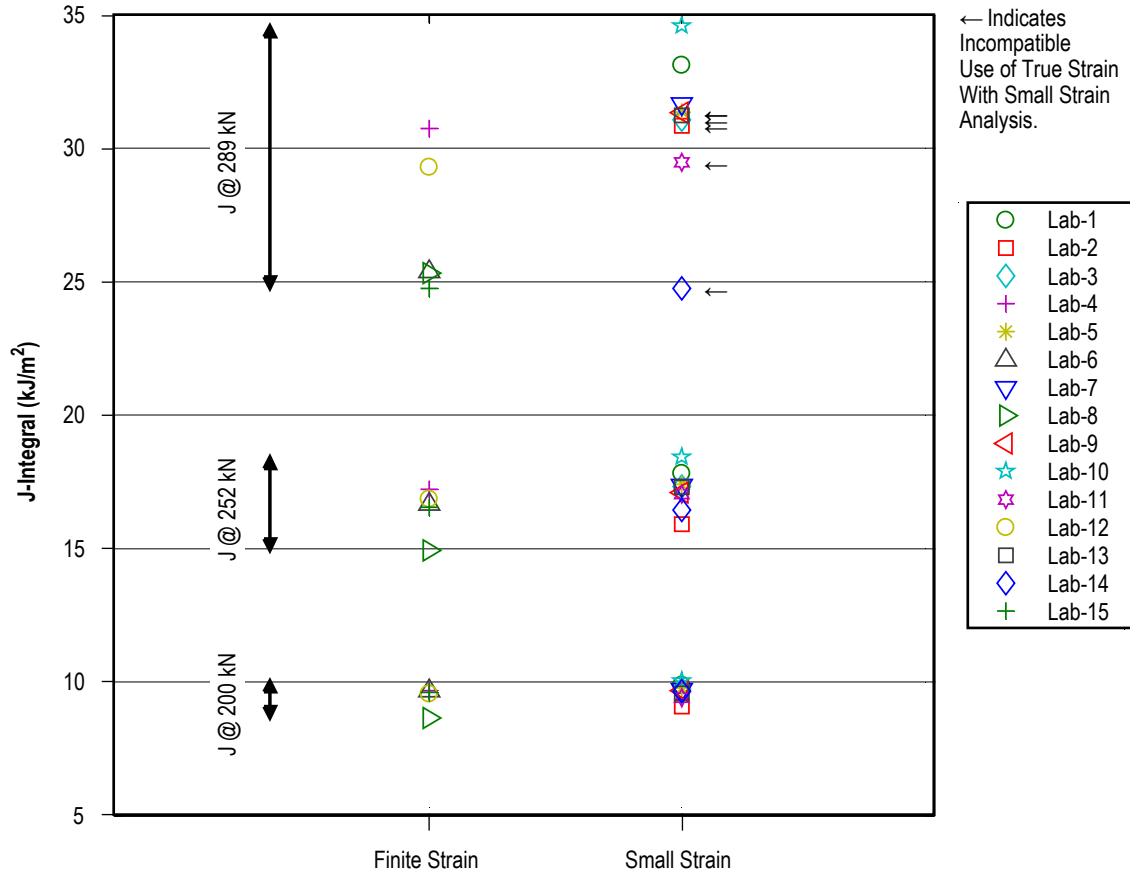


Figure 27. J-integral at  $\phi = 17^\circ$  versus use of small-strain or finite-strain formulation.

The changes in the early post-yield portions of the stress-strain curve due to the true stress-strain transformation are small, yet they noticeably affect the J-integral results reported at the specified force values. Based on this observation, a closer evaluation of each of the lab's stress-strain inputs is warranted. To provide a consistent basis for comparison, the provided data were converted into a consistent format to eliminate differences due to units, plastic versus total strain, and the use of true stress-strain versus engineering stress-strain. Figure 28 shows the provided data along with the inputs of all labs using engineering stress and strain. In this larger view, the consistency across labs appears good, likely well within the variability one would expect from typical material property scatter. To isolate when each analysis would begin to accumulate plastic strain, the curves are plotted as engineering stress versus plastic strain in figures 29a and 29b. In these figures, a range of proportional limit is visible from approximately 315 to 385 MPa, represented by star-shaped symbols. This range is due in part to a lack of a standardized treatment for rendering experimental tensile data into constitutive inputs for an analysis code. For example, a likely explanation for the higher proportional limits chosen is the use of a 0.2% offset definition of yield strength that is standard in engineering practice, versus setting the proportional limit when the first substantial plastic strain occurs. The J results are plotted versus the proportional limit used in each lab's analysis in figure 30. With the exception of the lab-8 result, the choice of proportional limit effectively isolates each of the results that provide lower J results at 289 kN. This follows clearly

since the higher proportional limit delays the onset of plastic contributions to J because the plastic area under the stress-strain curve for a given stress level is reduced.

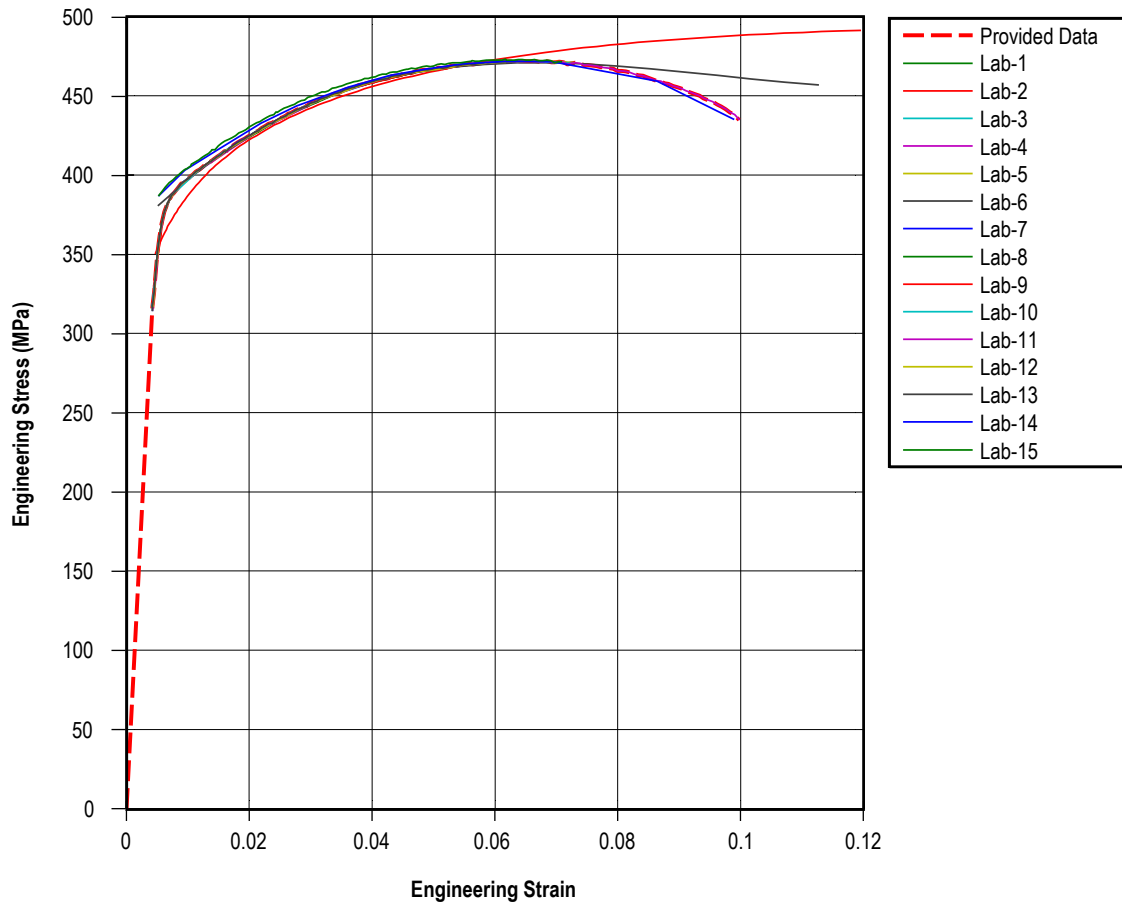


Figure 28. Stress-strain inputs in engineering stress-strain space.

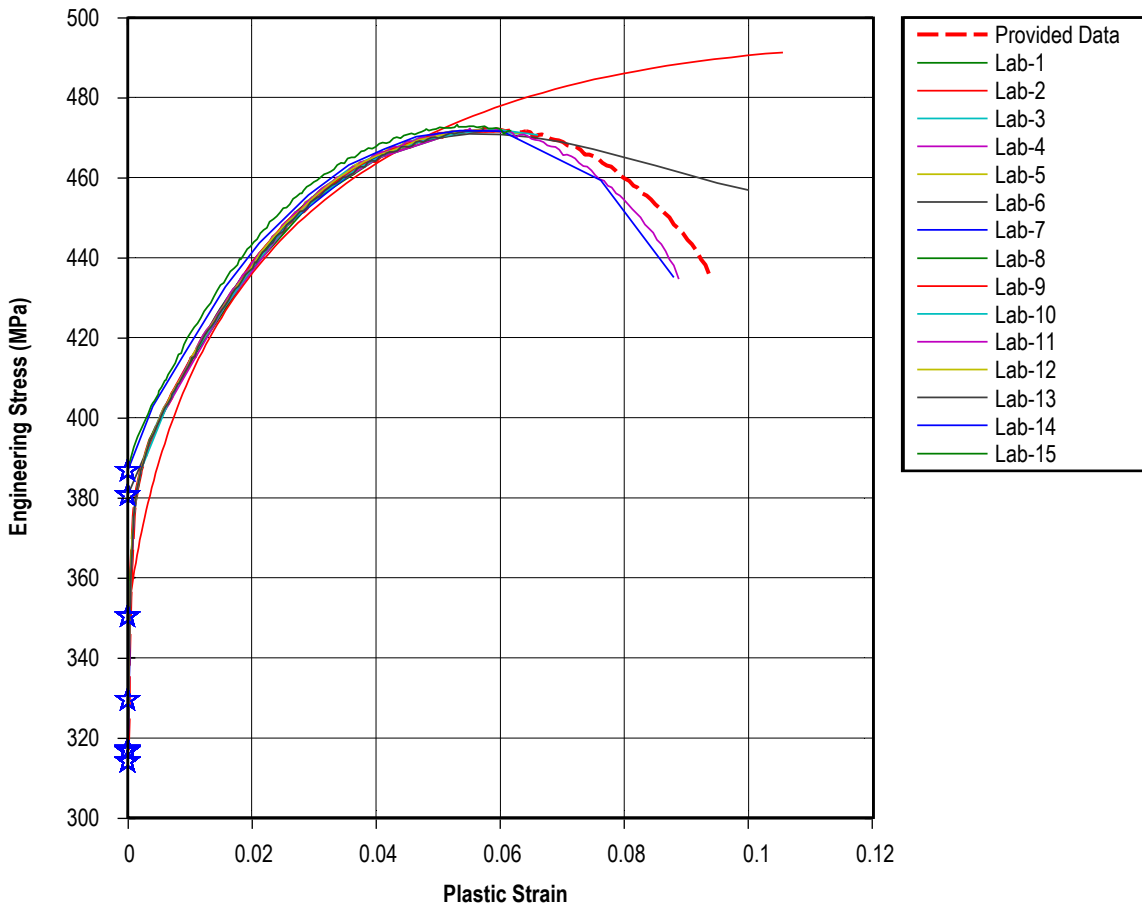


Figure 29a. Engineering stress versus plastic strain.

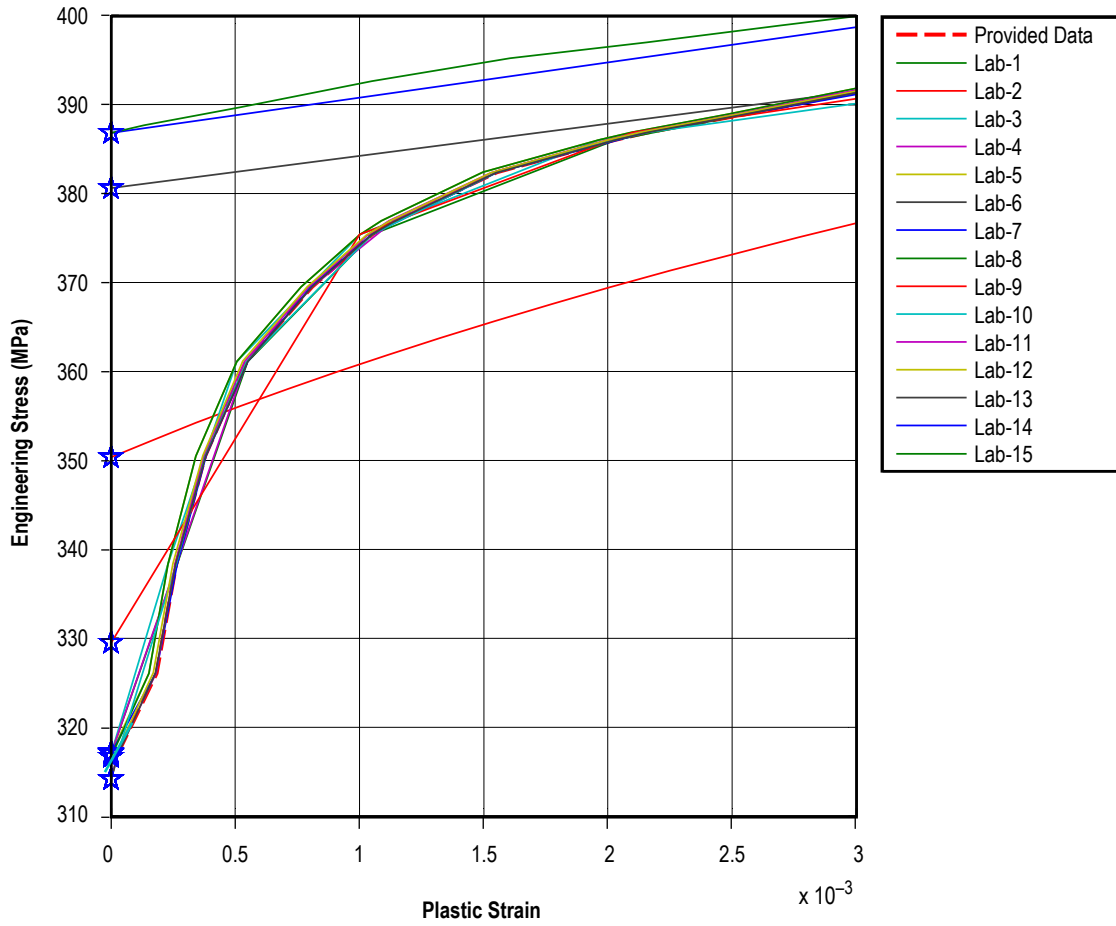


Figure 29b. Engineering stress versus plastic strain illustrating range of proportional limits.

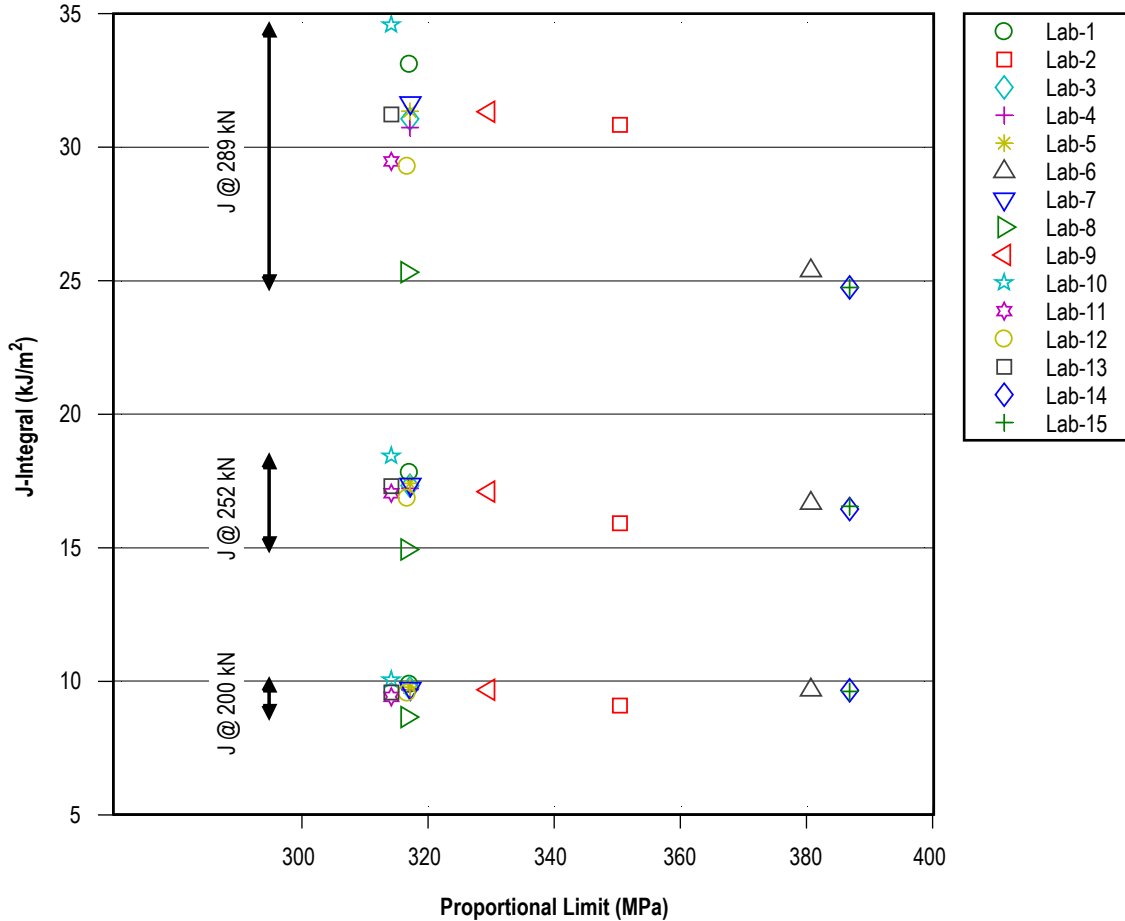


Figure 30. J-integral at  $\phi=17^\circ$  versus proportional limit in constitutive inputs.

Figure 31 illustrates the area under the stress versus plastic strain curve. In the figure, the area is normalized relative to the area under the provided stress-strain curve and plotted versus stress. Thus, inputs exactly matching the provided data produce a normalized area of unity. The curves with higher proportional limits (labs -6, -14, and -15) do not begin accumulating plastic area until the local stresses exceed 380 MPa. Also clear from this plot is that though the curve fit chosen by lab-2 has a slightly higher than average proportional limit, it accumulates plastic area quicker than average in the range of 360 to 400 MPa, and the overall result is that the lab-2 estimate of J at 289 kN is typical of the larger population. Of further interest is the deviation among labs in normalized area under the plastic strain curve converges as the stress-strain state increases. This suggests that variability in the analysis due to the precision of the proportional limit in the constitutive input should decrease as deformation increases.

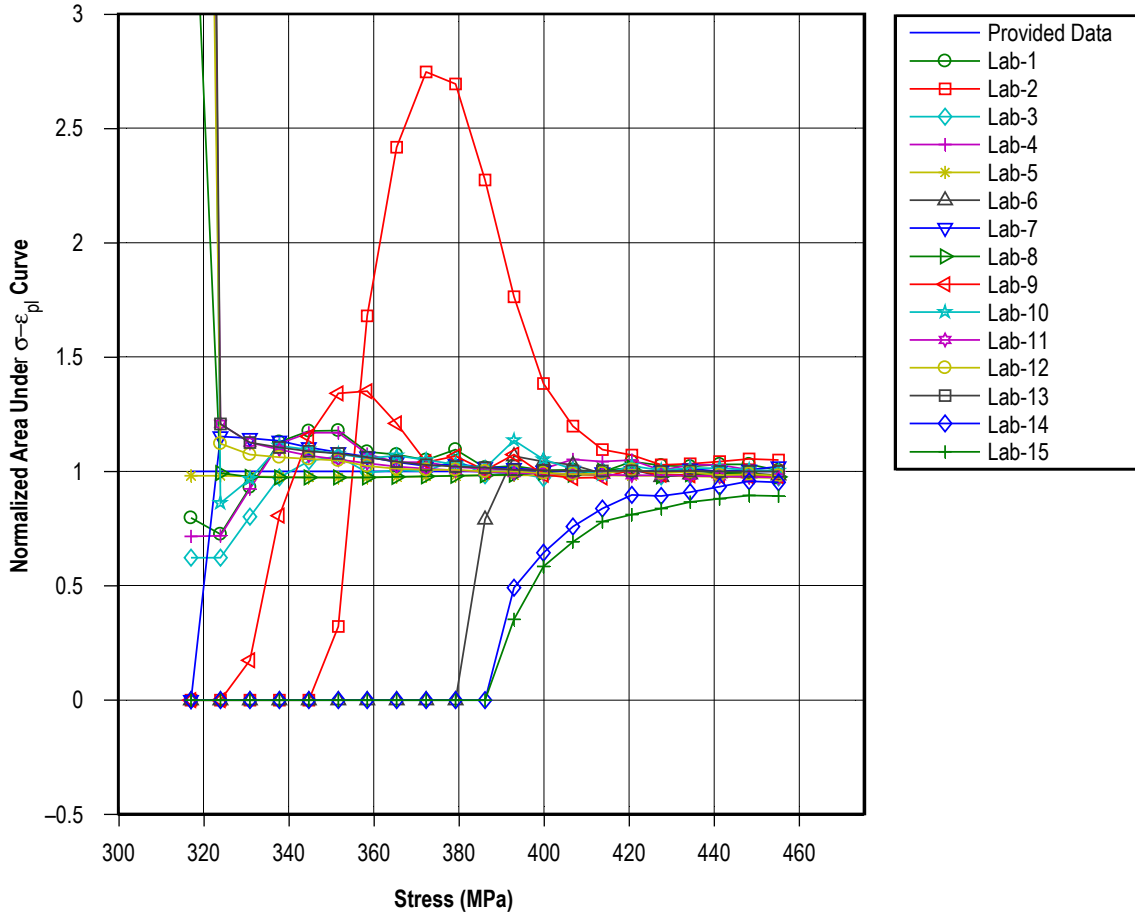


Figure 31. Area under the engineering stress-plastic strain curve as function of stress.

To directly study the effects of proportional limit variation in the constitutive inputs, the lab-1 model was run under four scenarios, where only the proportional limit was altered. Figures 32a and 32b illustrate the stress-strain curves used in the assessment. The differences are subtle, with the proportional limit changing from 276 to 379 MPa, yet the curve remaining identical to the provided input data after a plastic strain of 0.002, the typical engineering yield point. The smallest proportional limit value of 276 MPa was purposefully chosen below the actual proportional limit of the test data on the linear portion of the stress-strain curve to illustrate no issues arise with a low proportional limit as long as the curve is properly followed. An area evaluation similar to that previously reviewed for the participant inputs is shown in figure 33. In this case, the normalizing curve is the one with the lowest proportional limit (276 MPa). The delay in accumulation in plastic area in the early region of the curve is clear as the proportional limit increases. These plastic area differences quickly dissipate once the stress-strain curves converge and large amounts of plastic area develop.

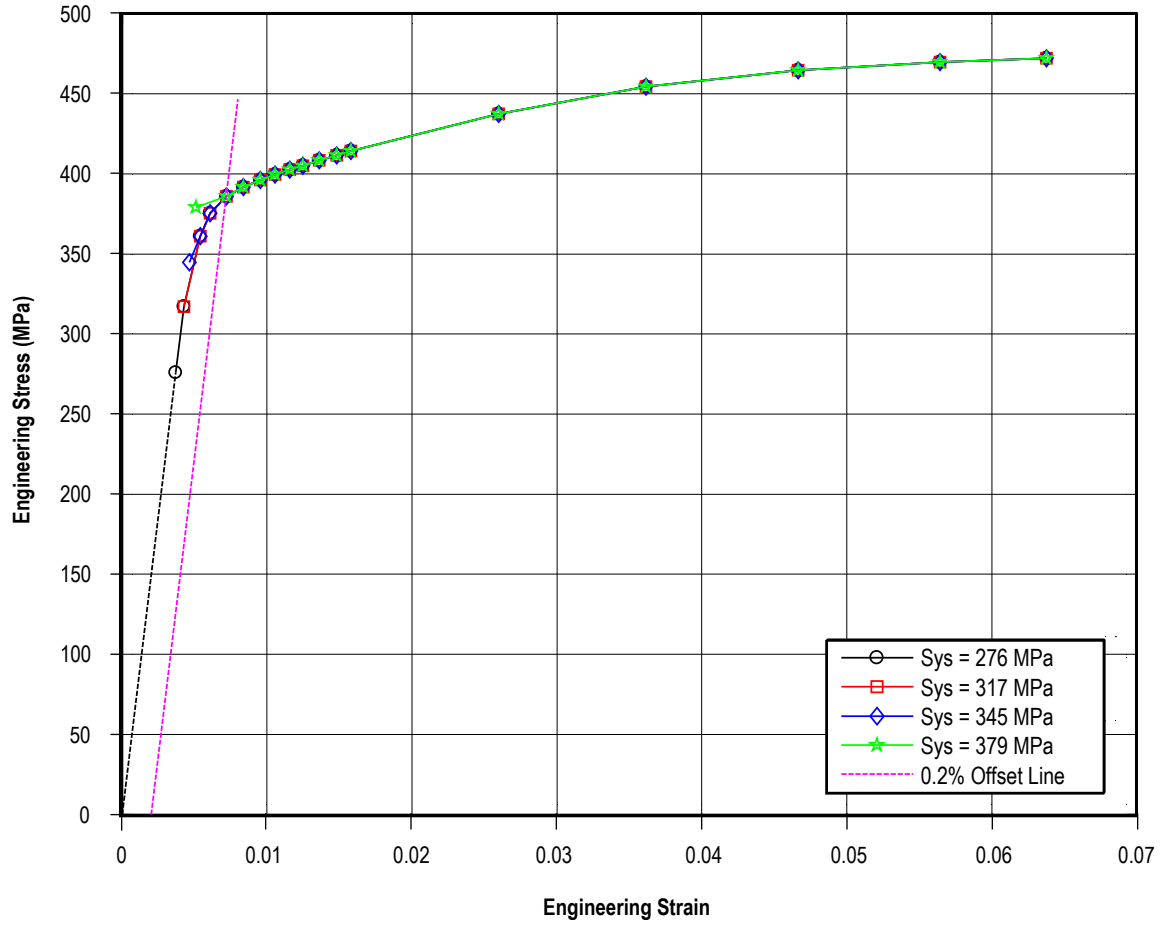


Figure 32a. Engineering stress-strain curves used in the proportional limit substudy.

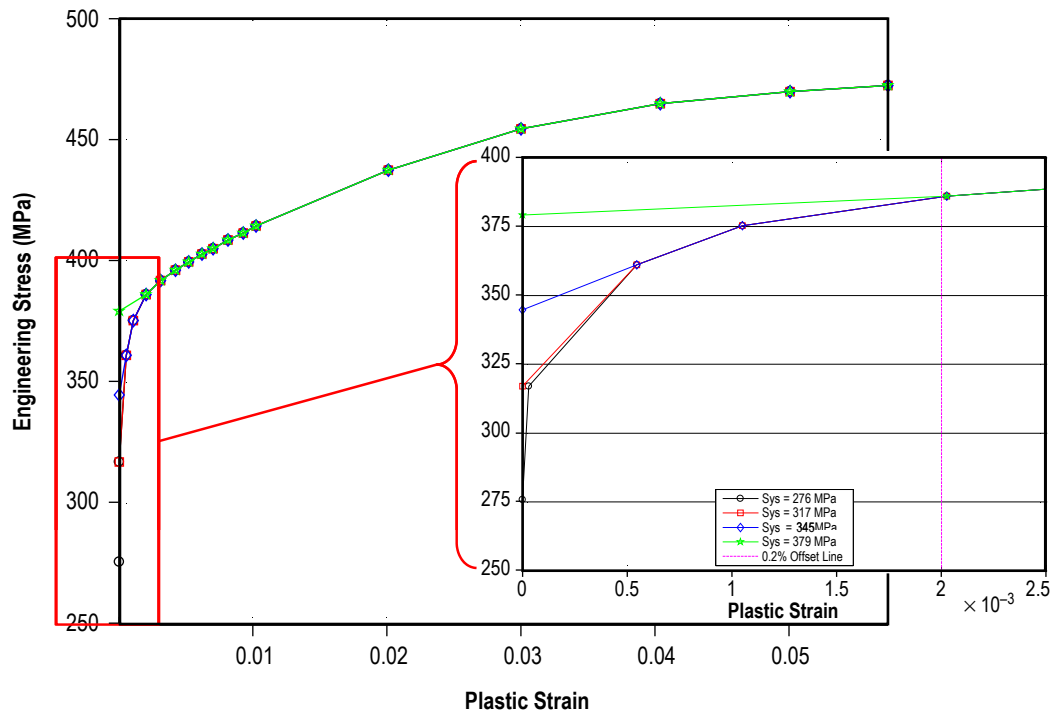


Figure 32b. All variations in proportional limit occur prior to standard 0.2% offset strain yield definition.

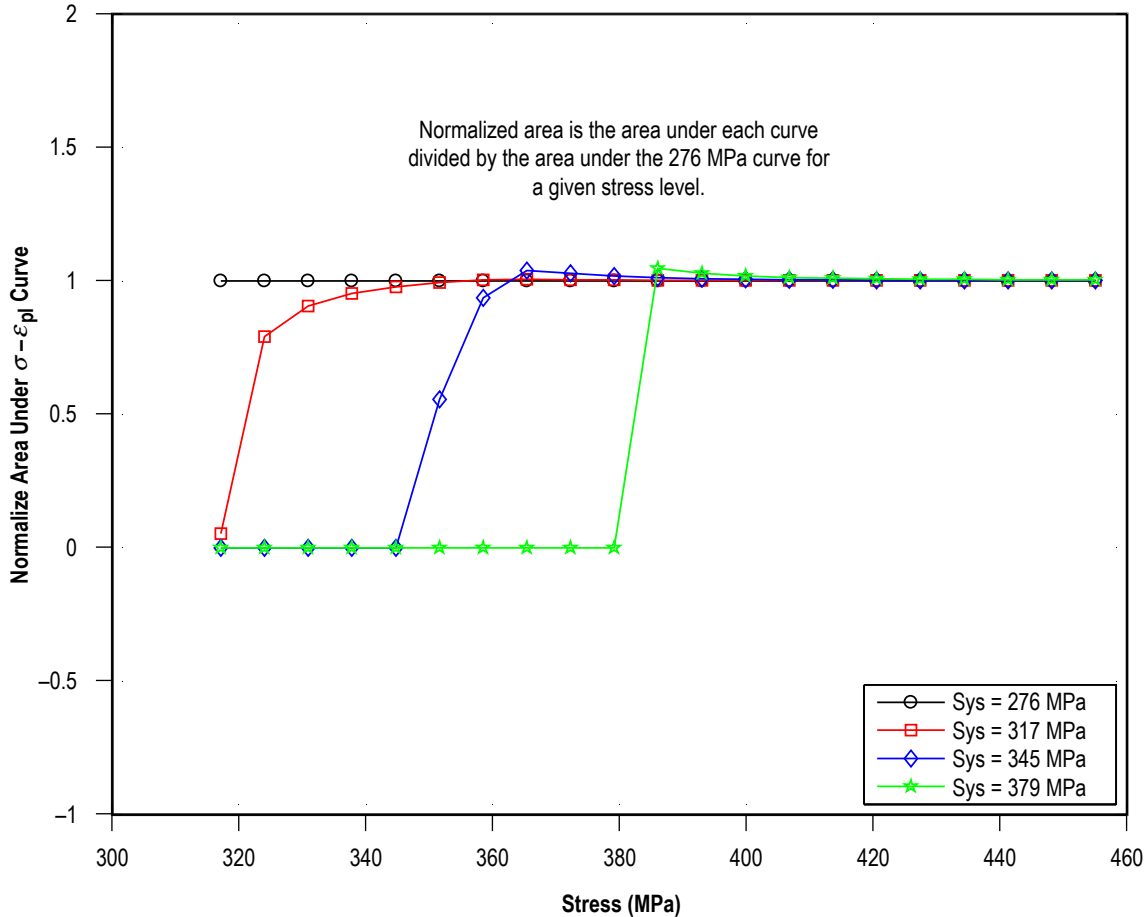


Figure 33. Area under the engineering stress-plastic strain curve as function of stress for the proportional limit substudy.

Figures 34a through 34j present the results from a series of load steps from each of the four models in this substudy superimposed, each illustrating both the force versus CMOD response and the  $J(\phi)$  results around the crack perimeter at the indicated force. The force values of interest in the ILS are highlighted along the force axis and the deformation level as defined in the test standard is shown for crack length and ligament at  $\phi = 17^\circ$ ,  $r_{\phi a}$  and  $r_{\phi b}$  in figure 34a. The load step producing the  $J(\phi)$  result is indicated along the force-CMOD trace. In figure 34a, at step 11, the response is predominantly linear-elastic and the four results are nearly identical. Figure 34b, at step 12, corresponds closely with the 200 kN force of interest in the ILS and very little deviation in  $J(\phi)$  is present among the models, particularly at  $\phi = 17^\circ$ . As the analysis progresses through steps 13–15 (figs. 34c–34e), separation in the  $J(\phi)$  results becomes clear and is ordered based on the proportional limit. Step 15 corresponds closely to the 252 kN force where results were requested in the ILS. Note that the variability in the proportional limit leads to approximately 6% variation in  $J(\phi = 17^\circ)$ . At steps 16 and 17 in figures 34f and 34g, respectively, the two models with lower proportional limits have converged, yet the overall variation in  $J(\phi)$  has increased across the models, accounting for almost a 20% deviation in  $J(\phi = 17^\circ)$ . At step 18, which is slightly above the 289 kN force value reported in the ILS, the lower proportional limit models are further converging, leaving the model

with the 379 MPa proportional limit lagging as a separate family (fig. 34h). At even higher levels of deformation, the early influence of the proportional limit dissipates. Figures 34i and 34j illustrate that the variation in J has decreased to approximately 4% for  $J(\phi = 17^\circ)$ . The model violates the current deformation limit on crack size in the test standard ( $M_a \geq 25$ ) between steps 19 and 20.

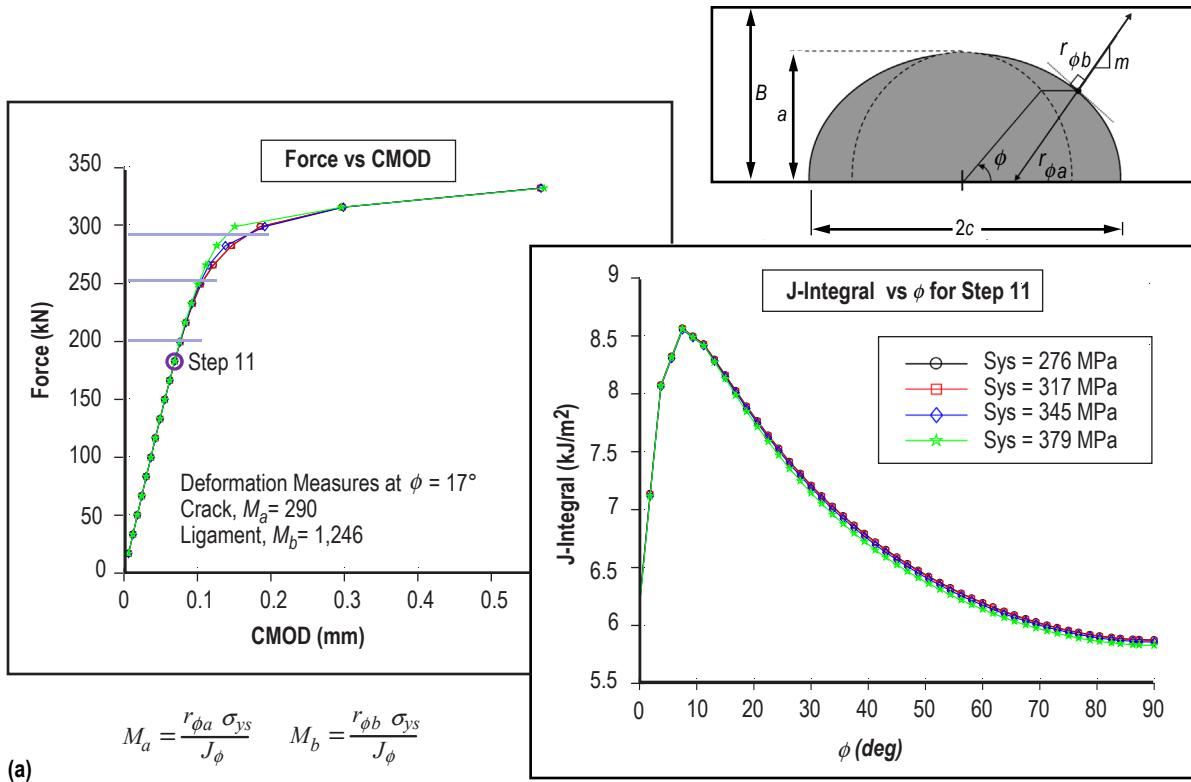
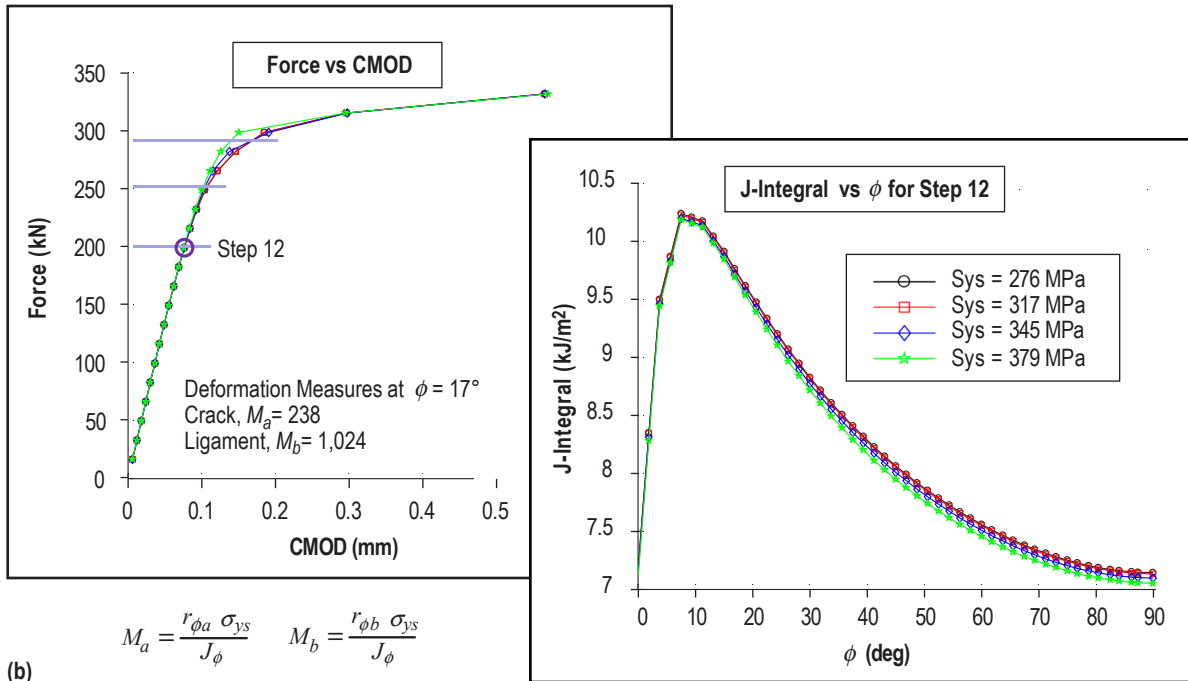
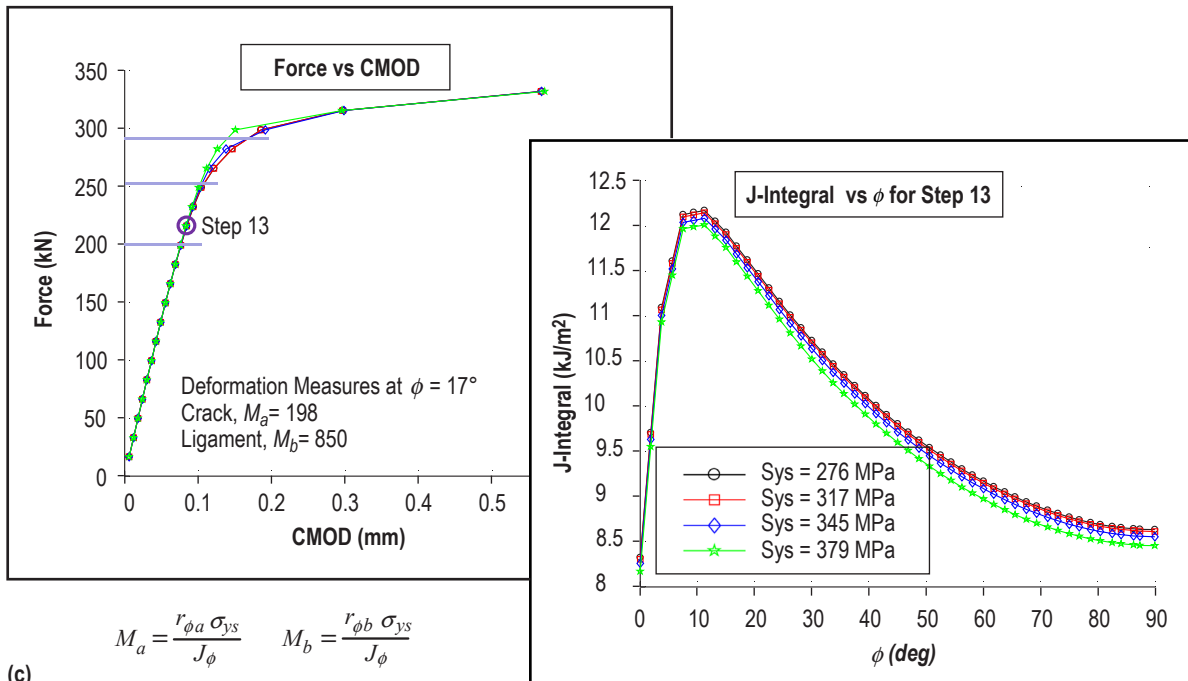


Figure 34. Images (a) through (j) illustrate the effects of proportional limit on the resulting J-integral value as the model is loaded through the ILS load regime and beyond.



(b)



(c)

Figure 34. Images (a) through (j) illustrate the effects of proportional limit on the resulting J-integral value as the model is loaded through the ILS load regime and beyond (Continued).

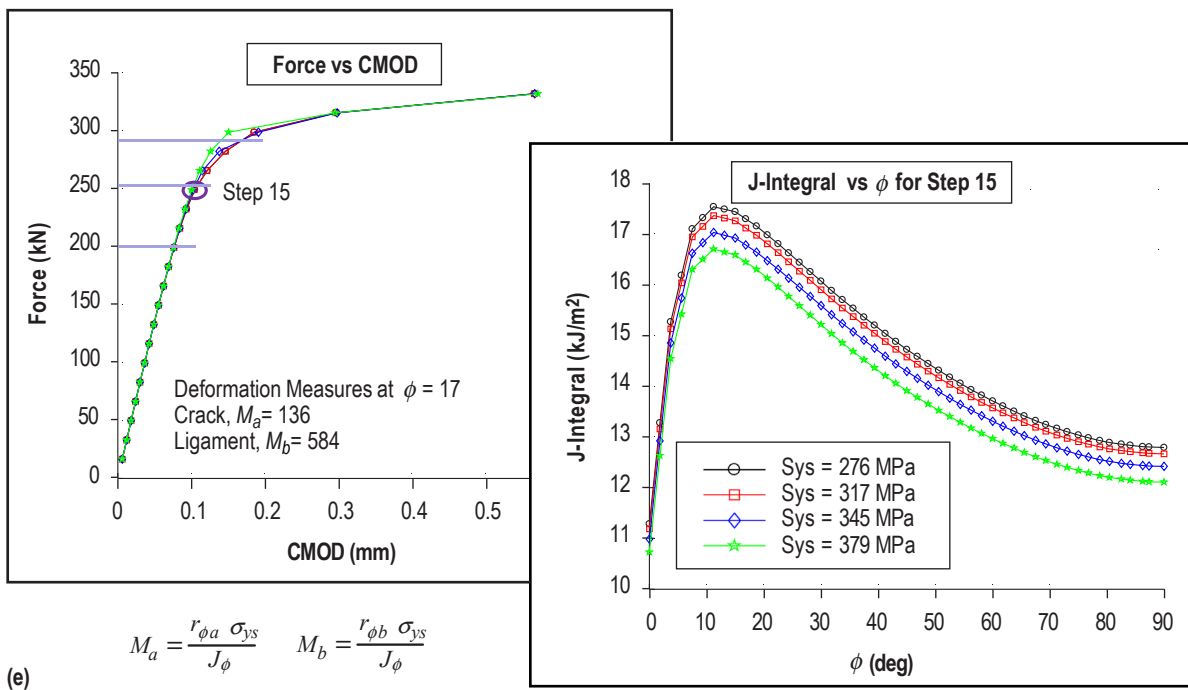
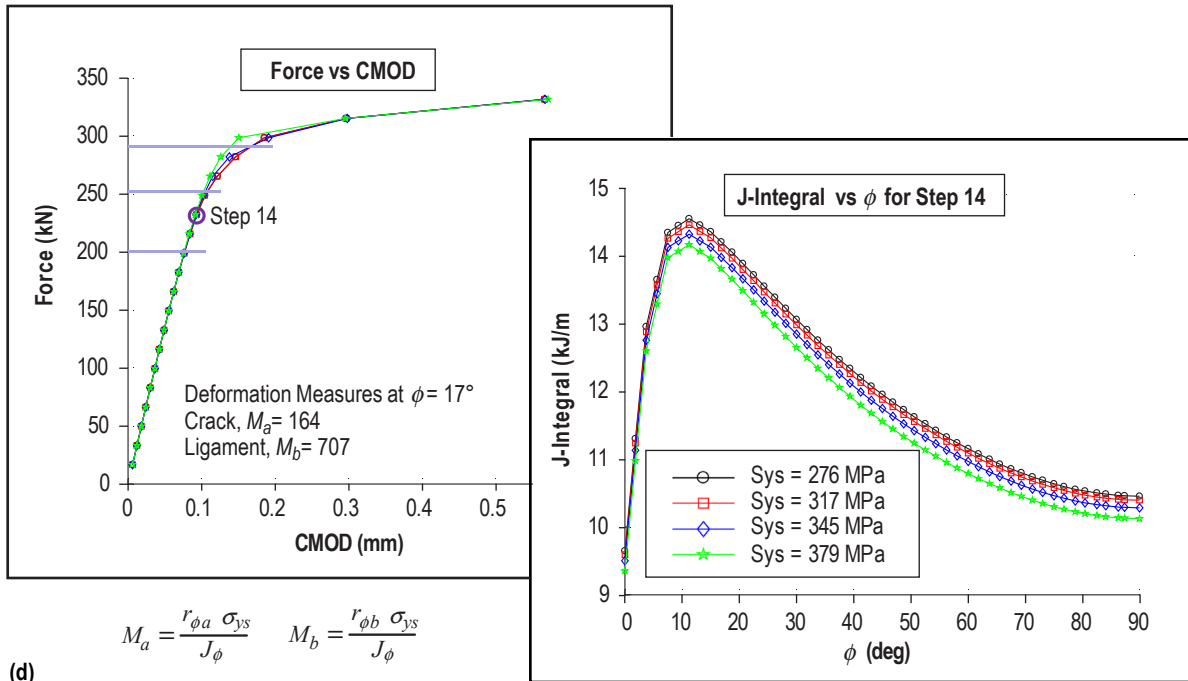
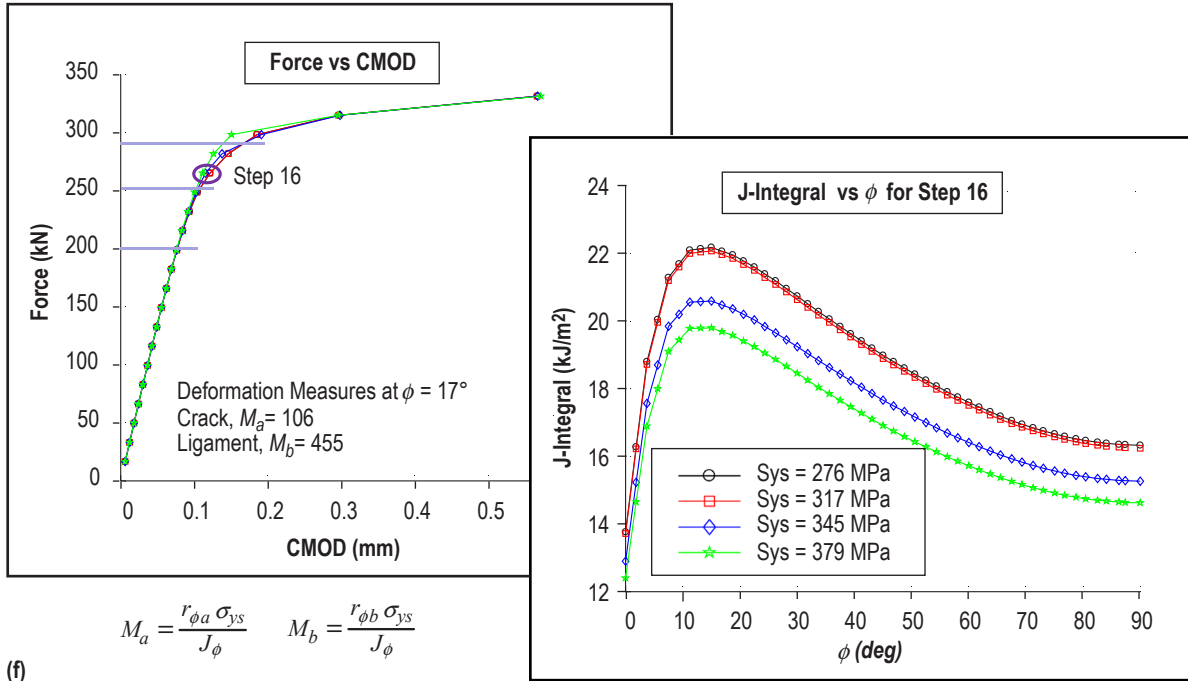
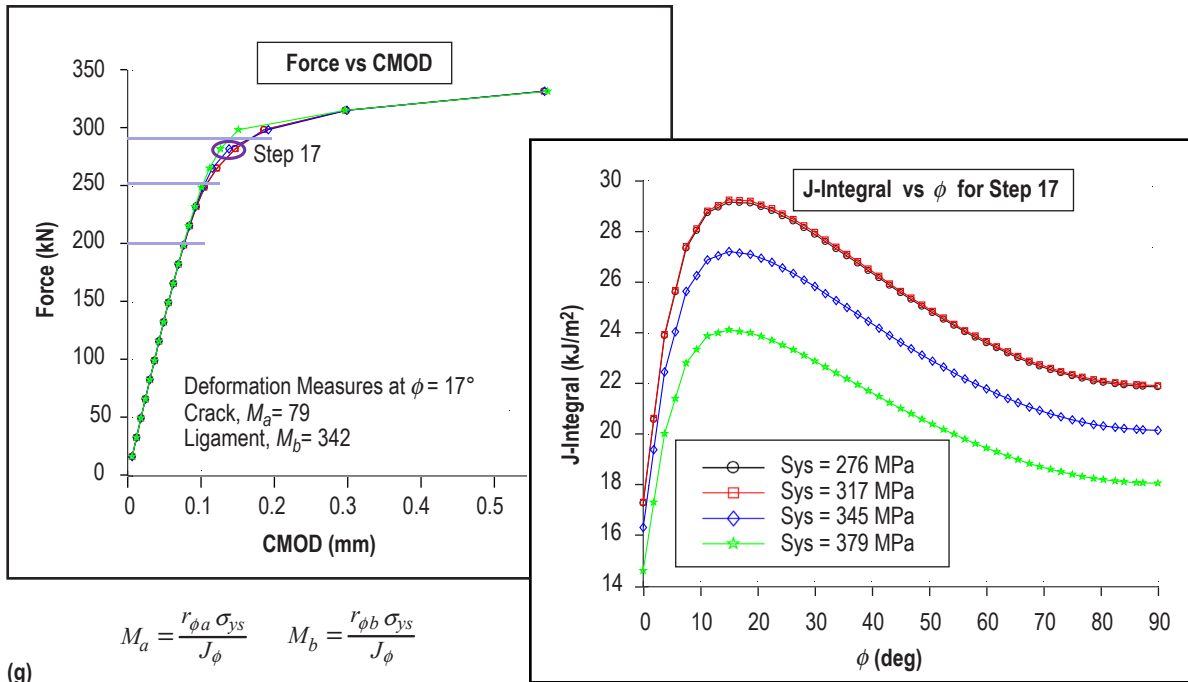


Figure 34. Images (a) through (j) illustrate the effects of proportional limit on the resulting J-integral value as the model is loaded through the ILS load regime and beyond (Continued).

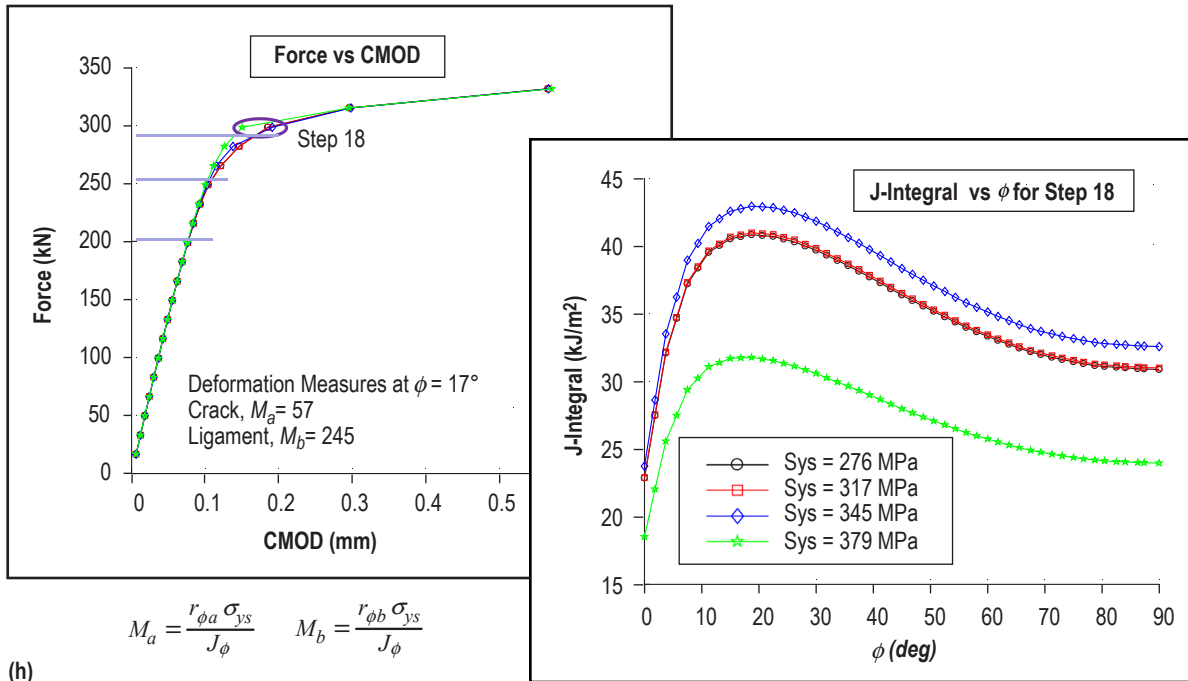


(f)

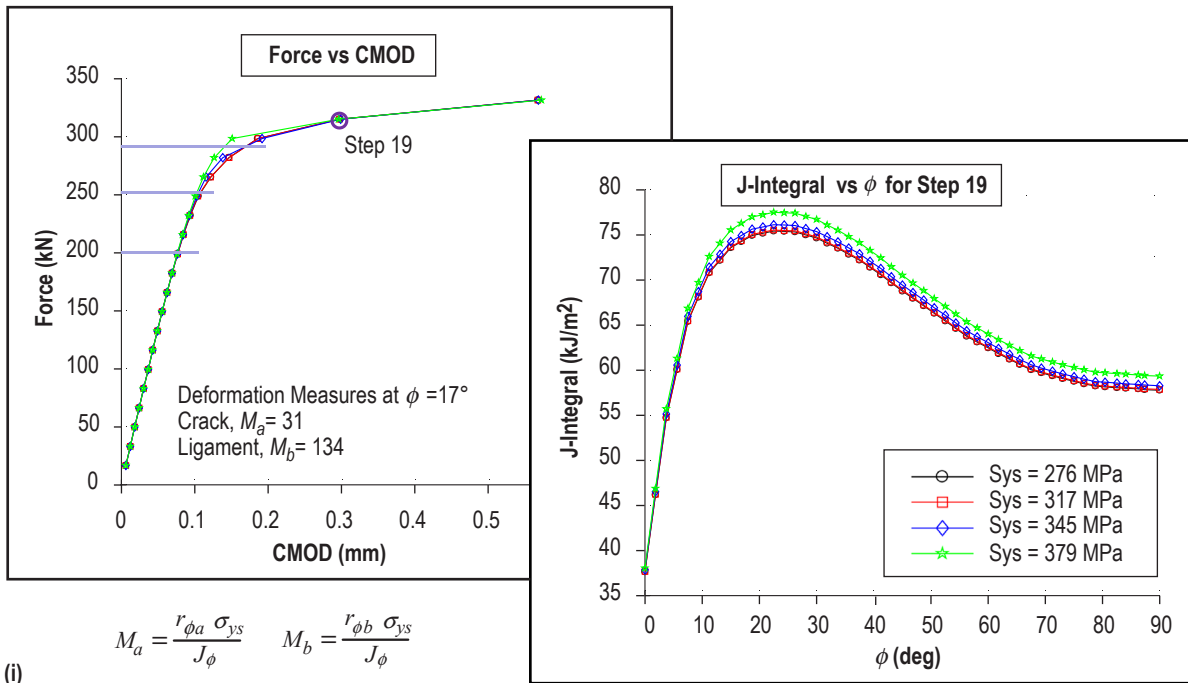


(g)

Figure 34. Images (a) through (j) illustrate the effects of proportional limit on the resulting J-integral value as the model is loaded through the ILS load regime and beyond (Continued).



(h)



(i)

Figure 34. Images (a) through (j) illustrate the effects of proportional limit on the resulting J-integral value as the model is loaded through the ILS load regime and beyond (Continued).

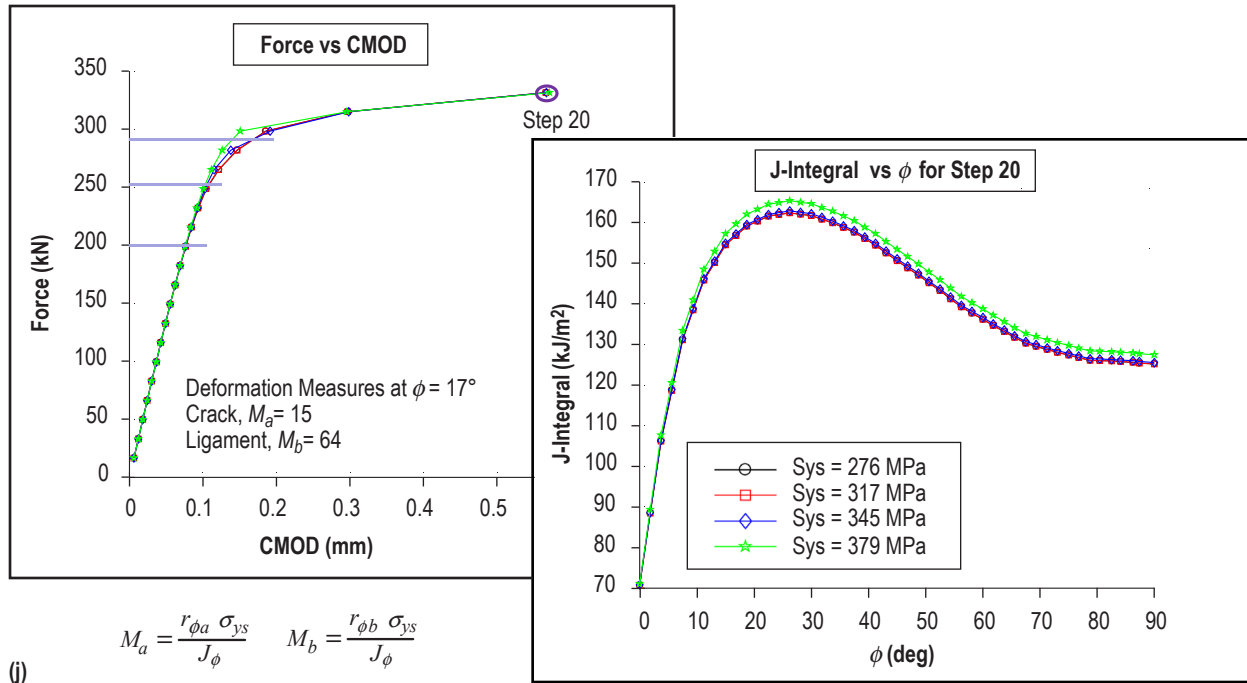


Figure 34. Images (a) through (j) illustrate the effects of proportional limit on the resulting J-integral value as the model is loaded through the ILS load regime and beyond (Continued).

The sequence of plots showing J-integral and force versus CMOD results in figure 34 illustrates the variability in J-integral assessment due to constitutive input when the criterion used to match the experiment is enforced at the far-field boundary conditions, in this case, matching the experimentally measured force to the reaction force in the model. Similar J-integral variability is observed if the experimental displacement at the end of the specimen is used to match displacement-controlled boundary conditions on the model. The constitutive model must convey these far-field conditions through the specimen (or structure) to the crack, resulting in considerable sensitivity once nonlinear conditions prevail. These constitutive sensitivities require significant consideration for typical structural defect assessments, when local knowledge of crack conditions are not known and remote boundary conditions are (at best) all that are available. In the case of surface crack toughness experiments in the laboratory, the presence of the CMOD gauge provides an option to enforce the tie from experiment to analysis based on conditions local to the crack. As hinted during previous discussion of figures 11 and 12, the CMOD provides a more direct and less sensitive indicator of crack tip conditions. Moreover, tying experiment and analysis using CMOD should lessen constitutive sensitivities because of the local nature of the criterion.

To evaluate the benefit of using a CMOD-based criterion to reduce the sensitivity of constitutive inputs to the J-integral results, the authors conducted a second substudy using the lab-1 model. In this substudy, the constitutive inputs were altered to target a  $\pm 5\%$  deviation in predicted

force when the model's CMOD matches the experimental CMOD. The constitutive inputs were modified using a simple multiplicative factor on the stress values of the stress-strain curve. A factor of 0.96 applied to the stress inputs resulted in a very close match to the force and CMOD at the initiation of tearing in the experiment. This result is designated "analysis A" and "material A" in table 4 and figure 35, respectively. Further iteration developed material inputs B and C to target the  $\pm 5\%$  bounds for prediction of force on the specimen at the tearing CMOD. As tabulated in table 4, the resulting range in J-integral prediction is only  $\pm 3.2\%$  when interpolated at the tearing CMOD. The modified constitutive inputs are illustrated in figure 36. In stark comparison to the previous substudy, which allowed zero deviation in the 0.2% offset yield strength, bounding assessments B and C incorporate a 57 MPa (14%) difference in the 0.2% offset yield strength, and yet, by matching the CMOD, the results maintain very small errors in the J-integral.

Table 4. Summary of results from CMOD-matching substudy.

CMOD-Matched Analysis at Tearing CMOD					
Analysis	Factor on Stress*	0.2% Offset Yield Strength (Mpa)	Force Difference** (%)	J-Integral (kJ/m <sup>2</sup> )	J Difference*** (%)
Lab-1†	1.000	386	2.92	19.8	1.67
A	0.960	370	0.01	19.4	0
B	1.040	401	5.03	20.0	3.17
C	0.893	344	-4.94	18.8	-3.23
CMOD-Matched Analysis at Deformation-Limited CMOD					
Analysis	Factor on Stress*	0.2% Offset Yield Strength (Mpa)	Force Difference‡ (%)	J-Integral (kJ/m <sup>2</sup> )	J Difference*** (%)
A-2	0.960	370	0	159	0
D	1.010	390	5.02	167	4.88
E	0.910	351	-5.17	152	-4.70

\* Multiplication factor applied to the material stress inputs of the Lab-1 analysis.

\*\* Percent difference in predicted force at tearing CMOD.

\*\*\* Percent difference in J at  $\phi=17^\circ$  relative to analysis "A".

† Material properties as used in Lab-1 results.

‡ Percent difference in predicted force at CMOD from analysis A-2.

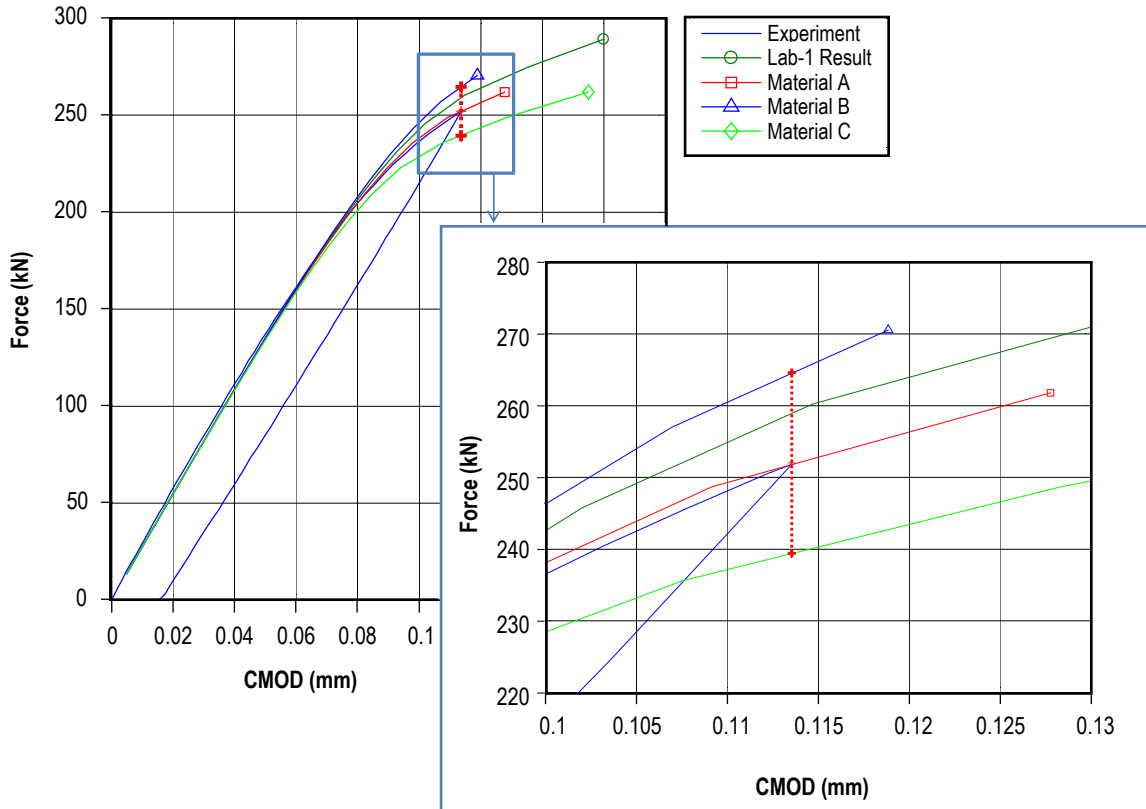


Figure 35. Bounding models at the tearing CMOD for the CMOD-matching substudy.

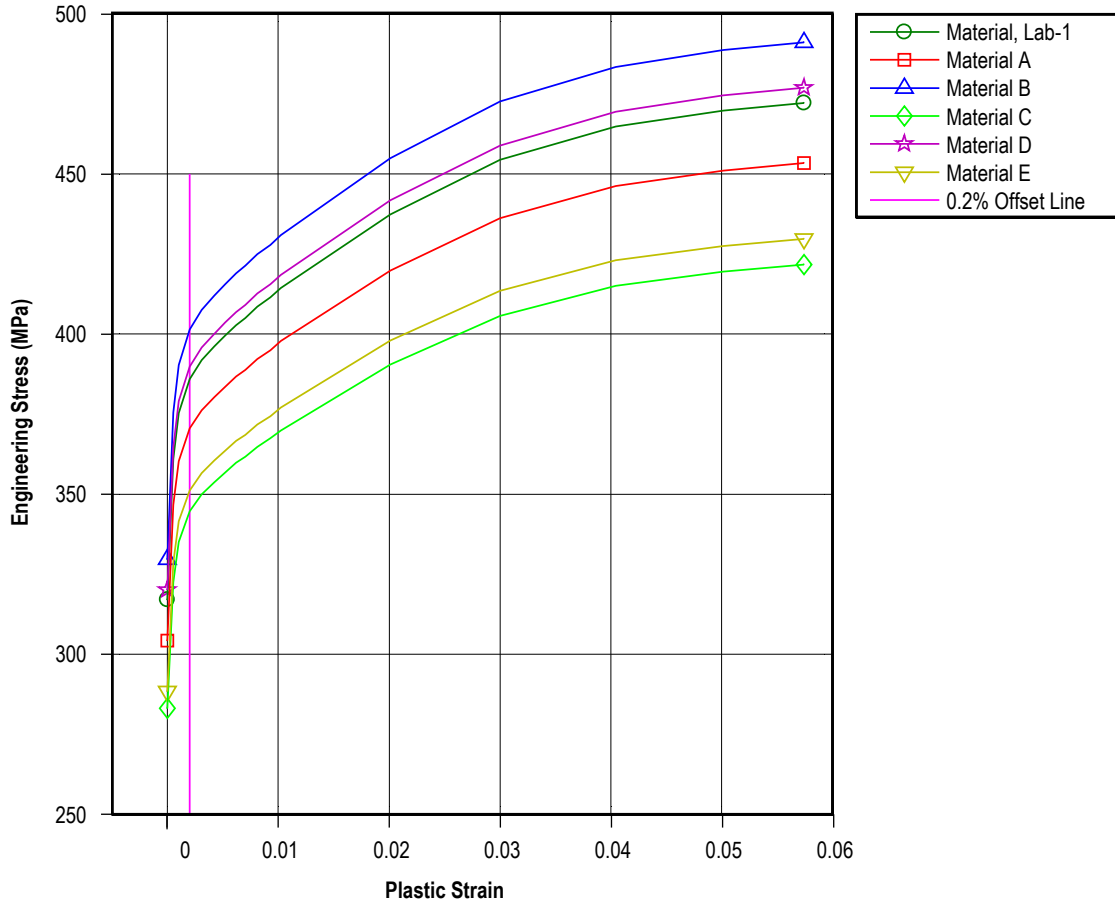


Figure 36. Comparison of scaled material property inputs for the CMOD-matching substudy.

There is only a small amount of plasticity in the round robin experiment at tearing. To evaluate the same sensitivities at higher levels of plasticity, the analysis using material A was run to the maximum allowed deformation in the proposed surface crack standard, resulting in analysis A-2 in table 4. Using this analysis as a baseline, materials D and E (fig. 36) were developed to target the allowable  $\pm 5\%$  force range at this deformation-limited CMOD, as illustrated in figure 37. Interpolating J-integral values from analyses D and E at the final CMOD of analysis A-2, the resulting range in J is approximately  $\pm 4.8\%$ . For comparison, the original tearing CMOD bracket is also shown in figure 37. Note that the factors on stress input for materials D and E are smaller than those for materials B and C, resulting in a range of 39 MPa for offset yield strength.

Though the issue of constitutive modeling sensitivity remains for most elastic-plastic assessment of defects in structures, the advantage of measuring the CMOD during surface crack toughness testing allows the proposed test method to mitigate much of this sensitivity during the analytical assessment of the experiment, thus exacting knowledge of the material's stress-strain response is not necessary to reasonably evaluate the toughness result.

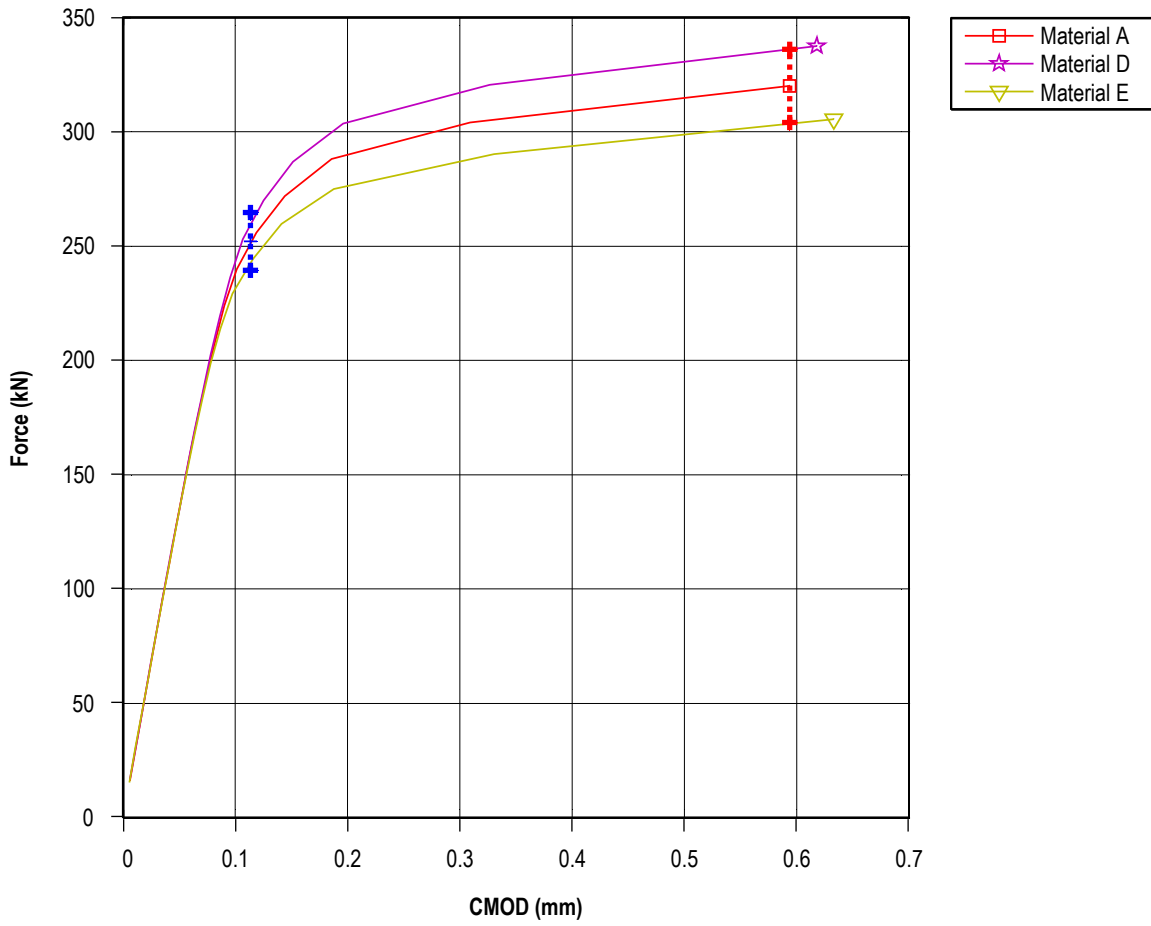


Figure 37. Bounding models at the deformation-limited CMOD for the CMOD-matching substudy.

## 5. CONCLUSIONS

Regarding the overall state of the art for elastic-plastic J-integral analysis, the results from phase I of the ILS are encouraging. Providing a request for analysis with no further instruction regarding methodology has yielded results with surprisingly little variation. Many of the commonly assumed sources of error in finite element analysis appear less significant than they once were, when computing resources for mesh building and equation solving were at a higher premium. General modeling choices such as analysis code, model size (mesh density), crack tip meshing, or boundary conditions were not found to be sources of significant variability. This finding is made possible by the almost ubiquitous standardization toward the finite element implementation of the domain integral method for numerical estimation of the J-integral. The method has been adopted by numerous commercial and open source codes and provides a robust and reliable method to evaluate elastic-plastic J-integral values, as long as the domains are defined by elements of reasonable quality.

Because the ILS called for results at specified force values, the most pressing source of variability in the J-integral assessment is introduced through the constitutive model. The ILS has illustrated, for assessments controlled only by far-field boundary conditions, the representation of the material's stress-strain relation can influence elastic-plastic J results more strongly than most other choices left to the analyst, within commonly accepted modeling practices. In fact, the first substudy which evaluated proportional limit effects in force control would argue that constitutive model sensitivity is likely inherent to the process despite best efforts of the analyst since the degree of material property variability reflected in the study is reasonably representative of the expected variability in flow properties within any given piece of structural metal. The vast majority of structural assessments for J will be based on applied forces or a resulting stress field where the local displacements (CMOD) are unknown. In this case, the substudy illustrates the importance of representing the stress-strain curve faithfully throughout. For most J-integral evaluations related to structural integrity, other structural factors of safety are likely to limit stresses such that the stress-strain conditions in the vicinity of the crack span the range through the proportional limit and out only modestly onto the tangent modulus of the curve. Analysis in this region of the stress-strain curve is highly prone to introducing variability into the estimated elastic-plastic values of J.

In the controlled case of surface crack toughness testing, the advantage of having the CMOD data is significant. The second substudy illustrates that the extreme sensitivity to constitutive input can be largely avoided by using the CMOD as the basis for evaluating the experimental results. The resulting error in the J-integral will be bounded by the percent error in the predicted force at a given CMOD. The proposed surface crack standard will be updated to utilize only a CMOD-based assessment of surface crack tests in the elastic-plastic regime.

## 6. RECOMMENDED PRACTICES

In the development of a standardized test procedure, the objective is to provide all necessary controls to allow users to achieve a consistent test result. In the case of the elastic-plastic surface crack test, the approach used by other test standards to contain all needed relations to evaluate the test record is not currently feasible. The variations possible due to nonlinear material behavior add sufficient complexity that an external, stand-alone analysis is required. This ILS has provided strong evidence that such a method is feasible without the introduction of excess variability, even without any significant guidance regarding the analysis methodology. However, the ILS has also provided clear insight into what common practices are in use, such that they could be standardized without undue burden on the user of the standard. This allows the test result to be standardized to the extent possible by providing specifics regarding what analysis practices are considered “standard.” The following list of recommended practices is proposed for inclusion in the surface crack test standard. These are a combination of accepted best practices and observations garnered through this phase of the ILS. They are not to be construed as the only acceptable way to perform elastic-plastic J-integral analysis of surface cracks, but rather as a set of rules that help users achieve a more standardized answer when evaluating test records according to the test standard:

- (1) The analysis shall be performed using the finite element method.
- (2) The model shall consist of three-dimensional elements with quadratic shape functions and utilizing reduced integration. Crack tip deformations should be monitored for spurious zero energy deformation modes.
  - (a) Full integration may be used for elements near the crack tip to avoid spurious zero energy deformation modes.
- (3) The domain integral method shall be used for J-integral calculations.
  - (a) The domains should be as large as possible without compromising mesh integrity.
  - (b) The domains should consist of elements without excessive skew and should be normal to the local crack front within 30°.
  - (c) A minimum of five domains shall be used to monitor path dependence.
  - (d) All domain solutions shall be checked for path dependence, reporting only the highest fully converged value from the outermost domain(s). Unconverged domains indicate the physical size of the domain is too small for the deformation state in the model.
  - (e) All domain solutions shall be checked for oscillatory J-integral results along the crack front. Solutions with oscillations >5% shall not be used.
  - (f) Small strain assumptions shall be used, such that the nodal geometry is not updated due to displacements.

- (4) The following procedures shall be followed to develop constitutive model inputs:
- (a) Tensile test data from ASTM E8 or equivalent is required to establish the stress-strain curve. Tensile specimens should come from the same material and metallurgical orientation used for surface crack testing. Multiple tests are preferable to evaluate a typical response.
  - (b) The finite element constitutive model shall follow Mises plasticity (incremental plasticity).
  - (c) Stress-strain data shall be input as a table look-up, developed as follows:
    - (i) Elastic modulus values shall come from either handbook values or dedicated modulus testing per ASTM E111 or equivalent. Do not rely on tensile test results for accurate elastic modulus values.
    - (ii) Use engineering stress-strain values to be compatible with the small strain assumption in the element formulation.
    - (iii) Separate plastic strain from experimental stress-strain data by subtracting the elastic strain based on the best fit modulus to the actual tensile test response (not the handbook value). If required, the quality of the linear fit should be biased toward the proportional limit region. Define the proportional limit when the plastic strain value is consistently  $>0.0001$ .
    - (iv) Develop the input table as required by the analysis code (stress versus total strain or plastic strain). If the FEA code requires total strain input, then use the elastic modulus value (4)(c)(i) to calculate the elastic strain for a given stress value and sum the elastic and plastic strain components to calculate total strain. The table should have a sufficient number of entries to accurately define the proportional limit, rollover, and tangent modulus characteristics of the stress-strain curve. The material model should be linear-elastic up to the proportional limit.

## APPENDIX A—PHASE I PROBLEM STATEMENT AND TABULAR DATA

ASTM Committee on Fatigue and Fracture  
E08.07.03 Task Group on Surface Cracks

### Analytical Round Robin on Elastic-Plastic Analysis of Surface Cracks in Flat Plates

**Introduction:** The task group on fracture toughness of surface cracked plates is in the process of developing a new material test standard for the assessment of surface crack toughness tests in the linear-elastic and the elastic-plastic regime. While evaluation of stress intensity factor,  $K$ , is well-accepted for surface crack geometries through the Newman-Raju equations or other existing tabulations, the evaluation of elastic-plastic J-Integral values requires the user to perform an analytical assessment of the experiment using methods that cannot be explicitly dictated by the test standard. The feasibility of allowing this latitude in assessment methodology in a testing standard requires validation through an inter-laboratory study.

**Objective:** Determine the variability in J-Integral values from analytical assessment of experimental surface crack tests under elastic-plastic conditions providing minimal guidance. Phase I of the study is conducted “blind.” No test results are provided to the participants at this time.

#### Phase I, Problem A Surface Cracked Plate in Tension

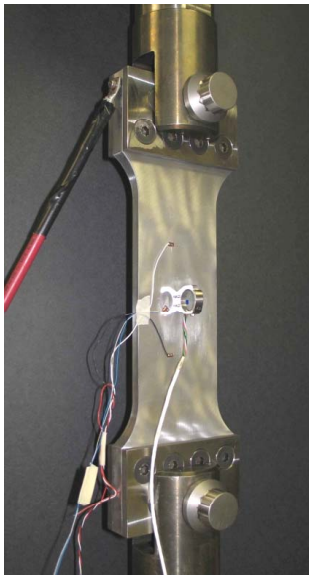


Figure 2. Experimental test set-up for specimen A.

**Requested Analysis:** Elastic-plastic analysis with sufficient quantity of load steps to report the following data:

1. Force versus CMOD from 0 to 289kN (65kip)
2. J-Integral versus  $\phi$ , for at least the following force values
  - a. 200kN (45kip)
  - b. 251.8kN (56.6kip)
  - c. 289kN (65kip)Request sufficient data to plot J vs  $\phi$

3. J-Integral versus Force from 0 to 289kN (65kip) at  $\phi \approx 17^\circ$

Any consistent system of units is fine, *but ksi and inches would be helpful* for consolidating the data. See the draft surface crack test standard for definition of  $\phi$  and CMOD for the surface crack specimen.

**Material Properties:** Stress-strain data shall be provided to all participants in an Excel spreadsheet. Interpretation of the data and type of constitutive model is left to the discretion of the user. For consistency, all analysis should utilize the following elastic properties:

$$E = 74.46 \text{ GPa (10.8E3 ksi)}$$

$$\nu = 0.33$$

**Test Cross Section A-A:** Dimensions taken directly from test specimen A. Dimensions are mm(inches). See Figure 3 for complete specimen geometry.

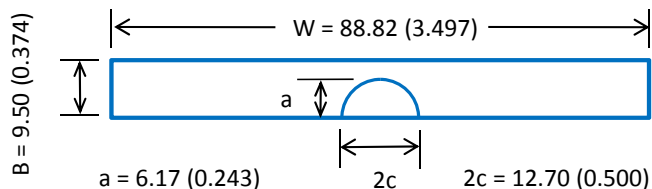


Figure 1. Cross-section A-A and crack size definition.

Crack assumed centered with respect to  $W$ .

**Questions?** Please email us:  
Douglas.N.Wells@nasa.gov  
Phillip.A.Allen@nasa.gov

**Scope and Schedule:** This is the first of at least two problems in Phase I of this Analytical Round Robin. A similar problem under 4-pt bending should follow shortly. Future phases of the round robin will be defined as needed to develop the necessary minimum guidance for the surface crack test standard to sufficiently control analytical variability, or to determine sources of variability observed in Phase I. We request that results of this first problem be returned by email (see "Questions?" box on other side) by July 11, 2011. As always, earlier would be very helpful.

**THANK YOU for participating in this very helpful study! Doug Wells and Phillip Allen, NASA MSFC.**

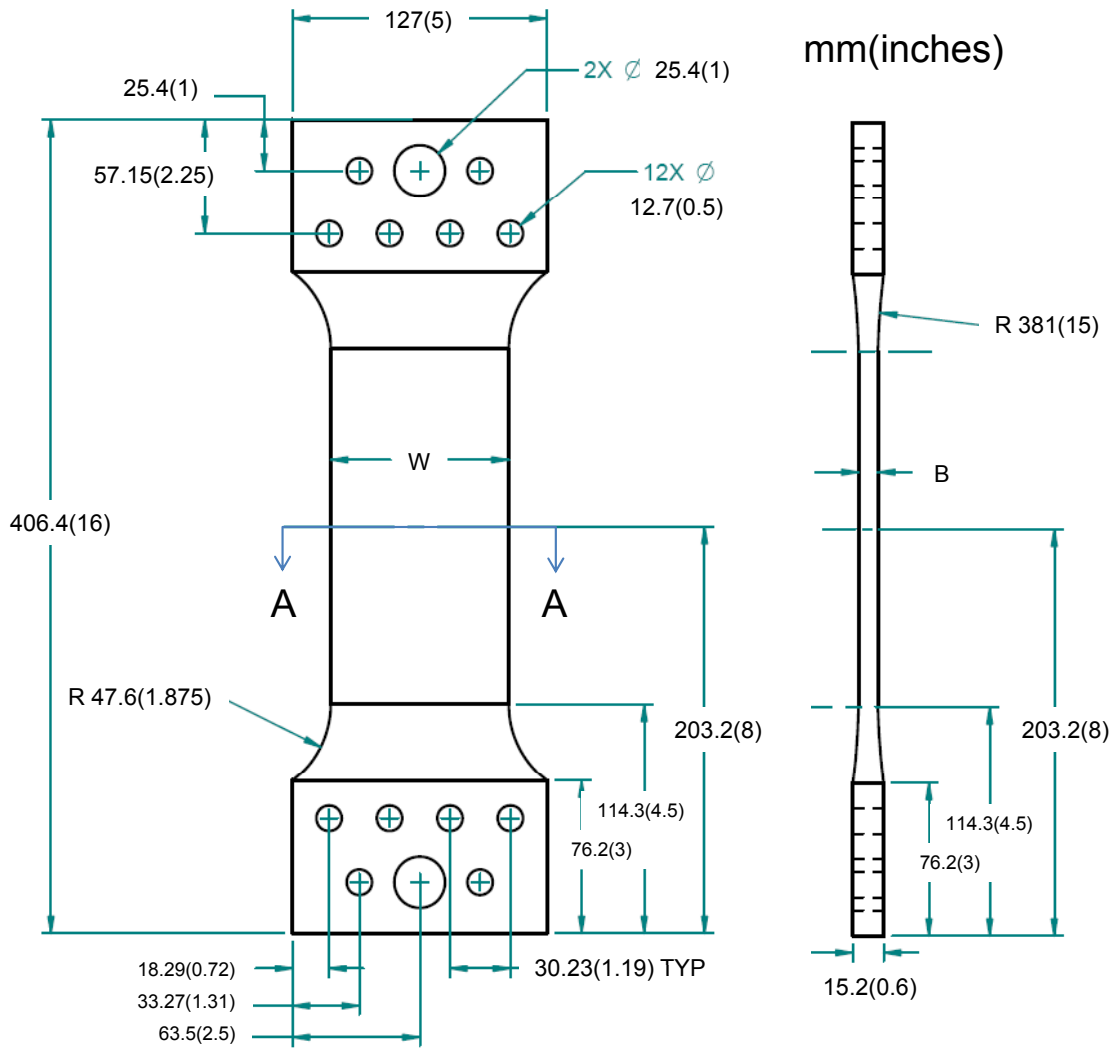


Figure 3. Surface Crack Tension Specimen Geometry

Table A1. Tabular data, full engineering stress-strain data provided to the ILS participants.

Provided Data		Provided Data, Cont'd									
Strain	Stress (MPa)	Strain	Stress (MPa)	Strain	Stress (MPa)	Strain	Stress (MPa)	Strain	Stress (MPa)	Strain	Stress (MPa)
0.00000	0.0	0.00577	369.5	0.02034	425.7	0.03792	456.7	0.05704	470.2	0.07115	468.1
0.00016	11.6	0.00609	375.3	0.02089	426.8	0.03850	457.4	0.05823	470.6	0.07786	467.8
0.00031	23.3	0.00620	376.9	0.02147	427.9	0.03909	458.0	0.05839	471.2	0.07858	467.6
0.00047	34.9	0.00669	382.3	0.02203	429.5	0.03968	458.5	0.05839	471.2	0.07927	467.0
0.00062	46.5	0.00721	386.0	0.02260	430.9	0.04026	459.1	0.05886	470.8	0.07991	465.7
0.00078	58.2	0.00736	386.9	0.02318	432.2	0.04083	459.9	0.05950	471.1	0.08058	465.8
0.00094	69.8	0.00777	388.9	0.02373	432.9	0.04142	460.1	0.06013	471.2	0.08130	465.3
0.00109	81.4	0.00835	391.9	0.02430	434.4	0.04201	460.6	0.06076	471.6	0.08199	464.8
0.00125	93.1	0.00895	394.4	0.02486	435.7	0.04259	461.1	0.06140	471.5	0.08267	463.7
0.00141	104.7	0.00954	396.2	0.02544	436.5	0.04314	462.2	0.06205	471.5	0.08336	462.9
0.00156	116.3	0.01011	398.1	0.02600	437.4	0.04374	462.8	0.06264	471.5	0.08408	462.7
0.00172	128.0	0.01057	399.5	0.02642	438.8	0.04434	462.7	0.06327	471.6	0.08478	461.8
0.00187	139.6	0.01072	400.1	0.02666	438.7	0.04494	463.8	0.06377	472.2	0.08548	460.6
0.00203	151.2	0.01130	402.2	0.02712	439.9	0.04553	464.2	0.06393	471.7	0.08622	459.7
0.00219	162.9	0.01159	402.8	0.02769	441.2	0.04612	464.1	0.06457	471.8	0.08693	459.1
0.00234	174.5	0.01187	403.4	0.02826	442.0	0.04666	464.8	0.06522	471.7	0.08761	457.9
0.00250	186.1	0.01247	405.1	0.02883	443.1	0.04725	465.6	0.06588	471.9	0.08828	457.6
0.00266	197.8	0.01261	405.9	0.02936	443.7	0.04771	465.7	0.06654	471.8	0.08900	456.1
0.00281	209.4	0.01304	406.9	0.02991	445.2	0.04786	465.9	0.06719	471.5	0.08969	455.4
0.00297	221.1	0.01362	408.5	0.03049	446.0	0.04847	466.4	0.06785	471.7	0.09040	454.5
0.00312	232.7	0.01377	408.7	0.03104	446.5	0.04909	466.3	0.06852	471.9	0.09112	453.3
0.00328	244.3	0.01421	410.0	0.03158	448.1	0.04969	466.7	0.06917	471.4	0.09186	452.1
0.00344	256.0	0.01481	411.4	0.03216	448.8	0.05031	467.6	0.06983	471.4	0.09258	451.1
0.00359	267.6	0.01537	412.8	0.03273	449.4	0.05093	467.7	0.07050	471.5	0.09330	450.1
0.00375	279.2	0.01579	414.3	0.03328	450.4	0.05154	467.6	0.07117	471.2	0.09400	448.3
0.00391	290.9	0.01593	415.0	0.03385	451.4	0.05211	467.9	0.07179	470.0	0.09467	447.3
0.00406	302.5	0.01642	415.2	0.03439	451.6	0.05273	468.9	0.07238	470.6	0.09541	446.3
0.00422	314.1	0.01693	417.5	0.03496	452.4	0.05333	469.1	0.07308	470.8	0.09612	444.5
0.00428	317.0	0.01750	419.1	0.03556	453.8	0.05396	468.9	0.07376	470.4	0.09684	443.3
0.00456	326.1	0.01807	420.6	0.03613	454.3	0.05459	469.5	0.07441	469.7	0.09758	441.6
0.00481	338.3	0.01864	421.8	0.03672	455.1	0.05521	469.9	0.07510	469.4	0.09828	439.6
0.00509	350.5	0.01919	422.7	0.03701	455.2	0.05584	470.1	0.07578	469.2	0.09898	438.1
0.00540	361.1	0.01976	424.1	0.03731	455.8	0.05645	469.8	0.07647	468.8	0.09979	434.7

Table A2. Useful data for independent evaluation of the ILS problem. These data were not provided to ILS participants.

<b>Experiment</b>		<b>Experiment, Cont'd</b>		<b>Lab-1 Analysis</b>		<b>Lab-1 Constitutive Input</b>	
Force kN	CMOD mm	Force kN	CMOD mm	Force kN	CMOD mm	Strain mm/mm	Stress MPa
0.0	0.00000	128.5	0.04674	0.0	0.00000	0.00426	317.0
1.2	0.00051	134.2	0.04877	14.5	0.00528	0.00540	361.1
3.6	0.00127	139.7	0.05105	28.9	0.01057	0.00609	375.4
6.8	0.00229	145.3	0.05334	43.4	0.01586	0.00721	386.0
10.6	0.00356	150.8	0.05563	57.8	0.02116	0.00835	391.8
14.8	0.00483	156.3	0.05791	72.3	0.02649	0.00954	396.2
19.2	0.00635	161.7	0.06020	86.7	0.03184	0.01057	399.6
23.9	0.00813	167.1	0.06248	101.2	0.03724	0.01159	402.9
28.8	0.00991	172.4	0.06477	115.7	0.04269	0.01247	405.1
33.9	0.01168	177.7	0.06706	130.1	0.04821	0.01362	408.5
39.2	0.01346	183.0	0.06934	144.6	0.05382	0.01481	411.4
44.2	0.01524	188.3	0.07188	159.0	0.05955	0.01578	414.3
49.6	0.01727	193.6	0.07442	173.5	0.06545	0.02600	437.4
54.9	0.01905	198.8	0.07696	187.9	0.07159	0.03613	454.4
60.5	0.02108	204.2	0.07976	202.4	0.07807	0.04666	464.8
65.9	0.02311	209.2	0.08255	216.9	0.08506	0.05645	469.8
71.5	0.02515	214.5	0.08560	231.3	0.09285	0.06377	472.2
77.1	0.02718	219.7	0.08865	245.8	0.10202		
82.6	0.02921	224.9	0.09169	260.2	0.11470		
88.5	0.03150	230.2	0.09550	274.7	0.13530		
93.9	0.03353	235.3	0.09906	289.1	0.15986		
99.9	0.03581	240.3	0.10312				
105.7	0.03785	245.6	0.10770				
111.7	0.04013	250.6	0.11227				
117.3	0.04242	252.0	0.11354				
123.1	0.04445						

## APPENDIX B—EVALUATION OF INTER-LABORATORY STUDY RESULTS ASSUMING A NORMAL DISTRIBUTION

In many cases, the ILS results have been reduced to report average and standard deviation information. In doing so, the results are assumed to be distributed normally. To evaluate the quality of that assumption, many of the parameters in the study have been plotted on normal probability axes to evaluate the degree to which they follow the normal distribution. The J-integral results at  $\phi = 17^\circ$  are plotted in figure 38 for each of the specified force levels. The majority of responses at the 200 and 252 kN force levels are described well with the linear fit in this space. The lower values of J fall below what would be expected from the normal distribution fit. At 289 kN, the trends are stronger, with the family of  $J \approx 25 \text{ kJ/m}^2$  standing alone and influencing the fit. The slope of the result subset with  $J \approx 30 \text{ kJ/m}^2$  looks to be a better match to the slope at the previous force levels and indicates that this subset of models likely better fits the normal distribution. In this case, the extreme values in the ILS result population for J are not perfectly fit to the normal distribution and will cause errors in the standard deviation estimates; however, the use of these statistics within this TM are still useful for indicating the relative variability in the result set.

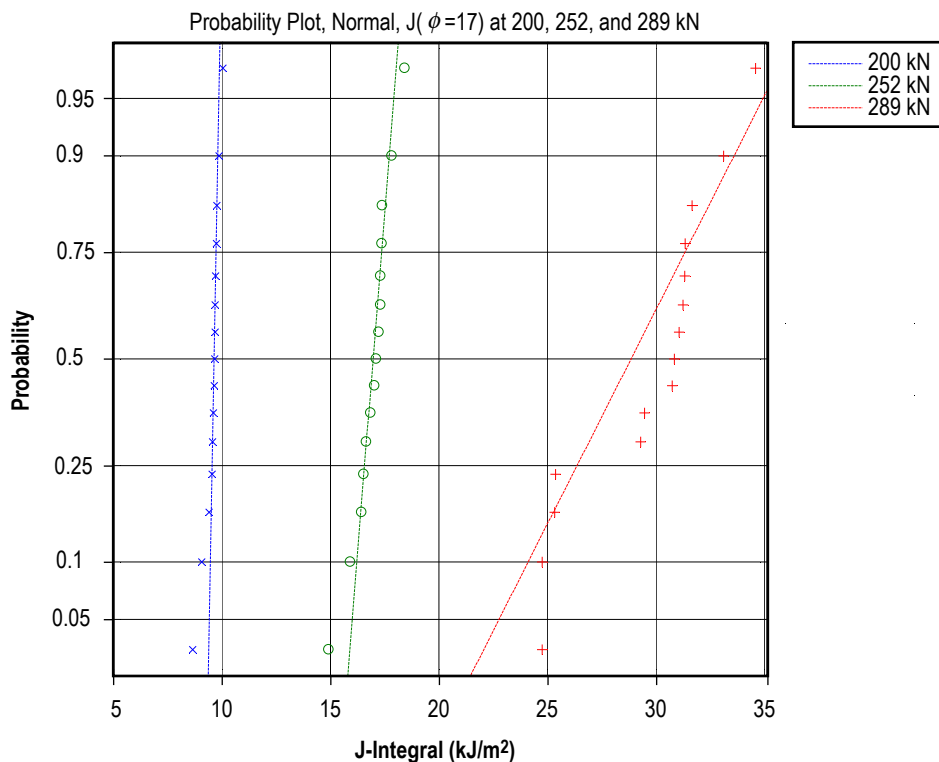


Figure 38. Probability plot for normal distribution of J-integral values.

Figure 39 illustrates the distribution of data regarding the elastic stiffness of the ILS models. This figure can be compared with figure 7. Again, the central values of stiffness reasonably reflect a normal distribution, but the slightly less stiff models are more so than the normal distribution would predict. The result from lab-2 stands unique in this view as well, with stiffness well outside the expected upper bound predicted by a normal fit.

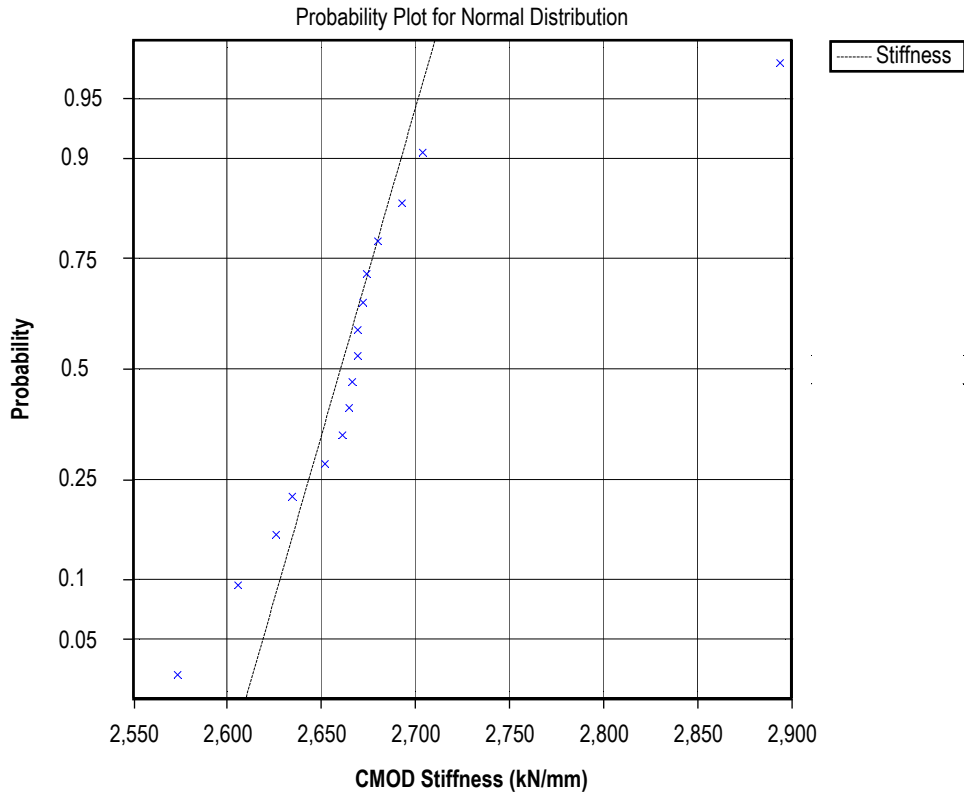


Figure 39. Probability plot for normal distribution of elastic stiffness of modeled CMOD response.

Figures 40 and 41 relate to the use of the model size statistics. In figure 40, the size of the model as measured by the number of crack front nodes is plotted in normal space. In this case, the quality of fit to the normal distribution is not very good. This raises some question regarding the rigorous validity of the MSP that uses the average and standard deviation of the model nodal counts as shown in equation (1). The MSP sums two values that have been transformed into a standard normal space under assumptions that the values are normally distributed. The result in figure 41 shows that the central set of models characterized by  $-1 < \text{MSP} < 2$  are somewhat normally distributed, but relative to those, the smallest models are a bit larger than predicted. As in the case of the J-integral results, the distributions are not rigorously normal, but sufficiently so to conclude that normal statistics derived from the results are sufficient for relative comparison within the context of this study.

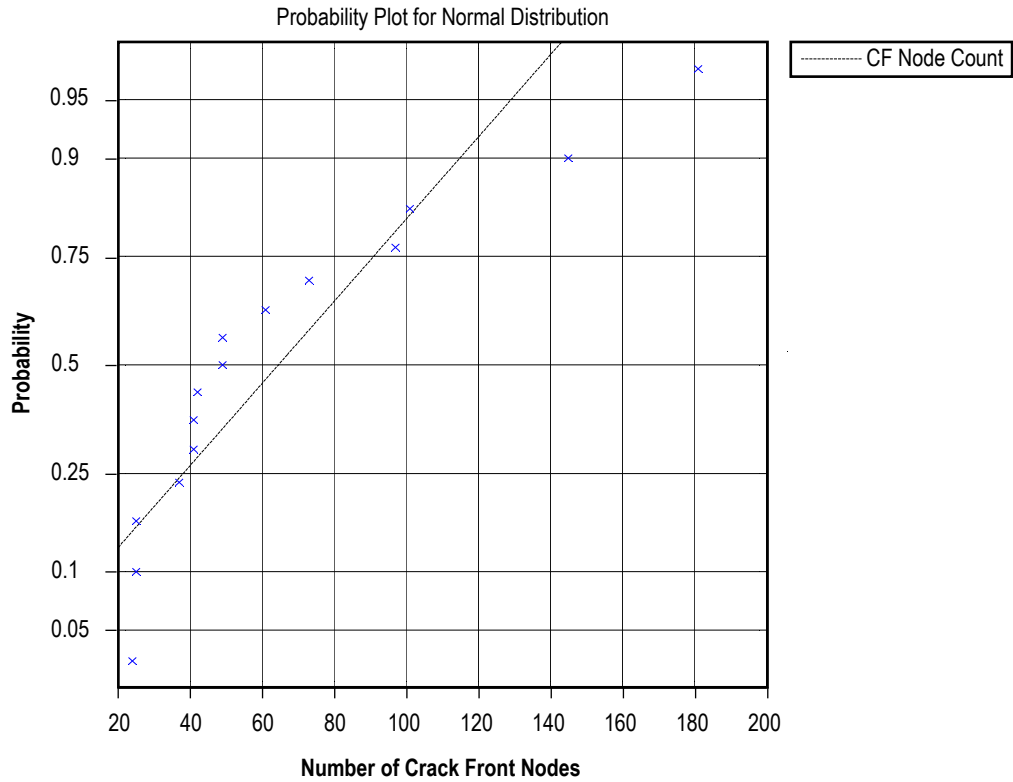


Figure 40. Probability plot for normal distribution of the number of nodes used to model the crack front.

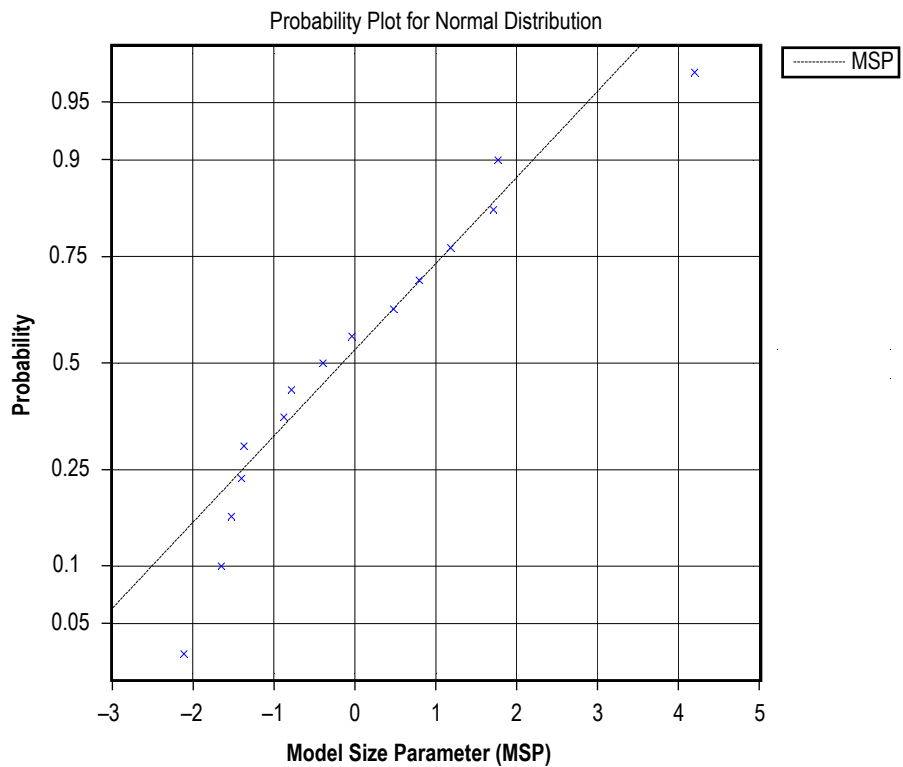


Figure 41. Probability plot for normal distribution of the model size parameter from equation (1).



## REFERENCES

1. Newman, J.C.; and Raju, I.S.: “Stress-intensity Factor Equations for Cracks in Three-Dimensional Finite Bodies Subjected to Tension and Bending Loads,” *Computational Methods in the Mechanics of Fracture*, Vol. 2, pp. 311–334, 1986.
2. Newman, J.C.; Reuter, W.G.; and Aveline, C.R.J.: “Stress and Fracture Analyses of Semi-Elliptical Surface Cracks,” *ASTM Special Technical Publication*, STP1360, pp. 403–423, 2000.
3. API A, *API Recommended Practice 579-1/ASME FFS-1, Fitness-For-Service*, 2nd Ed., Ed: American Petroleum Institute, 2007.
4. E1820-09, Standard Test Method for Measurement of Fracture Toughness, American Society for Testing and Materials, Philadelphia, PA, 2011.
5. Bleackley, M.H.; and Luxmoore, A.R.: “Comparison of Finite Element Solutions With Analytical and Experimental Data for Elastic-Plastic Cracked Problems,” *International Journal of Fracture*, Vol. 22, pp. 15–39, 1983.
6. Larrson, L.H.: “A Computational Round Robin in Elastic-Plastic Fracture Mechanics,” *International Journal of Pressure Vessels and Piping*, Vol. 11, pp. 207–228, 1983.
7. ABAQUS., Dassault Systèmes, <[http://www.simulia.com/products/unified\\_fea.html](http://www.simulia.com/products/unified_fea.html)>, Verified January 11, 2011.
8. WARP3D, Static and Dynamic Nonlinear Analysis of Fracture in Solids, Dodds, R.H., University of Illinois at Urbana-Champaign, <<http://code.google.com/p/warp3d/>>, Verified January 11, 2011.
9. ANSYS, ANSYS, Inc., <<http://www.ansys.com/>>, Verified January 11, 2011.
10. ADINA, ADINA R&D, Inc., <<http://www.adina.com/index.shtml>>, Verified January 11, 2011.
11. Dodds, R.H.: “Effects of Reduced Integration on the 2-D Quadratic Isoparametric Element in Plane Strain Plasticity,” *International Journal of Fracture*, Vol. 19, pp. R75–R82, 1982.
12. Rice, J.R.: “A Path Independent Integral and the Approximate Analysis of Strain Concentration by Notches and Cracks,” *Journal of Applied Mechanics*, Vol. 35, pp. 379–386, 1968.
13. Brocks, W.; and Scheider, I.: “Reliable J-Values; Numerical Aspects of the Path-Dependence of the J-integral in Incremental Plasticity,” *MP Materialprüfung*, Vol. 45, p. 264, 2003.

# REPORT DOCUMENTATION PAGE

*Form Approved*  
OMB No. 0704-0188

The public reporting burden for this collection of information is estimated to average 1 hour per response, including the time for reviewing instructions, searching existing data sources, gathering and maintaining the data needed, and completing and reviewing the collection of information. Send comments regarding this burden estimate or any other aspect of this collection of information, including suggestions for reducing this burden, to Department of Defense, Washington Headquarters Services, Directorate for Information Operation and Reports (0704-0188), 1215 Jefferson Davis Highway, Suite 1204, Arlington, VA 22202-4302. Respondents should be aware that notwithstanding any other provision of law, no person shall be subject to any penalty for failing to comply with a collection of information if it does not display a currently valid OMB control number.

**PLEASE DO NOT RETURN YOUR FORM TO THE ABOVE ADDRESS.**

<b>1. REPORT DATE (DD-MM-YYYY)</b> 01-03-2012			<b>2. REPORT TYPE</b> Technical Memorandum			<b>3. DATES COVERED (From - To)</b>		
<b>4. TITLE AND SUBTITLE</b>  Analytical Round Robin for Elastic-Plastic Analysis of Surface Cracked Plates: Phase I Results						<b>5a. CONTRACT NUMBER</b>		
						<b>5b. GRANT NUMBER</b>		
						<b>5c. PROGRAM ELEMENT NUMBER</b>		
<b>6. AUTHOR(S)</b>  D.N. Wells and P.A. Allen						<b>5d. PROJECT NUMBER</b>		
						<b>5e. TASK NUMBER</b>		
						<b>5f. WORK UNIT NUMBER</b>		
<b>7. PERFORMING ORGANIZATION NAME(S) AND ADDRESS(ES)</b> George C. Marshall Space Flight Center Huntsville, AL 35812						<b>8. PERFORMING ORGANIZATION REPORT NUMBER</b>  M-1332		
<b>9. SPONSORING/MONITORING AGENCY NAME(S) AND ADDRESS(ES)</b> National Aeronautics and Space Administration Washington, DC 20546-0001						<b>10. SPONSORING/MONITOR'S ACRONYM(S)</b> NASA		
						<b>11. SPONSORING/MONITORING REPORT NUMBER</b> NASA/TM-2012-217456		
<b>12. DISTRIBUTION/AVAILABILITY STATEMENT</b> Unclassified-Unlimited Subject Category 39 Availability: NASA CASI (443-757-5802)								
<b>13. SUPPLEMENTARY NOTES</b> Prepared by the Damage Tolerance Assessment Branch, Materials and Processes Laboratory, Engineering Directorate								
<b>14. ABSTRACT</b>  An analytical round robin for the elastic-plastic analysis of surface cracks in flat plates was conducted with 15 participants. Experimental results from a surface crack tension test in 2219-T8 aluminum plate provided the basis for the inter-laboratory study (ILS). The study proceeded in a "blind" fashion given that the analysis methodology was not specified to the participants, and key experimental results were withheld. This approach allowed the ILS to serve as a current measure of the state of the art for elastic-plastic fracture mechanics analysis. The analytical results and the associated methodologies were collected for comparison, and sources of variability were studied and isolated. The results of the study revealed that the J-integral analysis methodology using the domain integral method is robust, providing reliable J-integral values without being overly sensitive to modeling details. General modeling choices such as analysis code, model size (mesh density), crack tip meshing, or boundary conditions, were not found to be sources of significant variability. For analyses controlled only by far-field boundary conditions, the greatest source of variability in the J-integral assessment is introduced through the constitutive model. This variability can be substantially reduced by using crack mouth opening displacements to anchor the assessment. Conclusions provide recommendations for analysis standardization.								
<b>15. SUBJECT TERMS</b> surface crack, finite element, elastic-plastic fracture, J-integral, round robin								
<b>16. SECURITY CLASSIFICATION OF:</b>			<b>17. LIMITATION OF ABSTRACT</b>		<b>18. NUMBER OF PAGES</b>	<b>19a. NAME OF RESPONSIBLE PERSON</b>		
<b>a. REPORT</b>	<b>b. ABSTRACT</b>	<b>c. THIS PAGE</b>	UU		94	STI Help Desk at email: help@sti.nasa.gov		
U	U	U				<b>19b. TELEPHONE NUMBER (Include area code)</b> STI Help Desk at: 443-757-5802		



National Aeronautics and  
Space Administration  
IS20  
**George C. Marshall Space Flight Center**  
Huntsville, Alabama 35812